UNIVERSITÄT DUISBURG ESSEN

Open-Minded

PROCESS ENGINEERING WATER TECHNOLOGY

Studies on Graphite as model adsorbent in aqueous solutions

Master thesis to obtain the degree of a Master of Science

Faculty of Engineering Science,
Chair of Mechanical Process Engineering/Water Technology

University of Duisburg-Essen

Editing period:	29 June 2018 – 20 December 2018
Author:	Marco Vernillo
Student ID number:	[redacted]
Course of study:	Water Science (M. Sc.)
First supervisor:	Prof. Dr.-Ing. Stefan Panglisch
Second supervisor:	Dr.-Ing. Ralph Hobby
External supervisor:	Prof. Dr. Ivana Ivancev-Tumbas

Versicherung an Eides Statt

Ich versichere an Eides statt durch meine untenstehende Unterschrift,

- dass ich die vorliegende Arbeit - mit Ausnahme der Anleitung durch die Betreuer - selbstständig ohne fremde Hilfe angefertigt habe und
- dass ich alle Stellen, die wörtlich oder annähernd wörtlich aus fremden Quellen entnommen sind, entsprechend als Zitate gekennzeichnet habe und
- dass ich ausschließlich die angegebenen Quellen (Literatur, Internetseiten, sonstige Hilfsmittel) verwendet habe und
- dass ich alle entsprechenden Angaben nach bestem Wissen und Gewissen vorgenommen habe, dass sie der Wahrheit entsprechen und dass ich nichts verschwiegen habe.

Mir ist bekannt, dass eine falsche Versicherung an Eides Statt nach § 156 und nach § 163 Abs. 1 des Strafgesetzbuches mit Freiheitsstrafe oder Geldstrafe bestraft wird.

_____ _____

Ort, Datum Unterschrift

Summary

Adsorption processes from aqueous solutions for the removal of aromatic compounds by activated carbon are influenced by various adsorption mechanisms. In contrast to activated carbon, graphite is a homogeneous sp2-hybridized material, which is excellently suited for the investigation of adsorption mechanisms. In particular, functional oxygen groups on the graphite surface weaken the hydrophobic character of pristine graphite by using of special modification methods. Various modification methods such as ozonation for the production of graphite oxide were carried out experimentally and analytical methods were used to examine the modified material for changes in surface chemistry. By Adsorption batch tests the adsorption affinity of selected aromatic compounds were compared between pristine graphite and graphite oxide. Amongst other results, it was found that bicyclic aromatics better adsorb onto both, pristine and ozonised graphite surface than monocyclic aromatics. Further tests were carried out to investigate the concentration behaviour of the test substances and factors that could influence the adsorption process. More in-depth studies on this topic for more comprehensive results and improved method developments, for instance to modify the graphite surface properties, are required.

List of contents

List of figures

List of tables

1. Introduction

Activated carbon (AC) is a widely proved adsorbent in removal of various organic and inorganic pollutants dissolved in aqueous media (Yin, Aroua and Daud, 2007). Already in 1927 activated carbon was used in Germany and the USA for drinking water treatment to remove unpleasant odours and bad taste, but also to remove phenolic compounds (Kienle and Bäder, 1980b). Today, drinking water can contain hundreds of organic compounds released into the environment from industrial, domestic and agricultural wastewater (Pollard *et al.*, 1992). Improved analytical techniques with high sensibility have increased the number of detected chemicals present in water (Ivančev-Tumbas, 2014). The polar characteristics of some newly emerging micropollutants is increasingly concerning the drinking water industry because many of these substances cannot be easily removed by traditional drinking water treatment operations (Verliefde *et al.*, 2007). In the removal of micropollutants, the adsorption mechanisms between the adsorbent and the adsorptive play an important role. Three known of these mechanisms are the π-π dispersion interactions, the hydrogen bonding formation mechanism and the electron-acceptor complex mechanism (Moreno-Castilla, 2003). With the help of specially developed AC modifications, the affinity for certain contaminants could be improved. For enhancing the adsorption properties of activated carbon for certain contaminants, studies are required for modification via a chemical or physical treatment for introducing special designed functional groups onto the surface structure of AC (Yin, Aroua and Daud, 2007). Activated carbon is constituted of a wide range of amorphous carbon-based materials and exhibits a high degree of porosity and an extended surface area (Çeçen and Aktaş, 2012a). Structurally, activated carbon is heterogenous and consists of a mixture of graphite-like crystallites and non-organized phases composed of complex aromatic-aliphatic forms. The presence of functional groups bond to the edges of the basal planes have a great importance for the adsorption behaviour of carbon adsorbents (Menéndez-Díaz and Martín-Gullón, 2006). Due to the heterogeneous structure, the adsorption mechanisms on activated carbon are difficult to detect. In contrast, graphite is nonporous and to a large extent a crystalline material, ideal for studying the adsorption mechanisms. For this purpose, virgin graphite is used in this work and for the profound comparison of the adsorption properties the usage of modified graphite with oxygen-containing surface groups is applied.

2. Objectives

Activated carbon is a common adsorbent for removing organic contaminants from the aqueous phase, such as in drinking and wastewater treatment. However, since the various organic substances have different adsorption properties in the interaction with the adsorbents, it is necessary for the activated carbon to meet the requirements for obtaining high efficiencies in the adsorption capacity. To date, the exact adsorption behaviour of many substances on activated carbon has not been thoroughly researched. In order to investigate the adsorption mechanisms in more detail, adsorption tests in this work were suggested with chosen differently substituted aromatic substances. By the application of pristine and oxidized graphite as adsorbent the different adsorption behaviour should be investigated by the uptake of adsorption isotherms from adsorption batch tests. An essential part in the preparation of the adsorption experiments is the modification of pristine graphite via chemical and thermal oxidation treatments. The characterization of the graphite species should to be carried out by elementary or physico-chemical investigations via surface-sensitive analytical methods, such as XPS, EDX, BET surface analysis, zeta potential measurement, particle size analysis etc. The determination of the adsorptive concentration in the adsorption systems is performed by spectrometric fluorescence analysis. Subsequently, by the evaluation of the data and measurements, the results should to be analysed adequately.

3. Theoretical background

3.1 Basics of the adsorption process

Adsorption is the accumulation of substances on the surface of liquids or solids. The adsorption takes place by interactions of the active centres with atoms, molecules or ions of an adjacent liquid or gaseous phase (Kümmel and Worch, 1990c).

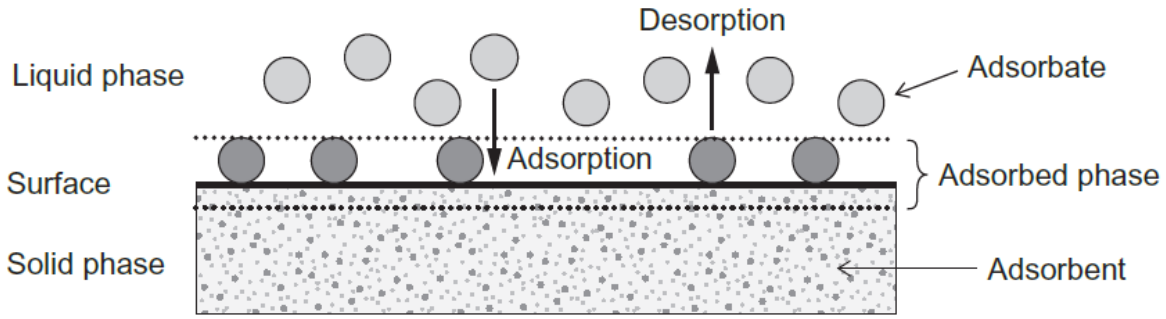

Figure 3.1: Schematic illustration of the adsorption process

(Worch, 2012)

The basic terms of adsorption in the schematic illustration (Figure 3.1), which represents the model of the adsorption process, are explained in more detail. The adsorbent is the adsorbing solid. The adsorbate, also indicated as adsorptive, refers to the particles of the substance to be adsorbed from the liquid phase and attached as adsorbed phase to the surface of the adsorbent. Adsorbent and adsorbate form the adsorption complex (Kümmel and Worch, 1990c). In aquatic solution typically monolayer adsorption occurs in contrast to gas phase adsorption, where a multilayer forming is commonly found (Moreno-Castilla, 2003).

Adsorption isotherms describe the adsorption process and have been developed to assess the capacity of, for example, activated carbon for the adsorption of a particulate molecule. The shapes of isotherms are classified into several types (Figure 3.2), and five of them are found mainly in carbon materials. Mostly, long-linear isotherms are found in the initial part of all isotherms concerning with carbon adsorption. The Langmuir isotherms (type L) often occur, even if the preconditions of the Langmuir theory are not obvious. The most common Freundlich-Isotherm (type F) is typical for heterogeneous surfaces. Adsorption processes with a very steep initial rise, followed by a pseudo-plateau, are described by high-infinity isotherms. The latter sigmoidal isotherm occurs with homogenous surfaces observed at graphitized carbon black Graphon and V3G (Moreno-Castilla, 2003).

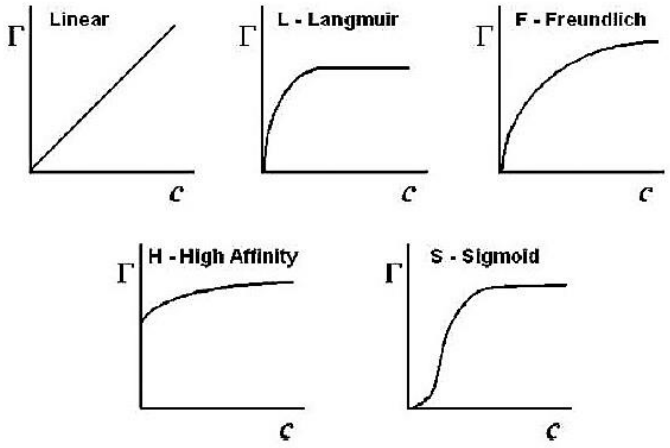

Figure 3.2: Types of adsorption isotherms found from dilute aqueous solution on carbon materials (Moreno-Castilla, 2003)

For description of adsorption isotherms, the Freundlich equation (1) can be applied. Freundlich's empirical relationship is often suitable for describing measured values for adsorption from aqueous solutions to activated carbon.

$$q = K_F \, c^n \qquad (1)$$

q	solid phase concentration (mass of adsorbate related to the mass of adsorbent)
K_F	Freundlich constant
c	equilibrium concentration of adsorptive in aqueous solution
n	Freundlich exponent

The two isotherm parameters K_F and n from the Freundlich equation can be determined by regression calculation or by graphical methods after plotting the measured values on a double logarithmic scale by the following equation (2).

$$\log q = \log K_F + n \log c \qquad (2)$$

From the illustrated linear function (2), the slope can be used to obtain the Freundlich exponent n. The Freundlich constant K_F is obtained when the load q is set to c = 1 (log c = 0) (Sontheimer, Frick, Fettig, *et al.*, 1985).

3.2 Graphite as adsorbent

3.2.1 Graphite structure and chemical properties

Graphite allotrope is the most thermally stable form of carbon under standard conditions and it was discovered in 1787 (Yaya *et al.*, 2012), (Nikam and Hydarali, 2018). In addition, graphite has a good electrical conductivity, but is also thermally conductive (Menéndez-Díaz and Martín-Gullón, 2006). Various graphites within the same classification may vary in their crystallinity. Graphite itself describes an ideal crystallite material without defects resulting in a perfect graphite structure built from the trigonal units of sp^2 hybridized carbon atoms (Pierson, 1993a). Two different types of bonds, the σ-bonds directional between carbon neighbors, and the π-bonds, spread out above and below the carbon sheet, engender the unique properties of graphite (Yaya *et al.*, 2012). Under real conditions, crystallite imperfections can be observed, caused by a number of structural defects. Therefore, these materials are considered rather as “graphitic carbon” (Pierson, 1993a). In nature, graphite commonly occurs in crystalline flakes, but also occurs in an amorphous microcrystalline form or is found in graphite veins as a lump form. Graphite has a layered crystal structure in which the carbon atoms are arranged in hexagonal or rhombohedral unit cells (Figure 3.3). In hexagonal crystal structures, mostly found in synthetic graphite, each of these unit cells has a size of a = 2.46 Å and c = 6.708 Å (Pierson, 1993a). A single atomic graphite layer of sp^2 carbon atoms is termed as graphene and forms the basal plane of a 3D graphite crystal (Marcano *et al.*, 2010). The individual graphene layers in graphite are stacked in ABAB sequence in hexagonal crystal structure and in ABC sequence in rhombohedral crystal structure on top of each other at a distance of 3.354 Å (Pierson, 1993a).

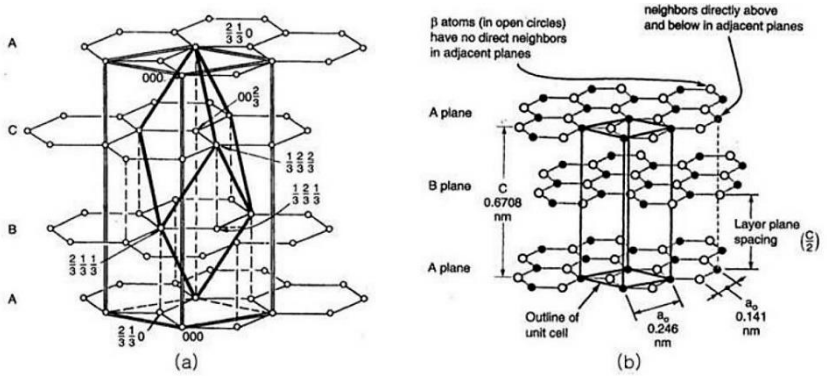

Figure 3.3: The crystal structure of graphite, a) rhombohedral, b) hexagonal (Yaya et al. 2012).

The individual graphene layers in graphite are stacked on top of each other at a distance of 3.354 Å. (Chung, 2002)

The chemical bonds within the graphene layers are strong and covalent while the affinity between the individual stacked graphene layers is due to van der Waals forces and weak electrostatic interatomic interactions. (Yaya et al. 2012). Naturally, rhombohedral graphite, which is thermodynamically unstable, is never found in pure form but in combination with hexagonal graphite, but also in synthetic material it may

contain up to 40 % (Pierson, 1993a). The resistance to most non-oxidising acids, alkalis and corrosive gases of pure graphite is due to the fact, that it is one of the most chemically inert materials. Under real conditions, impurities are present in the material to some degree, which increases the chemical reactivity by its catalytic effect. Furthermore, active sites present at the end of the basal planes of the graphite crystal and defect sites, such as dislocations, vacancies, and edge defects form chemical reaction sites. In contrast, reactions with the basal plane surfaces are much less represented. This is because of the reason, that the graphite crystals exhibit large differences in the surface energy in the different crystallographic directions accounting for the different rate of reaction. At the prismatic plane the energy amounts to 5 J m^{-2} whereas at the basal plane, according to the literature, the amount of energy is only 0.11 J m^{-2}. Therefore, graphite materials with large crystals and few defects are more chemically resistant. Large porosity as it is found in activated carbon increase the surface area resulting to an increase of the chemical reactivity in contrast to dense, pore-free materials (Pierson, 1993a). The true material density of graphite, which is determined according to the guidelines (Sontheimer, Frick, Fettig Joachim, *et al.*, 1985) in a pycnometer, is with 2.26 g cm^{-3} (at 300 K, 1.01325 bar) greater than that of conventional activated carbon with about 2.0 – 2.1 g/cm^3 (Kienle and Bäder, 1980a) (Pierson, 1993a). An increase in the reactivity of graphite with water, oxygen, some oxides or other substances may also be observed at higher temperatures at, for example, above 450 °C. The chemical resistance of graphite is less pronounced with respect to the elements of the 6th main group (oxygen, sulphur, selenium and tellurium) from the periodic system. Generally, oxidising acids and acid solutions (boiling H_2SO_4, Br_2, $H_2Cr_20_7$, HNO_2, $HClO_4$), oxidising alkalis and alkaline solutions (permanganate, perchlorate, perborates), gases (air, F_2, H_2 He, methane, N_2, O_2, N_2O_4), etc. react under given physical conditions more or less strong with graphite materials. For instance, graphite does not react with hydrogen at ordinary temperatures but at an increased temperature in the range of 1000 – 1500 °C methane is formed (Pierson, 1993a). An oxidation treatment of graphite with strong oxidants, such as sodium nitrate ($NaNO_3$) (98 %), sulfuric acid (H_2SO_4) (98 %), potassium permanganate ($KMnO_4$) (99 %), H_2O_2 solution (30 %) and HCl (98 %), as used in the modified Hummer's method, lead to the synthesis of graphene oxide (Gupta *et al.*, 2017). The synthesis of graphite oxide having functional groups on the external surface can only be realized with a mild oxidation treatment of graphite, such as ozonation (Razumovskii *et al.*, 2007).

3.2.2 The structure of Graphite oxide

Graphite oxide (GO) was discovered by B. C. Brodie in 1859 (Brodie, 1859). There are four different preparation methods, that have been developed: the Brodie process, the Staudenmaier process, the Hummers-Offeman process and anodic oxidation of graphite electrodes in nitric acid. Four different main structural models of graphite oxide have so far been proposed: the Hofmann model, the Rues model, the Scholtz-Boehm model, and the Lerf-Klinowski model (Lee *et al.*, 2010). In the Hofmann model, the

oxygen atom is linked to the carbon atoms of hexagon layer planes via epoxy (1,2-ether) linkages. The Rues model states that in the crumpled carbon layers, trans-linked cyclohexane compounds are assumed to which functional OH and epoxy groups are bound (Szabó *et al.*, 2006). Rues was the first scientist who accounted for the hydrogen content in GO (Lee *et al.*, 2010). In addition, this model was supplemented by C=C double bonds, ketone and enol groups on the graphite surface in the work of Claus and co-workers. In addition, they observed an acidity caused by enolic OH groups along the layer planes and by carboxyl groups around the edges of the lamellae. Scholtz and Boehm revised this model, suggesting that there are only a few ether groups onto the surface of graphite oxide, and graphite oxide also consists of corrugated carbon layers bound to rigid quinoid-structured ribbons. The Lerf-Klinowski model presented a completely new graphite oxide structure. The graphite oxide layer consists of a random distribution of flat aromatic regions with unoxidized benzene rings and alicyclic six-membered rings bearing C=C double bonds, C-OH, ether, and carboxyl groups (Szabó *et al.*, 2006). In the general model of graphite oxide (Figure 3.4) various oxygen functional groups are distributed across aromatic regions (Yong *et al.*, 2015).

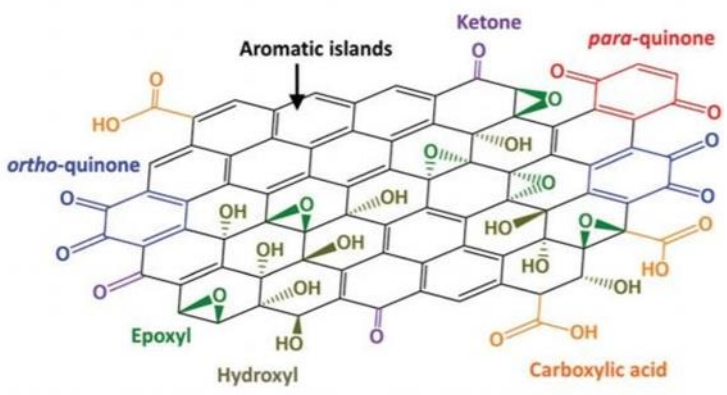

Figure 3.4: General structural model of oxidized graphite

(Yong *et al.*, 2015)

3.2.3 Surface functionalities of carbon materials

The chemical properties of carbon materials are strongly influenced by functional groups present on the surface (Figure 3.4). In particular, even small amounts of heteroatoms introduced onto the carbon surface by chemical or thermal oxidation methods can greatly alter these properties, and also the adsorption properties. Hence, the adsorption properties can be tailored by a variety of chemical surface modifications. The most common acidic and basic functionalities, besides nitrogen-containing functional groups or functionalities with other heteroatoms, are oxygen-containing groups such as carboxyl, lactone, hydroxyl, carbonyl, quinone, ether, pyrone, phenol, carboxylic anhydride, and lactol groups (Bandosz and Ania, 2006). Specific methods for the modification of carbon materials, such as activated carbon, have been described by a number of scientists (Moreno-Castilla *et al.*, 1995) (Bhatnagar *et al.*, 2013) (Moreno-Castilla *et al.*, 1995) (Rivera-Utrilla *et al.*, 2011) (Yin, Aroua and Daud,

2007). The amount of oxygen fixed on carbons by thermal oxidation get higher with increasing temperature (max. 676 – 773 K). Other oxidation methods with chemical oxidants such as ammonium peroxydisulfate, hydrogen peroxide, nitric acid and ozone are also performed (Bhatnagar *et al.*, 2013), (Rivera-Utrilla *et al.*, 2011).

3.2.4 Production of synthetic graphite

The transformation of turbostratic carbon material into a well-ordered graphitic structure may be termed as graphitization. A series of steps are necessary for graphitization of e.g. cokes. At increasing temperatures of about 1200 °C hydrogen, sulphur and other elements are gradually removed from the carbonized precursor material and are disappearing totally at 2000 °C. The conversion of a turbostratic to a graphitic structure takes place at 1800 °C to 2200 °C. The higher the temperature is, the faster is the graphitization process. This procedure leads to weight loss, because of the removal of interlayer chemical species, such as interstitial carbon. Thereby, most graphitizable materials require a temperature of 3000 °C of about 2 to 3 hours for a full graphitization grade with minimum interlayer spacing. At lower temperatures, considerably more time is required. Besides, the usage of elevated pressures may yield to a higher degree of graphitization. Moreover, higher pressure results in a shorter heat-treatment time or respectively, a lower heat-treatment temperature may be applied. (Pierson, 1993b).

3.2.5 Surface chemistry carbons and adsorption mechanisms

The application about the adsorption of organic solutes from the aqueous phase by activated carbon has been very important, since by the more thorough removal of pollutants from potable and waste waters, the use of carbons and the demands placed on their performance are expected to increase. In recent years, the understanding about the chemistry of the carbon surface has reached a significant progress, which poses a crucial basis for the understanding of adsorption processes of organic and inorganic solutes. Several monographs concerning with carbonaceous adsorbents have been published in the last decades but they held more attention to gas-phase-adsorption than to liquid-phase-adsorption, in particular the surface physics is discussed in more details than the surface chemistry. Scientific studies lead to the conclusion that a direct comparison of the gas-phase-adsorption of organics in the presence of water vapor to the separation of organics from liquid water is not possible. The adsorption of organics in association with the role of the carbon surface for determining the adsorption uptakes is a complex process. Thus, the focus of the scientific investigation engagement has to be directed on the removal of phenols or other organic compounds and in particular on their adsorption mechanisms (Radovic, Morena-Castilla and Rivera-Utrilla, 2001).

Adsorption mechanisms

The adsorption of organic molecules from dilute aqueous solutions is a complex process that depends on electrostatic and non-electrostatic interactions. Non-electrostatic interactions generally consist of dispersive forces and hydrophobic interactions, whereas electrostatic interactions (coulomb interactions) occur through ionized electrolytes with ionized surface functional groups on the absorbent. The interactions involved in the adsorption process depend on the physicochemical properties of the adsorbent, the adsorptive, and the solvent chemistry.

Adsorbent characteristics

The characteristic properties of the adsorbents involved in the adsorption process include pore structure, surface chemistry, and mineral matter content. The adsorption of organic molecules from aqueous solutions is conventionally carried out with activated carbons of high porosity. The pore texture is an important factor in the adsorption process. Graphite usually has no pore structure in the original and inactive state. The presented overview of the characteristic properties of adsorbents is mainly concerned with graphite, by means of which the adsorption mechanism is to be symbolized. Therefore, this chapter does not discuss the influence of the pore structure in the adsorption process. The surface chemistry of the graphite layers is determined by the content of the heteroatoms. In particular, oxygen complexes which are formed by the functional surface groups play an essential role. These functional groups form a surface charge during immersion in an aqueous solution, which is caused by the degree of dissociation of the surface groups or the adsorption of ions from the solution (Figure 3.5). The resulting hydrophobic forces and electron density have an influence on the adsorption property. Negative surface charges result from dissociation of functional oxygen groups that are acidic, such as carbonyl and phenolic groups. Positive surface charges occur through nitrogen functionalities. In addition, the state of the surface charge depends on the pH of the solution. When carbons do not have nitrogen-containing functional groups, positive charges may be due to basic oxygen surface complexes with, for example, pyrones and chromenes. Moreover, also the existence of electron-rich regions within the graphene layers act as electron pair donators (Lewis bases), which take up protons from the aqueous solution, giving the surface a positive charge character (Moreno-Castilla, 2003). For the estimation of the surface charge, titrations methods, indicating the point of zero charge (pH_{PZC}) for the measure of the total surface charge or, alternatively, an electrophoretic method, indicating the isoelectric point (pH_{IEP}) for the degree of surface charge on the outer surface of the particle, may be used. If the difference between the two values is small, the distribution of the surfaces is homogeneous (Radovic, Morena-Castilla and Rivera-Utrilla, 2001) (Moreno-Castilla, 2003). The hydrophobicity of the carbon surface is generally reduced by the increase in oxygen content because hydrogen molecules are bound to the surface of the oxygen complexes by hydrogen bonding, thereby reducing the accessibility of the hydrophobic aliphatic chains (Moreno-Castilla, 2003).

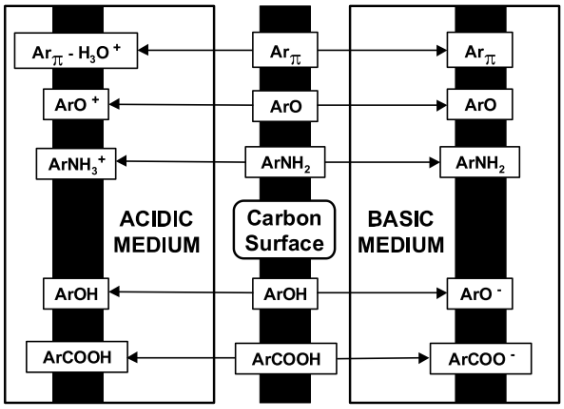

Figure 3.5: Carbon surface chemistry.

Dependence of the pH value and of the aqueous medium on a macroscopic scale. The functional groups are covalently linked to aromatic ring systems (AR) at the graphite surface. (Moreno-Castilla, 2003)

In addition, surface oxygen complexes also affect the electronic density of the graphene layers, which affects the dispersion interactions between the carbon surface and the adsorptive molecules. Carboxyl groups, which are fixed at the edges of the graphene layers, can withdraw electrons, while phenolic groups achieve an electron-releasing effect. Many studies have shown that an increasing of the surface acidity by oxidation of activated carbons causes a reduction in phenol adsorption from aqueous solutions (Moreno-Castilla, 2003).

Adsorptive characteristics

Adsorptive factors that play a key role in the adsorption process include molecular size, solubility, pK_a, and the nature of the substituent on aromatic molecules. The pK_a value, which depends on the pH of the aqueous solution in the adsorption system, determines the degree of dissociation of the adsorptive and thus the adsorption affinity to the adsorbent. In the case of aromatic substances, their substituents can influence the electron distribution in the molecule and thereby withdraw or release electrons from the aromatic ring. This process affects the dispersion interaction between the aromatic ring of the adsorptive and the graphene layers of the adsorbent. Many scientific studies have attempted to elucidate the adsorption mechanism of phenolic compounds on carbon materials. The following adsorption mechanisms have been suggested by various scientists since the late 1960s, π-π-dispersion interactions and hydrogen bonding, proposed by (Coughlin and Ezra, 1968) and the electron-acceptor complexation proposed by (Mattson *et al.*, 1969). It has long been known that phenol is adsorbed in the flat position onto the graphene layers by adsorption driving forces due to π-π interactions between the aromatic ring of phenol and the aromatic structure of the graphene layers (Moreno-Castilla, 2003). Acidic surface oxygen groups, located at the edges of the basal planes of the graphene layers remove electrons from the π-electron system, creating positive holes in the conducting π-band of the graphitic planes. Thus, weaker interactions between π-electrons of the phenol aromatic ring and the π-electrons of the basal planes are established and this reduces the phenol uptake. Some scientific works from the last decades give evidences for such π-π dispersion

interaction mechanisms (Haydar *et al.*, 2003), (Mahajan, Moreno-Castilla and Walker, 1980). In these works, it was also indicated that phenol and water compete to form H-bonds with surface oxygen groups, such as carboxyl groups, whereas H-bonds are formed preferentially by water molecules. For this thesis an experiment about an adsorption system with phenol in cyclohexane showed, that phenol uptake by oxidized absorbents is preferred by the surface oxygen complexes. This result confirmed in a study (Franz, Arafat and Pinto, 2000) by experiments studying the adsorption of phenol aniline, nitrobenzene and benzoic acid from aqueous and cyclohexanic solutions. In these scientific works the conclusion was indicated, that the adsorption mechanism is forced by both, H-bonding with carbonyl groups and π-π dispersion interactions between the aromatic ring of the adsorptive and the graphene layers. Some scientific studies about regeneration experiments with activated carbon revealed that adsorption of phenolic compounds is partly physical and partly chemical. Heat treatments or heating of activated carbon by different solvents could remove the part of phenolic compounds that was physisorbed, but not the chemisorbed part even at high temperature. This result indicates that chemisorbed phenolic compounds are strongly bound by other forces than π-π dispersion interactions or H-bonds, probably by electron-acceptor-complex-mechanism as it was proposed by (Mattson *et al.*, 1969).

Solution chemistry and adsorption temperature

The solution pH, the ionic strength, and the temperature are crucial factors that influence the process in an adsorption system. The electrostatic interaction of organic weak electrolytes and polyelectrolytes between the adsorptive and a carbon material adsorbent is strongly controlled by the pH of the solution. This is because the carbon surface charge and the dissociation and protonation grade of the electrolyte solution is a function of the solution pH. Hence, external or the total surface charge of the absorbent particles will be on average positive at a solution pH lower than pH_{IEP} or pH_{PZC} and on average negative at a solution pH higher than pH_{IEP} or pH_{PZC}. In addition, the dissociation or ionization of the electrolyte relating to its pK_a is also influenced by the solution pH. Therefore, at a pH > pK_a acidic electrolytes are dissociated, whereas at a pH < pK_a electrolytes can be protonated. Therefore, electrostatic interactions are depending on the solution pH and have a strong effect on the adsorption process. Using substituted phenols as an example, it could be shown that in an acidic pH milieu a maximum adsorption uptake was achieved due to the undissociated phenol derivatives, whereby the dispersion interactions prevail. Conversely, for a basic solvent, pH, adsorption uptake was lower because under these conditions electrostatic repulsion predominated between the negative surface charge and the phenolate anions and the phenolate-phenolate anions (Moreno-Castilla, 2003). Also, the temperature influences the adsorption processes. At elevated temperature, less organic molecules are adsorbed to an absorbent because of the exothermic behavior of adsorption processes (Moreno-Castilla, 2003),(Çeçen and Aktaş, 2012b). However, some exceptions in this phenomenon has been reported where the adsorbed amount increased with rising temperature, as it was for example the case for paracetamol from a diluted aqueous solution (Terzyk *et al.*, 2003), (Moreno-Castilla, 2003).

3.3 Characterization of graphite structure and surface functionalities

3.3.1 The theory of zeta potential

Dispersed particles in distilled water or in electrolyte-containing water have a surface charge (Nernst potential), that depends on the existing dissociated functional groups located on the particle surface. In this case, dissociated groups can be of different types, i.e. they can be positively or negatively charged. The sum of the surface charge of all dissociated groups gives the total surface charge, which may be positive or negative depending on the nature of the surface functional groups. The extent of the surface charge is also dependent on the pH and degree of dissociation. Around the charged particle surface, an ion layer is formed which, depending on the electrolyte content of the water, has a different layer thickness. For highly dilute electrolyte solutions, the concentration of counterions is very low and the thickness of the diffused layer extends over a long distance. In contrast to this, the layer of counterions is rather compact in concentrated solution. Two ion-layer models are postulated, the Gouy-Chapman model for electrolyte-free water and the Stern model for electrolyte-containing water (Müller and Hildebrand, 1996).

Gouy-Chapman model for dispersed particles in electrolyte-free water

An ideal electrolyte-free water does not exist in practice. After purification, there is always a certain residual concentration of electrolytes due to the self-dissociation of water, so that the minimum possible conductivity is approximately 0.5 µS cm^{-1}. Dispersed particles which have predominantly proton donating group (carboxyl groups, sulfate groups) receive a negative surface charge. The dissociated cations (H^+, Na^+) present in the surrounding water are deposited in the form of a cloud of counterions around the negatively charged particles, in the so-called diffuse layer. The potential drop in the diffuse layer is exponential and decreases to zero with increasing distance, so that the particle appears neutrally charged to the outside. The concentration of positive counterions is higher in the vicinity of the particle surface than at a greater distance. At the end of the diffuse layer, the concentration equilibrium between positive and negative ions is restored (Müller and Hildebrand, 1996).

Stern's model for dispersed particles in electrolyte-containing water

The Stern model describes the attachment of ionic layers to dispersed particles in electrolyte-containing water. By the example of particles with negative surface charge, a monolayer of negative ions is adsorbed to the particle surface, the so-called inner Helmholtz layer, which is not present in the Gouy-Chapman model. The adsorption of negative ions on a negatively charged particle surface is caused by van der Waals forces, which dominate at small distances of a few angstroms the electrostatic forces. The negative ions are striping off their hydration shell during the adsorption process and can thus move closer to the particle surface. The inner Helmholtz layer thus consists of dehydrated negative ions to which a second monolayer of positively hydrated ions is fixed, the so-called outer Helmholtz layer. The surface potential is not fully compensated by the outer Helmholtz layer, because the positively charged ions

have a larger space requirement due to their hydration shell and thus are present in smaller numbers than the negative ions on the particle surface. As a result, there is still a negative stern potential (Figure 3.6), which is compensated by further counterions surrounding the particle as diffuse layer, also indicated as the Goy-Chapman layer. With increasing distance, the potential drops to zero and there is a charge equalization parallel to the Gouy-Chapman model (Müller and Hildebrand, 1996).

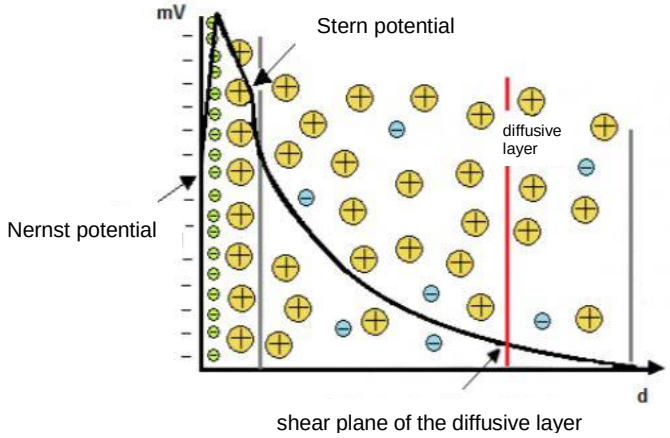

Figure 3.6: Schematic illustration of the attachment of ionic layers to a negatively charged particle surface in electrolyte containing water according to the Stern's model (Schirmer, 2018)

The first layer consisting of the negatively charged ions (Inner Helmholtz layer) attached to the negatively charged particle surface (Nernst potential). The second layer, consisting of positive ions (Outer Helmholtz layer), forms in association with the Inner Helmholtz layer the stern layer, to which the stern potential attaches. This is followed by the diffuse layer in which the concentration of counterions continuously drops to a potential of zero - the particle appears neutral to the outside. The zeta potential is located within the diffuse layer and is measured at the shear plane created by applying an electric field (Müller and Hildebrand, 1996).

Measurement of the zeta potential

The zeta potential is determined by an electrophoretic measurement by applying an electric field to a dispersion. The electric field energy accelerates the moving particles to the oppositely charged electrode, thereby stripping off a part of the diffused layer, creating a shear plane. The stripped portion of the diffuse layer increases with increasing field strength. The stern layer remains intact in this process because it is firmly fixed to the particle surface. The potential arising at the shear plane is slightly smaller than the stern potential and is indicated as zeta potential. The zeta potential can be calculated by the particle velocity within the electric field. Zeta potential measurements can be used to determine differences in the surface charge density of particles. For this, the concentration and type of the electrolytes in the dispersion medium must be kept constant and extremely low, as it can be obtained via distilled water with an electrical conductivity of about 50 µS cm^{-1}. Due to the extremely low electrolyte concentration in the dispersion medium, a high measuring sensitivity can be achieved since this avoids a compression of the diffusive layer. This reduces the differences between the measured zeta potentials. In general, for a low Nernst potential, a correspondingly lower zeta potential is measured and vice versa. (Müller and Hildebrand, 1996).

3.3.2 Laser diffraction particle size analysis

There are many techniques for the determination of the particle size. A particle is a coherent body bounded by a clearly recognizable surface. Few particles are spheres, whereby the smaller they are, often the greater is the deviance from sphericity. In particle analysis, the volume diameter of particles is generally equated with Stokes's diameter. Irregular particles are often characterized in terms of sphericity, by for instance an index to indicate the departure from sphericity and thereby, they may be related to a sphere by their volume, because only the dimension of a sphere can be specified by one number. The purpose of a particle size analysis is, for example to find the particle proportions in weight percent within a size class with a lower and upper limit. From this data the distribution of particles in different size classes may be calculated to construct particle size distribution curves. Particles may interact with incident electromagnetic wavelength by adsorption, scattering, refraction or reradiation. These interactions are useful to estimate the mass or the volume the analysed particles. The particle size measurement by scattering is a widely used technique today. In this method, the size information for smaller particles is mostly measured at a 90 ° angle to the plane of the incident light via a large angle scattering, according to the Mie theory. For larger particles the size information may be obtained by forward scattering, described by the Fraunhofer diffraction theory. With this process technology, modern instruments can determine particle sizes in the range between 0.04 µm to 2000 µm. When measuring by the scattering method, however, it is always assumed that all particles are spherical. (Loveland and Whalley, 2000).

3.3.3 Potentiometric Titration

Potentiometric titration is used to characterize carbon surfaces and provides suitable information on the composition and concentration of functional surface groups in aqueous media. Generally numerous techniques are combined for a qualitative and quantitative determination of surface characterization of carbons. Therefore, for example, the potentiometric titration in conjunction with the alternative surface characterizing method of Boehm titration delivers meaningful results on the acidic and basic species on the carbon surface (Bandosz and Ania, 2006). Boehm titration is the best-known method to determine chemical functionalities on carbon surfaces, especially for activated carbon. For estimating the amount of surface groups having pK values within certain ranges assigned to distinct categories different kinds of acid groups (carboxylic acids, lactones, or phenols) are classified by appropriate inorganic bases, whereas basic groups are titrated by hydrochloric acid (Bandosz *et al.*, 1993). However, potentiometric titration can be used to determine the acidic properties of the carbon surfaces in terms of their proton affinity distribution, which provides information on the number and strength of acid sites (Bandosz and Ania, 2006). With this method, acidic groups on carbon blacks may be classified as strong acids (pK < 7) and weak acids (7 < pK < 11) (Bandosz *et al.*, 1993). In the potentiometric titration, a very slow production of ion exchange equilibrium takes place. In addition, it is assumed that the

proton binding curve is influenced by the particle size and the titration curve of the sample material (Bandosz and Ania, 2006).

3.3.4 X-ray Photoelectron Spectroscopy (XPS)

XPS analysis is a non-destructive and highly surface-specific technique for the quantitative determination of the chemical composition of different material surfaces (Bandosz and Ania, 2006). With this measurement method it is possible to identify chemical elements (molecular weight ≥ lithium) from different sample materials (Haasch, 2014). Using XPS measurement, X-ray photons are directed onto the surface of a sample material using monochromatic X-radiation at ultrahigh vacuum conditions with energy from 1 up to 2 keV (Verma, 2007) (Bandosz and Ania, 2006). The X-rays emitted by the corresponding XPS instruments in the form of photons for sample analysis have a penetration depth of up to 1 nm (Bandosz and Ania, 2006), modern instruments even up to 10 nm (Haasch, 2014). The X-rays are absorbed by the atoms of the sample surface, releasing an electron from the atomic shell via energetic excitation. All the energy emitted by the X-ray photons is absorbed by the electrons and converted into kinetic energy. The kinetic energy of the ejected photoelectron depends on the binding energy characteristic to the elemental atom or atomic orbital and on the X-ray photon energy, whereby various chemical species can be identified. The XPS measurement results in characteristic peaks in a photoelectron spectrum for all elements detected on the sample surface. These peaks are proportional in their intensity to the concentration of the element within the scanned sample region. From this data, a semi-quantitative analysis of the surface composition of a sample material can be determined. However, the investigation of porous materials should be avoided, since the composition of the substance in the inner core often does not match to the surface composition due to a possible higher degree of oxidation. XPS is a useful tool for the characterization of oxygen and functional groups on carbon surfaces, since it provides meaningful information on the binding energy of photoelectrons from the 1s orbitals of carbon, nitrogen and oxygen in surface groups (Bandosz and Ania, 2006).

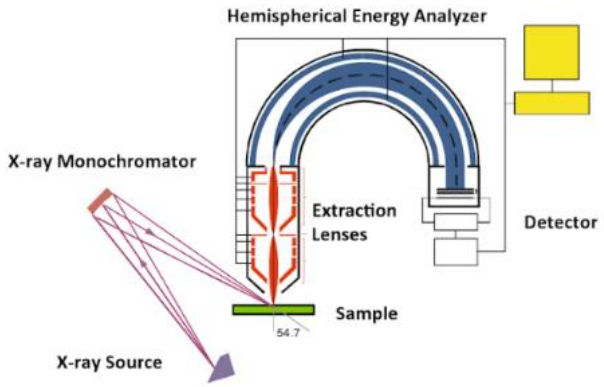

Figure 3.7: Schematic illustration of a typical high-resolution X-ray photoelectron spectrometer.

The instrument consists of a monochromatic X-ray source, extraction lenses with hemispherical energy filter for electron collection, an electron energy analyser, and a detector (Haasch, 2014).

Moreover, the X-ray excited Auger electron spectra (XAES), that is also provided by XPS analysis besides photoelectron spectra, gives information about the different hybridization states of carbon samples by the sp^2/sp^3 ratio from the first derivative of C KLL spectrum (Mizokawa *et al.*, 1987), (Mezzi and Kaciulis, 2010).

3.3.5 Energy Dispersive X-ray Spectroscopy (EDX)

Unlike XPS, a monoenergetic electron beam instead of X-rays is used for the EDX analysis as a radiation source for the characterization of the elemental material composition of a sample surface (Eggert, 2005). In general, an EDX spectrometer is used for the EDX analysis in conjunction with an electron microscope, such as a transmission electron microscope (TEM), a scanning electron microscope (SEM), or an electron probe microanalyzer (EPMA) (Kanda, 1991). By the emission of electron radiation, energy is transferred to the sample surface by the incident electrons via a photoelectric absorption and electrons in the inner atomic shell are energetically excited. When the excited electrons return to their ground state by relaxation, the excess energy is emitted in the form of characteristic X-radiation (Figure 3.8), that can be assigned to the source element by an EDX detector. Instead of the characteristic X-ray emission an Auger electron (Auger electron: ejected electron with atom specific kinetic energy corresponding to the chemical element species (Pratt, Muir and Nesbitt, 1993)) may be emitted when an excited electron from a higher energy level returns to its original state. In this case, the higher the atomic number of the atoms, the more likely the probability of X-ray emission, while the probability of the generation of Auger electrons decreases (Shindo and Oikawa, 2002b).

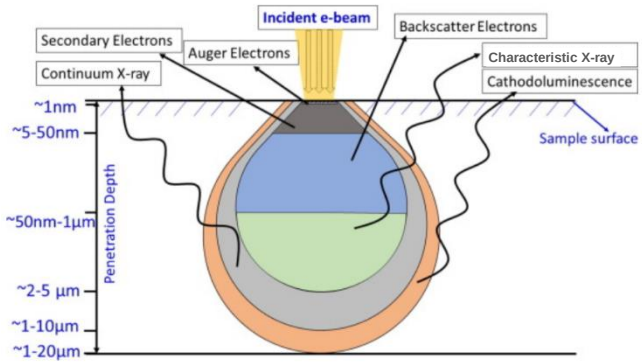

Figure 3.8: Schematic illustration about the principle of SEM technique

The figure shows the focusing of an electron beam source which is directed onto the surface of a sample material. As observed in the EDX analysis method, the energy transferred from the collimated electron beam to the sample surface leads to the emission of different types of radiation (secondary electrons, back-scattered electrons, characteristic X-rays, continuum X-rays (Bremsstrahlung), Auger electron, etc.). The imaging signals in SEM mainly come from low energy secondary electrons and backscattered electrons. The penetration depth of the electron beam is between 1 to 20 µm (Mazumder et al., 2018).

The property that the elements in the sample material produce characteristic X-rays of specific energy by treatment with the EDX method enables a qualitative and semi-

quantitative analysis of the elemental composition via the corresponding EDX spectrum (Eggert, 2005). Information about the binding partners of the detected elements can also be determined from the XPS spectra (Szabó *et al.*, 2006). Using modern methods of EDX analysis for samples with irregular surfaces or those consisting of particles even a standard absolute determination of the element concentration by the characteristic X-ray radiation including the Bremsstrahlung (Figure 3.8) can be performed (Eggert 2005). Each chemical element detected from the investigated surface area of the sample can be identified by the corresponding peak energy and the content of the respective element can be determined by integration of the appendant peak intensity by the peak area (Shindo and Oikawa, 2002a).

3.3.6 BET Surface area analysis

The BET surface area determination is an analytical method for characterizing the specific surface area of solids by gas adsorption according to the BET model named after the developers Stephen Brunauer, Paul Hugh Emmett and Edward Teller (Brunauer, Emmett and Teller, 1938). The determination of the specific surface area of disperse or porous solids by measuring the physisorbed amount of gas according to DIN ISO 9277 is based on the BET method. Reliable applicability to this process applies only to Type II adsorption isotherms for disperse, nonporous or macroporous solids, and to Type IV adsorption isotherms for mesoporous solids having a pore size between 2 nm and 50 nm. Applying the BET method to Type I isotherms or to solids that adsorb the measurement gas is not reliable. The BET method is used to determine the amount of gaseous adsorptive needed to fully cover the outer surface with a monolayer, along with an accessible inner pore surface, of the adsorbent. The capacity of the adsorbed monolayer can be calculated from the adsorption isotherm via the BET equation (3) taken from DIN ISO 9277.

.

$$\frac{\frac{p}{p_0}}{n_a[1-\left(\frac{p}{p_0}\right)]} = \frac{1}{n_m\,C} + \frac{C-1}{n_m\,C}\cdot\frac{p}{p_0} \qquad (3)$$

As the adsorbent gas, nitrogen is usually used because it is physically adsorbed onto the solid surface with weak bonds due to van der Waals forces. Nitrogen can also be easily desorbed by lowering the pressure at the same temperature. Depending on the sensitivity of the measuring device other adsorptive gases with heavier molecules and a lower saturation vapor pressure, such as krypton can be used. During the measurement, the temperature of the adsorptive gas is kept constant and fed to the sample container. The measured amounts of adsorbate are applied in equilibrium with the gas pressure *p* of the adsorptive against the relative pressure p/p_0 in an adsorption isotherm. The measurement for the preparation of the adsorption isotherms can be

carried out volumetrically, gravimetrically, calorimetrically, spectroscopically or with the carrier gas process in a continuous or discontinuous mode of operation.

3.3.7 Point of zero charge

The point of zero charge (PZC) of oxide surfaces immersed in an aqueous phase can be estimated by a method described by the surface ionization model of amphoteric oxides. The hydrated surface of oxides has ion exchange properties related to the pH-dependent net surface charge of a dispersed particle, as the functional surface groups can react as both Bronsted acid or base. The zero net surface charge at which a surface become neither positively nor negatively charged as a function of the pH, is indicated as the point of zero charge: One method for determining the zero point of the charge is the procedure of mass titration from the scientific publication "Estimation of the Point of Zero Charge of Simple Oxides by Mass Titration" by Noh & Schwarz, 1988 (Noh and Schwarz, 1989). Another parameter that can describe the electrical state of a carbon surface is the isoelectric point (IEP) (Bandosz and Ania, 2006). Electrophoretic measurements can be used to determine the isoelectric point, which is located at the zero point of the zeta potential (Noh and Schwarz, 1989). Temperature, concentration and contact time of an oxidizing agent to modify, for example, carbon surfaces affect the point of zero charge and the isoelectric point. Therefore, the PZC may also be an indicator of the oxidation of carbon surfaces, since the surface acidity or basicity changes after the modification treatment (Bandosz and Ania, 2006).

3.4 Analytical method for analysis of aromatic compounds

3.4.1 Fluorescence Spectrometry

Fluorescence spectroscopy is a highly sensitive analysis methodology for a wide range of molecular processes in which for instance the intensity of fluorescence of a sample substance is recorded for concentration measurement by the fluorescence technique (Lakowicz, 2006). Fluorescence describes the process in which electrons are excited to a higher energy state by the irradiation of a fluorescent analyte (fluorophore) with light photons. In this case, the light energy absorbed by the electrons is released time-displaced (fluorescence life time of about 10 ns) by a fluorescence emission via photons, while the energetic electron ground state is reached again. (Lakowicz, 2006) (Borlinghaus, 2016). Typically, fluorescence occurs from, e.g. aromatic molecules, and they all have π-bonds, whereby, also heteroatoms may participate in the π-conjugation (Orrit, 2016). Each fluorophore has a special absorbance maximum. Fluorescence spectrometers usually perform the possibility to produce excitation and emission spectra (Fig. 4). Such an emission spectrum constitutes the wavelength distribution of a fluorescence emission which is performed by a single constant excitation wavelength accordingly to the adsorption wavelength of the analyte. Conversely, an excitation

spectrum depicts the dependence of emission intensity measured at a single emission wavelength upon scanning the excitation wavelength (Lakowicz, 2006). The difference between the peak position of an emission spectrum and the absorption maxima of an excitation spectrum (Figure 3.9) is indicated as the Stokes Shift (McCelland and Mankin, 2018). Such an excitation spectrum enables to identify the wavelength of light which can be absorbed by the analyte (Sablinskas, 2003).

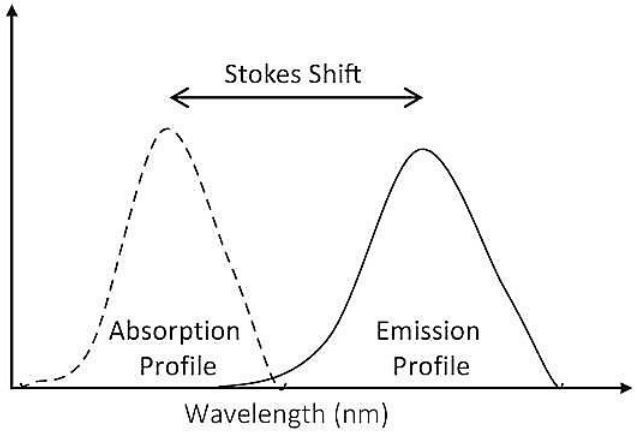

Figure 3.9: Schematic illustration of an emission and excitation spectrum of a fluorophore

The difference between the excitation and the emission maxima is referred as the Stokes Shift (McCelland and Mankin, 2018).

As a light source for spectral scanning usually high-pressure Xenon arc lamps are used because they provide a relatively continuous light output over a broad wavelength range from 250 – 700 nm in the UV/VIS range (Lakowicz, 2006). Thereby, the fluorescence intensity is proportional to the intensity of the light source. Generally, the fluorescence emission of an analyte by a fluorescence spectrometer is measured in a 90° angle (Figure 3.10) in order to avoid disturbances by non-absorbed excitation radiation. (Sablinskas, 2003).

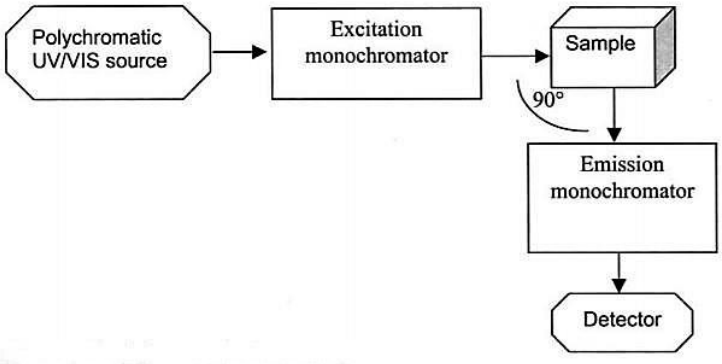

Figure 3.10: Schematic construction of a fluorescence spectrometer

Basically, the instrument consists of a single beam polychromatic UV/VIS light source, an excitation monochromator, a sample chamber an e.g. emission monochromator and a detector.

4. Material and Methods

4.1 Adsorbents and adsorptives

4.1.1 Adsorbents

Two adsorbents were used for the adsorption experiments with aromatic compounds, graphite UF1 99.5 (Graphit Kropfmühl GmbH, Germany) and chemically oxidized graphite UF1 99.5. For the experimental procedure, the graphite was washed with reverse osmosis (RO) water. The carbon content of the powdered virgin graphite UF1 99.5 was about 99.5 % and the particle size was given as an average of 2 to 4 µm according to the manufacturer's data sheet (see Appendix). According to the manufacturer, graphite UF 1 99.5 is a natural graphite that has been chemically pre-treated to increase its purity.

4.1.2 Adsorptives

To investigate the adsorption properties of graphite UF1 99.5 and chemically modified graphite UF1 99.5, seven different aromatic compounds (Phenol, Anisole, 1-Naphtol, Naphthalene, 2-Methoxynaphthalene, L-Tyrosine and L-Tryptophan) were used as adsorptives. The adsorptives or test substances used had analytical standard grade (purity ≥ 99 %) and were purchased from the following manufacturers: Carl Roth GmbH (Germany), Sigma-Aldrich CHEMIE GmbH (Germany), Merck KGaA (Germany) and ThermoFisher (Kandel) GmbH (Germany).

4.2 Matrix for modelling approaches of adsorption systems

4.2.1 Preparation of water matrix (Synthetic Model Water)

Synthetic Model Water (SMW) in which the test substances were dissolved was used to avoid competitive adsorption between these adsorptives and NOM and to reduce the risk of possible reduction of adsorption capacity. The SMW was prepared using reverse osmosis water (RO Water), which had a conductivity of about 20 µS/cm. For the preparation of the water matrix from inorganic salts, a $NaHCO_3$ stock solution (0.05 M) and a $MgSO_4$ stock solution (0.25 M) in reverse osmosis water were used. The final concentration of both salts in the SMW was 1.5 M.

4.2.2 Determination of buffer capacity

To ensure that the solvent pH of the water matrix maintains a stable pH, the buffer capacity was checked. The buffer capacity of SMW was determined by means of a titration curve using a titrator, TitroLine *easy*, SCHOTT Instruments GmbH (Germany). For the pH measurement, a Mettler TOLEDO InLab® routine pH electrode, Mettler-

Toledo GmbH (Germany), was used. For this purpose, 100 mL of SMW were titrated in 0.1 mL increments with NaOH (0.05 M) to pH 10 or with HCl (0.05 M) to pH 6. For the reference comparison, the buffer capacity of service water (treated process water from the University of Duisburg-Essen, Campus Duisburg) was also determined using the same method.

4.2.3 Titre determination of sodium hydroxide solution

The sodium hydroxide solution (0.05 M) used to determine the buffer capacity of SMW was prepared from sodium hydroxide (≥ 98.5 %), VWR International GmbH (Germany) and RO Water. For titre determination, 20 mL of the sodium hydroxide solution were titrated with a standard HCl solution (0.05 M), Berndt Kraft GmbH (Germany) until the equivalence point was reached. The exact concentration of the sodium hydroxide solution was calculated from the used volume of the standard solution, which was needed until reaching the equivalence point. In equation (4), the titre (t) of the NaOH solution is obtained from the quotient, which contains the actual concentration $c(X)_{actual\ value}$ in the numerator and the theoretical concentration $c(X)_{target\ value}$ in the denominator (Jander and Jahr, 1989):

$$t = \frac{c(X)_{actual\ value}}{c(X)_{target\ value}} \quad (4)$$

4.2.4 Measurement of the ionic strength

First the conductivity was measured using both, reverse osmosis water and service water (treated process water from the University of Duisburg-Essen, Campus Duisburg) by using the conductivity meter, WTW LF 197-S, Xylem Analytics Germany Sales GmbH & Co. KG. Subsequently, a model water was prepared in various concentrations (0.5 mM, 1 mM and 1.5 mM) served as water matrix and then the electrical conductivity was determined. The solution was shaken over night at 150 rpm. Furthermore, the pH was measured at the beginning and at the end of the experiment. From electrical conductivity measurement, the ionic strength could be calculated by the following equation (5):

$$I = \frac{1}{2} \sum_i \frac{c_i}{c_0} \cdot z_i^2 \quad (5)$$

I = ionic strength

i = ion species in solution

c_i = molar concentration of the ion species i

c_0 = 1 mol/L (since the ionic strength should be dimensionless)

z_i = charge number of the ion species i

Using a formula (6) based on the linear relationship between electrical conductivity (*EC*) and ionic strength (*I*), the ionic strength can be roughly estimated (*Electrical Conductivity (EC)*, 2015).

$$EC\left(\frac{\mu S}{cm}\right) = 6.2 \cdot 10^4 \cdot I\left(\frac{mol}{L}\right) \quad (6)$$

Inversion of the formula according to the ionic strength (7):

$$I\left(\frac{mol}{L}\right) = 1.6 \cdot 10^{-5} \cdot EC\left(\frac{\mu S}{cm}\right) \quad (7)$$

4.3 Characterization of graphite species

4.3.1 Potentiometric titration of graphite species

Potentiometric titration measurements were performed by using the titrator TitroLine *easy*, SCHOTT Instruments GmbH (Germany). The instrument was set to the modus that the titrant could be added to the sample in 0.01 mL increments at the touch of a button. For the pH measurement, a Mettler TOLEDO InLab® routine pH electrode, Mettler-Toledo GmbH (Germany), was used. The different graphite samples (2.5 g) were suspended in 50 mL $NaNO_3$ (0.01 M) at room temperature and allowed to equilibrate for 45 min. The suspension was continuously saturated with N_2 during the measurements, to eliminate the influence of atmospheric CO_2. As titrants volumetric standards of 0.1 M NaOH (VWR International GmbH, Germany) or HCl (Berndt Kraft GmbH, Germany) were used. The graphite suspension was stirred throughout the measurement. The experiments were carried out in a pH range of 3 – 10. Each sample was titrated with acid and base starting from the initial pH of the sample suspension. The titration solution was added in 0.01 mL increments approximately every two minutes to give time for adjustment of concentration equilibrium. As a reference value, $NaNO_3$ (0.01 M) was titrated without addition of graphite with the specified titration agents. The scientific paper “Surface Chemistry of Activated Carbons: Combining the Results of Temperature-Programmed Desorption, Boehm, and Potentiometric Titrations”, (Salame and Bandosz, 2001) was used as the source of literature for this method. For the electronic data acquisition and the operation of the titrator the software TitroLine-Chart, SCHOTT Instruments GmbH (Germany) was applied. The evaluation of the data was executed by the usage of Microsoft Excel (Microsoft Office 365 ProPlus).

4.3.2 Laser Diffraction Particle Size Analysis

In order to determine the particle size of the respective graphite species, a laser diffraction particle size analysis was performed. For this purpose, a small amount of the graphite sample was suspended in 30 ml of isopropanol. Alternatively, the graphite sample could be wetted with one drop of dispersant, SCHWEGO wett 6267, Berndt Schwegmann GmbH & Co. KG (Germany) prior to suspension. The measurement was carried out with a laser diffraction particle size analyser, LS 13 320, Beckman Coulter GmbH (Germany). For an optimum measurement, the sample suspension in the measuring cell should have an obscuration not higher than of 3 – 5 %.

4.3.3 Zeta potential Measurement

For the determination of the zeta potential of graphite UF1 99.5 and oxidized graphite UF1 99.5, a graphite suspension (20 mg/L) was prepared from the individual samples in RO-Water. The suspensions were treated for homogenization for 10 minutes in an ultrasonic bath, BRANSON 5200 Ultrasonic Cleaner, Branson Europa B.V (Germany), to dissolve particle agglomerations. The initial pH of the prepared suspensions was about 6.6 to 6.8. For the zeta potential analysis, the measuring system Zetasizer Nano ZS, Malvern Panalytical GmbH (Germany) with the corresponding software was used. For the individual measurements, aliquots of the respective graphite suspension were adjusted to various pH values in the range between 1 and 10 with diluted sodium hydroxide solution or hydrochloric acid. A clean measuring cell (DTS1071) was used for the measurement procedure, which was carefully filled bubble-free using a laboratory syringe. For the sample analysis, each measurement was repeated several times ($n \geq 9$), from which the statistical mean value was determined.

4.3.4 Energy Dispersive X-ray Spectroscopy (EDX)

The characterization of the elemental composition on the surface of the various graphite species was carried out by an EDX analysis in the central laboratory for scanning electron microscopy (SEM) of the University of Duisburg-Essen, Campus Essen (Germany). For the surface analysis of the graphite samples the Environmental scanning electron microscope (ESEM) Quanta 400 FEG (FEI Company) combined with an EDX analysis system was used. The operation of the analyzer was carried out by Dipl.-Ing. Smail Boukercha, research associate at the University of Duisburg-Essen.

4.3.5 X-ray photoelectron spectroscopy (XPS)

The surface analysis of the individual graphite species for determining the elemental composition and functional groups was carried out by XPS using the microfocus X-ray photoelectron spectrometer, PHI 5000 VersaProbe II (ULVAC-PHI, Inc.). The applied radiation source Al Kα (1486.5 eV) with a beam diameter of 100 µm and an X-ray

power of 25 W was used. The samples were outgassed for 90 min before analyses. The operation of the surface analysis instrument was carried out by Dr. Ulrich Hagemann, NanoEnergieTechnikZentrum (NETZ) at the University of Duisburg-Essen, Campus Duisburg.

4.3.6 BET-surface area analysis of graphite species

The BET surface and pore analysis of washed graphite UF1 99.5 and graphite UF1 99.5 (modified by ozone treatment) was carried out volumetrically with the use of the gas adsorption method by nitrogen adsorption. For this procedure, the benchtop BET surface and pore size analyser, SA^{TM} Coulter 3100 (Beckmann Coulter GmbH, Germany) was used according to the manufacturer's instructions (Beckman Coulter Inc., 2001). To carry out the test, the sample to be analysed was divided equally into three sample vessels and heated at 120 ° C for 60 min at vacuum conditions to desorb physisorbed material by outgassing, and then the dry matter was determined. The sample vessel with the sample was then filled with nitrogen gas at cryogenic temperatures in a series of controlled doses and then the pressure in the sample was measured after each dosing. Subsequently, the sample vessel was degassed for 600 min at 50 ° C. This was followed by the determination of the sample weight. The reduces pressure due to adsorption was able to be used to determine the volume of gas adsorbed by the sample, using the ideal gas law. The adsorption isotherm was obtained by the resulting relationship of the volume of the adsorbed gas and the relative pressure at a constant temperature. This data could be used to calculate the BET surface area. The measurement analysis was executed by Claudia Schenk, technical assistant at the University of Duisburg-Essen.

4.3.7 Point of zero Charge

The determination of the point of zero charge was carried out by the mass titration method, according to the scientific paper “Estimation of the Point of Zero Charge of simple oxides by Mass Titration” (Noh and Schwarz, 1989). For the implementation, six different amounts of graphite (0.0004 g, 0,004 g, 0.04 g, 0.4 g, 2 g and 4 g) were weighed into snap-top vials with a micro balance. Subsequently, in each case 10 mL NaCl solution with a concentration of 0.1 M was added to the graphite samples. As a reference, two samples without graphite were prepared. Subsequently, the snap top vials with the samples were sealed with the appropriate lids and shaken overnight at 150 rpm for 24 hours. After shaking, the pH of the supernatant of the samples and both reference samples has been measured. For the evaluation of the results, the measured pH values of the samples were plotted against the corresponding graphite masses per volume (m/V %) in a diagram. Finally, by approximating of the graphic curve to a certain pH, the point of zero charge may be determined.

4.4 Oxidation treatments of graphite UF1 99.5

For incorporation of functional surface groups on the carbon surface, the graphite UF1 99.5 was modified by various mild oxidation methods.

1st Method: Oxidation treatment with nitric acid

Graphite UF1 99.5 was treated with nitric acid (65 %) at 60 °C for 2 h.

2nd Method: Oxidation treatment with hydrogen peroxide

A weighted mass of 40 g of graphite UF1 99.5 was treated with 300 mL of hydrogen peroxide (30 %) at room temperature for 6 h with constant stirring. Alternatively, the same method was applied but for a longer reaction time of 48 h.

3rd Method: Thermal oxidation treatment in an oxygen-nitrogen atmosphere

In this procedure a weighted mass of 30 g of graphite UF1 99.5 was heated in a rotary furnace at 500 °C for 2 h while the graphite sample was constantly rotating. For the oxidation process, a reaction gas mixture (oxygen 100 L/h, nitrogen 200 L/h) was used. In a second experiment, the same method was carried out at a temperature of 350 °C.

4th Method: Thermal oxidation treatment in air atmosphere

A weighted mass of 5 g of graphite UF1 99.5 was heated in a muffle furnace at 500 °C (air atmosphere) for 3 h. The oxidation treatment was performed by Renate Schulz (chemical laboratory assistant) at IWW Zentrum Wasser (Water Research Institute), Mülheim, Ruhr (Germany).

5th Method: Oxidation treatment with sulfuric acid and ammonium peroxydisulphate

A weighted mass of 141.1 g $(NH_4)_2S_2O_8$ (≥ 98 %) was added to a volume of 200 mL sulfuric acid (1M) and stirred well with a stir bar such that the final concentration of the oxidizing salt in the reaction solution was 2.5 M. Thereafter, 20 g of graphite UF1 99.5 were mixed into the reaction solution at room temperature for oxidation and stirred well for 48 h. The method is described in the scientific paper “Activated Carbon Surface Modifications by Nitric Acid, Hydrogen Peroxide, and Ammonium Peroxydisulfate Treatments” (Moreno-Castilla *et al.*, 1995).

6th Method: Oxidation treatment by ozonation

The method for the oxidation of graphite with ozone was executed according to DIN EN ISO 10 121-1 (2014). A weighted mass of approximately 1.4 g graphite UF1 99.5 was through-flown with a mixture of O_3 (7 – 7.5 ppm) and air in a fixed bed flow reactor for 90 min at room temperature. The atmospheric humidity during the reaction was about 50 %. The oxidation treatment was performed by the PhD student, Roman Ligotski (M. Sc.), Faculty of Engineering (Nanoparticle Process Technology), University of Duisburg-Essen (Germany).

After the operation (Method 1,2 and 5), the treated graphite was washed with RO-water. For this purpose, the graphite was placed in a pleated filter (Rotilab® pleated filter, Type 113P, membrane diameter 320 mm, thickness 0.16 mm) and washed with

RO-water until the conductivity of the filtrate matched that of RO-Water. Thereafter, the graphite was dried in a drying oven overnight at 110 ° C. The treated graphite of all methods was stored in a desiccator for protection against moisture.

4.5 Analytical quantification of aromatic test substances

4.5.1 Fluorescence measurement

UV/VIS Spectroscopy was not applied, because no absorbance could be established. For the fluorescence measurement of the analytes, the SpectroFluorophotometer, SHIMADZU RF-6000 (Shimadzu Germany GmbH) was used. The software "LabSolutions" (Shimadzu Germany GmbH) was applied for the evaluation and operation of the fluorescence spectrometer. For determining the substance specific maximum excitation and emission wavelength pairs (Table 4.1), a 3-D fluorescence-excitation-emission scan (FEEM) was generated from each substance at a concentration of 0.1 mM using the fluorescence spectrometer. For calibration with external standard solutions to quantitate the analyte concentrations to be analysed in the samples of the adsorption batch tests a concentration range between 50 nM and 950 nM, with seven standard concentrations (50 nM, 200 nM, 350 nM, 500 nM, 650 nM, 800 nM and 950 nM) was selected. The practical quantification limits could be determined from the corresponding calibration curves. All prepared external standard solutions were prepared in 1.5 mM water matrix. The measurements were carried out without IHU 310 UV-transmitting filter. A 10 x 10 mm Hellma® fluorescence Suprasil® quarz cuvette, Hellma GmbH & Co. KG Germany was used to measure the samples. Further instrument settings for the fluorescence measurements were made. The spectral bandwidth for the measurement of the excitation and emission was set to 5 nm and the accumulation time was 10 ms. The required data for the excitation and emission wavelengths and for the adjustment of the sensitivity for all investigated substances can be found in the following table:

Table 4.1: Settings of aromatic analytes Fluorescence spectrometry.

Excitation and emission wavelengths and the adjustment of the sensitivity for all investigated substances.

Substance	Fluorescence wavelength [nm]		Sensitivity
	Excitation	Emission	
Naphthalene	265	330	low
Phenol	267 (270)	311 (330)	high
1-Napthol	233	500	high
Anisole	270	303	low
2-Methoxynaphthalene	270	350	low
4-Chlorophenol	265	310	high
L-Phenylalanine	No value	No value	-
L-Tyrosine	274	325	high
L-Tryptophan	278	356	low

For data analysis FEEM correction procedures were performed according to the scientific work “Measurement of Dissolved Organic Matter Fluorescence in Aquatic Environments: An Interlaboratory Comparison” (Murphy *et al.*, 2010), using a programmed Microsoft Excel file. The visualization of the corrected data set took place via a 3D fluorescence-excitation scans (FEEM) by the software OriginPro 2018G, OriginLab Corporation (USA).

4.6 Graphite adsorption batch tests

4.6.1 Degradation tests of pollutant solutions

For degradation tests a test solution of each substance (Naphthalene, Phenol, 1-Naphtol, Anisole, 2-Methoxynaphthalene, 4-Chlorophenol, L-Tyrosine and L-Tryptophan) with a concentration of 800 nM in water matrix was prepared. The samples were shaken for a certain time by the laboratory shaker, Laboshake, LS500 (C. Gerhardt GmbH & Co. KG, Germany) at room temperature. After the shaking procedure, the fluorescent intensity signal of the samples was measured at different time points (e.g. 0 h, 3 h, 6 h, 24 h and 48 h) using the SpectroFluorophotmeter, SHIMADZU RF-6000 (Shimadzu Germany GmbH). The data obtained were presented in a Microsoft Excel column diagram (Microsoft Office 365 ProPlus) to give an overview of the decay process as a function of time.

4.6.2 Adsorption experiments

First, test solutions of each substance (Naphthalene, Phenol, 1-Naphthol, Anisole, 2-Methoxynaphthalene, 4-Chlorophenol, L-Tyrosine and L-Tryptophan) with a concentration of 800 nM in water matrix were prepared from the respective 0.1 mM working solutions. The working solutions were prepared from a 1 mM stock solution of the respective substance. From the prepared single substance solutions, 100 mL was filled into 250 mL big-mouth bottles and then 20 mg of graphite UF 1 (washed) or modified Graphite (ozone-treated) were added for the adsorption kinetics tests. For 1-naphthol only 1.5 mg/L of the respective graphite powder was used for 700 mL of 1-naphthol solution, prepared in a 1 L laboratory bottle. In contrast, for the adsorption equilibrium tests several different amounts of graphite were used (see Table 4.2):

Table 4.2: Defined quantities [mg/L] of graphite UF1 (washed)/ozonised graphite) in the sample dispersions for the adsorption equilibrium tests.

Substance [800 nM]	Concentration [mg/L] of Graphite UF1 (washed)/modified, ozonised graphite
Naphthalene	50, 80, 110, 140
Phenol	50, 200, 350, 500, 800, 1000, 1200
1-Naphthol	5, 10, 15, 25
Anisole	50, 200, 350, 500, 650, 750
2-Methoxynaphthalene	50, 80, 110, 140, 165
4-Chlorophenol	50, 200, 350, 500
L-Tyrosine	50, 200, 350, 500, 800, 1000, 1200
L-Tryptophan	50, 200, 350, 500, 800, 1000, 1200

The graphite single substance solution dispersion was homogenized with a high-performance disperser, ULTRA-TURRAX® T25 (IKA-Werke GmbH & Co. KG, Germany) at a rotational frequency of 8000 min^{-1}. The samples were shaken intensively at 150 rpm until the measurement process with the laboratory shaker, Laboshake, LS500 (C. Gerhardt GmbH & Co. KG, Germany) at room temperature to bring the graphite species into contact with the solution. Before measuring the fluorescence signal of the samples every sample dispersion was filtered by ReliaDisc™ cellulose nitrate membrane filters (diameter 0,25 mm, pore size 0,45 µm, thickness 130 µm), Ahlstrom-Munksjö GmbH (Germany), to remove all graphite particles. The remaining contaminant concentration of the substances from the test solution after the adsorption process was determined at certain time points (e.g. 0 h, 3 h, 24 h and 48 h) via the fluorescence spectrometer SpectroFluorophotmeter, SHIMADZU RF-6000 (Shimadzu Germany GmbH). As a reference, the graphite-dispensed samples were prepared without addition of the substances in water matrix and then measured. The remaining equilibrium concentration c of the single substance and the solid phase concentration q describes the quantity of the absorbed substance. For the preparation of the adsorption isotherms the following equation of mass balance was used (8):

$$V \cdot c_0 + m \cdot q_0 = V \cdot c + m \cdot q \qquad (8)$$

V = Volume of solution with a single substance

c_0 = initial concentration of the single substance

m = quantity of graphite species

q_0 = initial solid phase concentration

c = equilibrium concentration

q = equilibrium solid phase concentration

The initial solid phase concentration of the unused graphite species is assumed to be q = 0. This results in the simplified equation (9) for calculating the equilibrium solid phase concentration q.

$$q = \frac{V}{m} \cdot (c_0 - c) \quad (9)$$

4.6.3 Background noise measurement of graphite suspension

For measuring the background noise of the adsorption batch tests, a graphite suspension was prepared with different graphite species mass concentrations (0 mg/L, 50 mg/L, 200 mg/L and 500 mg/L). The implementation of these tests was carried out according to the instructions of the adsorption experiments but without adding of any test substances to the graphite suspension. The fluorescence spectrometric measuring procedure was executed by measuring the membrane-filtered graphite suspension with all maximum excitation and emission wavelength of the corresponding substances (Phenol, Anisole, 1-Naphthol, Naphthalene, 2-Methoxynaphthalene, Tryptophan and Tyrosine).

4.6.4 Filter uptake test

The filter uptake test was performed for checking the loss of each dissolved substances (Naphthalene, Phenol, 1-Naphthol, Anisole, 2-Methoxynaphthalene, 4-Chlorophenol, L-Tyrosine and L-Tryptophan) from the sample dispersions, in the adsorption batch tests, by the ReliaDisc™ cellulose nitrate membrane filters (diameter 0,25 mm, pore size 0,45 µm, thickness 130 µm), Ahlstrom-Munksjö GmbH (Germany) during the filtration process. First, test solutions of each substance with a concentration of 800 nM in 1.5 mM water matrix were prepared from the respective 0.1 mM working solutions. The working solutions were prepared from a 1 mM stock solution of the respective substance. In the first series of tests, 50 mL of the substance solution with an initial concentration of 800 nM was filtered by the membrane filter. In the second series of tests, 25 mL of the substance solution with an initial concentration were filtered by the membrane filter. For each test series a total of seven repeated measurements were carried out. After the filtering process, the fluorescence signal of the filtrate was compared with the initial concentration of the substance solution by means of a spectrometric measurement.

4.7 Investigated substances for adsorption batch tests

4.7.1 Phenol

Phenol is a toxic, colourless, crystalline solid used as an antiseptic and disinfectant, in the preparation of cosmetics, for the productions of drugs, as weed killers and to

produce artificial resins, but it is also used as an agrochemical microbicide (Figure 4.1). In areas with a high level of motor traffic it can be found as traffic-derived phenol vapor in the ambient air. Phenol is a solid under standard conditions (Melting point of 40.9 °C), water-soluble (water solubility of about 82.8 g/L at 25 °C) and has a molecular mass of 94.11 g/mol (PubChem Substance and Compound databases, 2018). Under standard physical conditions at 25 ° C, the octanol-water partition coefficient is log *P* = 1.48 and the acid dissociation constant is pK_a = 9.99 (Lide *et al.*, 2005). Phenol possesses a negative inductive effect (-*I*), which withdraws the electron density from the aromatic system by the existing OH group at the aromatic ring system. However, the positive mesomeric effect (+*M*) predominates, pushing the negative charge density into the aromatic ring (Klein, 2015).

In general, inductive substituent effects (*I* effects) are electrostatic interactions between the polar substituent and the electron system of the substituted molecule. Polar substituents have an electron-withdrawing effect (-*I* effect). Substituents that exert a negative partial charge in their environment are electron repellent (+*I* effect). The mesomeric effect (*M* effect) alters the electron density in a molecular π-system. Substituents that have, for example, a free pair of electrons that interact with the π-system of the molecule can exert an increase in electron density (+*M* effect). Conversely, substituents with a polarized double bond, which are in mesomerism with the π-electron system of the molecule, are electron-withdrawing and reduce the electron density (-*M* effect) (Latscha, Kazmaier and Klein, 2016).

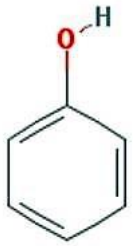

Figure 4.1: Structural formula of Phenol

(PubChem Substance and Compound databases, 2018)

4.7.2 Anisole

Anisole is a healthwise irritant aromatic compound used as flavouring agent, precursor to perfumes, insect pheromones and to produce pharmaceuticals (Figure 4.2). Anisole has a higher nucleophilicity than benzene due to the methoxy group attached as a substituent to the aromatic ring (PubChem Substance and Compound databases, 2018). The activating +*M* effect and -*I* effect of the methoxy group in anisole increases the electron density in the aromatic ring of the molecule (Smeljansky, 2006), (Polansky, 1963), (Wollrab, 2014). These effects influence the adsorption properties of anisole to

carbon materials. The molecular weight of Anisole is 108.14 g/mol. Anisole has a water solubility of 10.4 mg/L and its aggregate state under standard conditions is liquid (PubChem Substance and Compound databases, 2018). The octanol-water partition coefficient is log *P* = 2.11 (Lide *et al.*, 2005).

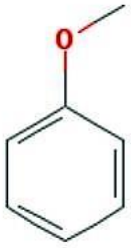

Figure 4.2: Structural formula of Anisole

(PubChem Substance and Compound databases, 2018)

4.7.3 1-Naphthol

1-Naphthol is a solid (Melting point = 96 °C) aromatic molecule with toxic properties and it is used as an agrochemical insecticide (Figure 4.3). 1-Naphthol is also used as a lubricant or lubricant additive in industry and for workshop needs. In water, 1-naphthol dissolves at 866 mg/L at 25 °C (PubChem Substance and Compound databases, 2018). The high octanol-water partition coefficient of log *P* = 2.85 indicates a lipophilic molecule. At standard conditions, the acid dissociation constant of the molecule has a value of pK_a = 9.39 (Lide *et al.*, 2005). As with phenol, 1-naphthol shifts the electron density from the OH group into the aromatic system.

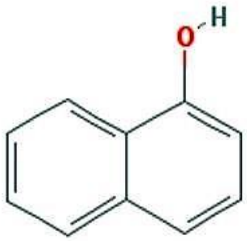

Figure 4.3: Structural formula of 1-Naphthol

(PubChem Substance and Compound databases, 2018)

4.7.4 Naphthalene

Naphthalene is a harmful non-heterocyclic aromatic compound, that is suspected for causing cancer (Figure 4.4). The substance is obtained by the distillation of petroleum or coal tar. The white crystalline volatile solid is used as agrochemical insecticide or moth repellent, also for domestic use. The molecular weight amounts to 128.17 g/mol (PubChem Substance and Compound databases, 2018). Due to the hydrophobic properties of this substance it is hardly soluble in water (31 mg/L) and therefore, it has

a relatively high octanol-water partition coefficient that amounts to log *P* = 3.34 (PubChem Substance and Compound databases, 2018), (Lide *et al.*, 2005).

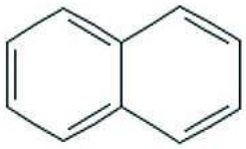

Figure 4.4: Structural formula of Naphthalene

(PubChem Substance and Compound databases, 2018)

4.7.5 2-Methoxynaphthalene

The aromatic compound, 2-Methoxynaphthalene is a powdery solid substance, and is considered to be harmful and dangerous to the environment (Figure 4.5). In everyday life, the substance finds its use in cleaning and care products, but also for the production of plastic and rubber products (PubChem Substance and Compound databases, 2018). 2-Methoxynaphthalene has a molecular mass of 158.2 g/mol and octanol-water partition coefficient at 25 ° C of log *P* = 4.0 (Lide *et al.*, 2005).

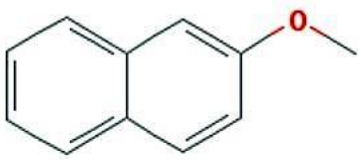

Figure 4.5: Structural formula of 2-Methoxynaphthalene

(PubChem Substance and Compound databases, 2018)

4.7.6 L-Tyrosine

L-Tyrosine is a non-essential laevorotatory aromatic amino acid compound and is synthesized in the biological organism from L-phenylalanine (Figure 4.6). In the body, the compound plays an important role in the production of proteins, enzymes and muscle tissue. The amino acid has a very high melting point of 343 °C and is readily soluble in water (479 mg/L) with an octanol-water partition coefficient of log *P* = -2.26 (PubChem Substance and Compound databases, 2018). The molecular weight of the molecule is 181.18 g/mol. The acid dissociation constants from the literature are log pK_{a1} = 2.24 (-COOH), pK_{a2} = 9.04 (-$NH3^+$) and pK_{a3} = 10.1 (phenyl group), the isoelectric point is at pH_{IEP} = 5.66 (Lide *et al.*, 2005).

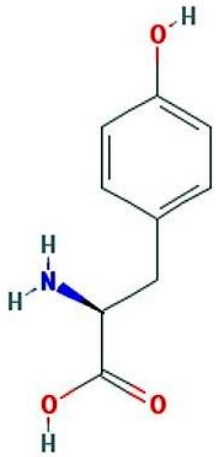

Figure 4.6: Structural formula of L-Tyrosine

(PubChem Substance and Compound databases, 2018)

4.7.7 L-Tryptophan

L-Tryptophan is an essential aromatic amino acid and a precursor product for the biosynthesis of proteins in the human organism (PubChem Substance and Compound databases, 2018). The melting point of the amino acid (Molecular mass = 204.23 g/mol) amounts to 289 °C and the compound is very soluble in water (11.4 g/L) with an octanol-water partition coefficient of log *P* = -1.06 (PubChem Substance and Compound databases, 2018), (Lide *et al.*, 2005). L-Tryptophan has a carboxyl group with a pK_{a1} of 2.38 and an amino group with a pK_{a2} of 9.34 (Figure 4.7). The isoelectric point amounts to pH_{IEP} = 5.89 (Lide *et al.*, 2005). The backbone of the aromatic ring structure of L-tryptophan consists of a benzene ring and an adjacent heterocyclic aromatic pyrrole ring (Zawadzki *et al.*, 2012).

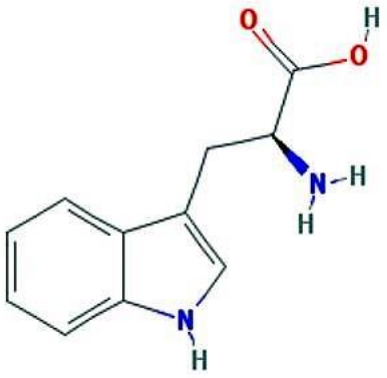

Figure 4.7:Structural formula of L-Tryptophan

(PubChem Substance and Compound databases, 2018)

5. Results and discussion

5.1 Characterization of water matrix

5.1.1 Ionic Strength

The electrical conductivity of both reverse osmosis water and service water (University of Duisburg-Essen, Campus Duisburg) was measured with the conductivity meter. From the measurement results, the ionic strength can be determined by a simplified equation (7). The results are shown in the following table (Table 5.1):

Table 5.1: Conductivity and ionic strength of reverse osmosis water and service water.

	Conductivity [µS/cm]	Ionic strength
Reverse Osmosis Water	20.1	0,000322
Service Water	480	0,00768

The model water (water matrix) produced at three different concentrations was examined in terms of pH, conductivity and ionic strength (Table 5.2). For the calculation of the ionic strength, the average of the measured conductivities per sample series was used.

Table 5.2: Investigation of water matrix related to the pH-value, electrical conductivity and ionic strength

Concentration of water matrix	**0,5 mmol/L**			**1 mmol/L**			**1.5 mmol/L**		
Sample No.	***1.1***	***1.2***	***1.3***	***2.1***	***2.2***	***2.3***	***3.1***	***3.2***	***3.3***
Electrical conductivity [µS/cm]	167.5	169.5	167.2	301	548	301	428	427	426
pH (Initial)	7.85	7.75	7.66	7.72	7.92	7.62	7.84	7.91	7.74
pH (End)	7.48	7.5	7.58	7.73	8.02	7.6	7.9	7.95	7.9
Ionic strength (equation (5)) (Ø)	$2.5 \cdot 10^{-3}$			$5 \cdot 10^{-3}$			$7.5 \cdot 10^{-3}$		
Ionic strength (equation (7)) (Ø)	$2.69 \cdot 10^{-3}$			$6{,}13 \cdot 10^{-3}$			$6{,}83 \cdot 10^{-3}$		

The equation (7) for the approximate calculation of the ionic strength from the measured electrical conductivity shows results which approximately correspond to the results from the equation (5) for the exact calculation of the ionic strength. In the second series of measurements of the sample 2.2 the measured values differ over the

pH and the electrical conductivity in comparison with the other two samples (2.1 and 2.3). It can therefore be assumed that the deviation of the values of this sample is due to impurities. Overall, it is noticeable that the electrical conductivity increases with increasing ion concentration, which corresponds to the assumptions, since ions promote the electrical conductivity in water.

5.1.2 Buffer capacity

The buffer capacity of model water 1.5 mM (water matrix) and service water (University of Duisburg-Essen, Campus Duisburg) was analysed by titration with HCL (0.05 M) and NaOH (0.05 M) as titrants. The initial pH of service water was 7.56 and that of the water matrix 8.18. The titration curves of the two samples were plotted in a line diagram (Figure 5.1).

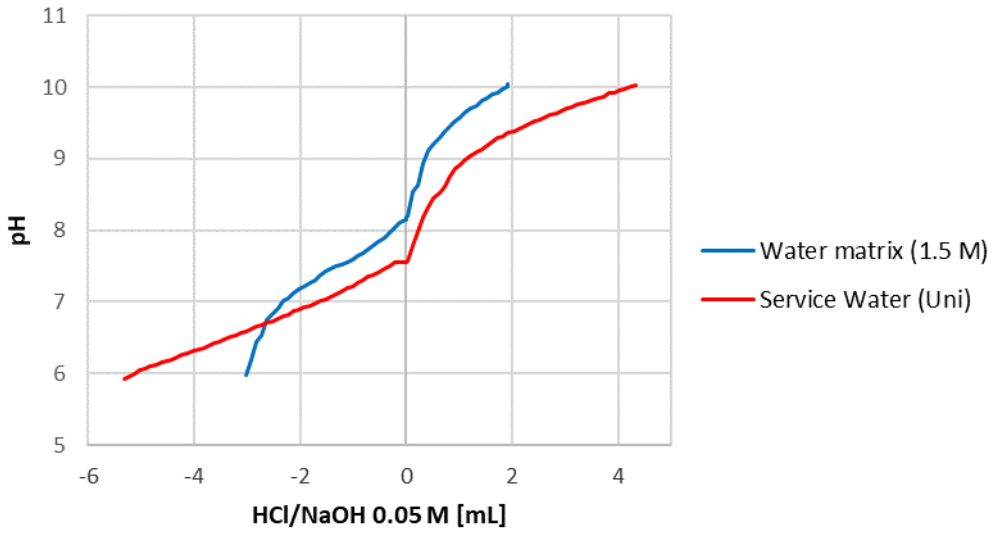

Figure 5.1: Titration curves for the visualization of the buffer capacity of the water matrix and service water.

The buffering capacity of the water matrix used for the experiments to determine the adsorption isotherms has no significant buffering property compared to the process water. Typically, buffers consist of a conjugate acid-base pair. However, the water matrix, containing $NaHCO_3$ (1.5 mM) and $MgSO_4$ (1.5 mM), consisted of a non-conjugated acid-base pair (HCO_3^-/SO_4^{2-}). In general, both aqueous sample solutions are more stable in the acidic medium than in the basic range. In the acidic pH range, the process water has a higher buffering capacity than the water matrix, the more acid the pH milieu becomes. For the experimental purposes in this work, the buffering capacity of the model water (water matrix) is sufficient.

5.2 Graphite species characterization and analysis

For the attempt of graphite modification different chemical or thermal oxidation methods were used. The modification by chemical oxidation was carried out via oxidation agents as nitric acid, hydrogen peroxide, ammonium peroxydisulfate, and ozone gas. The thermal modification was carried out under certain physical conditions, at elevated temperatures at 350 °C or 500 °C, with a certain mixed ratio of oxidative oxygen and nitrogen gas or with atmospheric oxygen. Special methods were applied, such as potentiometric titration, laser diffraction particle size analysis, zeta potential measurement, EPS, XPS and BET surface analysis, to analyse the oxidation grade and characterize the changing of surface charge of the treated graphite. In the following sections the results of the performed analysis techniques are presented.

5.2.1 Ozonation of Graphite UF1 99.5

Graphite UF1 was modified by ozonation with the aid of a fix bed flow reactor to introduce functional oxygen groups onto the graphite surface. By XPS analysis, the degree of the graphite surface oxidation was determined by the relative amount of chemisorbed oxygen (Table 5.5). The adsorbed O_3 masses to graphite UF1 99.5 after 90 min of ozonation is given in the line graph (Figure 5.2) below. After mixing all ozonised graphited samples the total ozonised graphite mass was 5.56 g and 0.63 mg of Ozone was adsorbed onto the graphite surface per m² relating to the graphite UF1 99.5 BET surface area of 19.489 $m^2\ g^{-1}$ (Table 5.6).

sample	time [min]	sample mass [g]	abs. mass [g_{Ozone}]	ads mass [$mg_{Ozone}/m^2_{graphite}$]
ads. mass 1	90	1.36	12.32	0.47
ads. mass 2	90	1.40	20.64	0.77
ads. mass 3	90	1.40	18.20	0.67
ads. mass 4	90	1.40	16.48	0.61
total	***90***	***5.56***	***16.91***	***0.63***

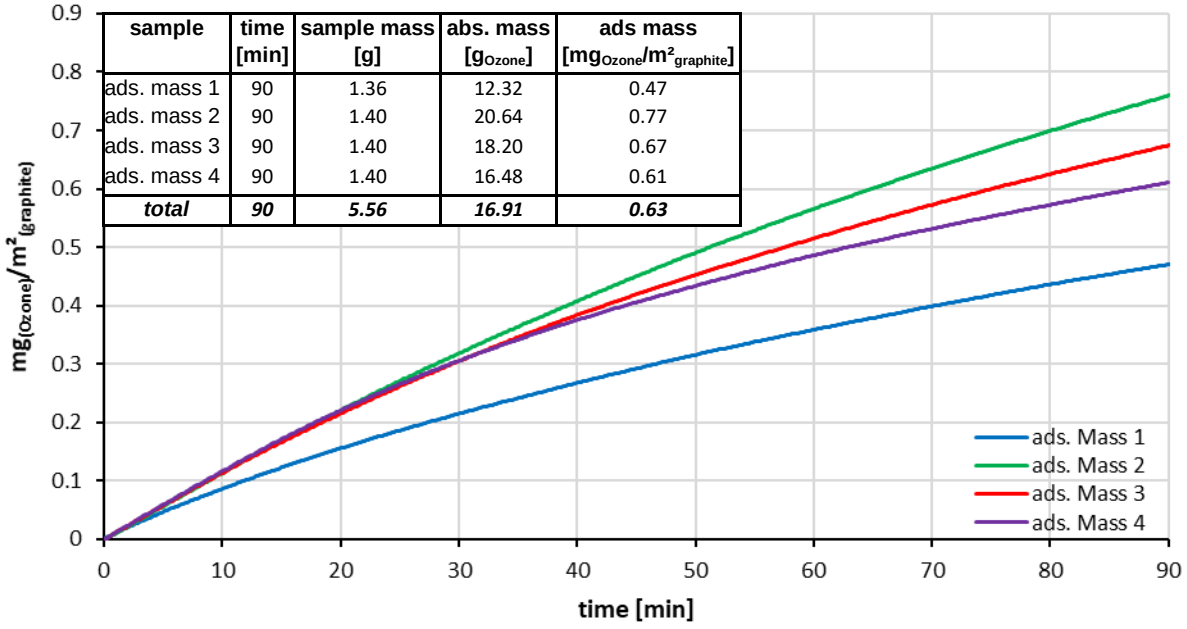

Figure 5.2: Adsorbed mass of ozone to graphite UF1 99.5

In an scientific study “Carbon Nanostructure Reactivity: Reactions of Graphite Powders with ozone, (Razumovskii *et al.*, 2007)” highly dispersed graphite powder with a specific surface area of 250 and 450 $m^2\ g^{-1}$ was ozonised at 20 °C. Allegedly to this

study, the adsorption rate was high and the ozone molecules react with the aromatic sp^2-hybridized six-membered carbon cycles at the graphite surface. After one-sixth of these six-membered cycles were consumed, the graphite surface did not react much with the ozone molecules. There was an indication for the formation of free radicals on the graphite surface that were converted to peroxide radicals. In Razumovskii's results was shown that functional groups formed at the graphite surface. The reaction led to the degradation of local zones, which reduced the reactivity of adjacent areas with ozone possibly due to the drastic destruction of the reactive centres and by a protective function of the functional groups. The reaction of ozonation was exothermic and accompanied by a degradation of the sample mass. At a weight of 0.39 g of the raw sample and specific surface area of 175.5 $m^2\ g^{-1}$ after the modification 1.36 moles of O_3 per m^2 were adsorbed onto the graphite surface (Razumovskii *et al.*, 2007).

Calculations in this master's work result in the adsorbed amount of 1.3125 x 10^{-5} mol ozone per m^2 of graphite surface (0.63 mg m^{-2}), which are with the aid of the avogadro's constant of 6,022 x 10^{23} converted to 7.904 x 10^{18} ozone molecules per m^2 of graphite accessible surface area. This result roughly corresponds to the amount of 8.2 x 10^{18} molecules estimated in the scientific work of Razumovskii, assuming that there are approximately 1.5 x 10^9 reactive six-members carbon cycles per m^2 at the graphite surface. In this regard, it is believed that the coverage is approximately one ozone molecule per two reactive cycles. (Razumovskii *et al.*, 2007). However, the actual adsorption amount of ozone may be negatively diminished in a humid atmosphere, since water vapor may reduce the catalytic activity of carbon by probably adsorbed water molecules (Subrahmanyam, Bulushev and Kiwi-Minsker, 2005). Another study also examined ozonation of activated carbon samples. In summary, the catalytic activity of woven-fibre fabric of activated carbon was lower in a humid atmosphere than in the dry atmosphere. In addition, ozonation resulted in the formation of oxygen containing surface groups at the sample surface (Subrahmanyam, Bulushev and Kiwi-Minsker, 2005). In the current ozonation experiment of this master's work, the relative humidity was about 50 %, which may have affected the reactivity of ozone at the graphite surface negatively. Further information on this experimental procedure about an exothermic reaction or loss of substance is not available.

5.2.2 Potentiometric Titration

The Potentiometric titration was performed to identify acid surface groups of the individual modified graphite species and to detect differences in relation to the untreated graphite. The following graphic (Figure 5.3) shows the plotted titration curves of the individual graphite samples, including the blank sample. The ozonised graphite sample was not investigated in this experiment because, because not enough modified graphite powder was left. In order to find the pK_a value of the individual samples in this experiment, first the equivalence point and the corresponding titration volume were determined by the titration curves. Subsequently, the sought pK_a value results from the

pH value which is reached when half of the titration volume has been consumed up to the equivalence point.

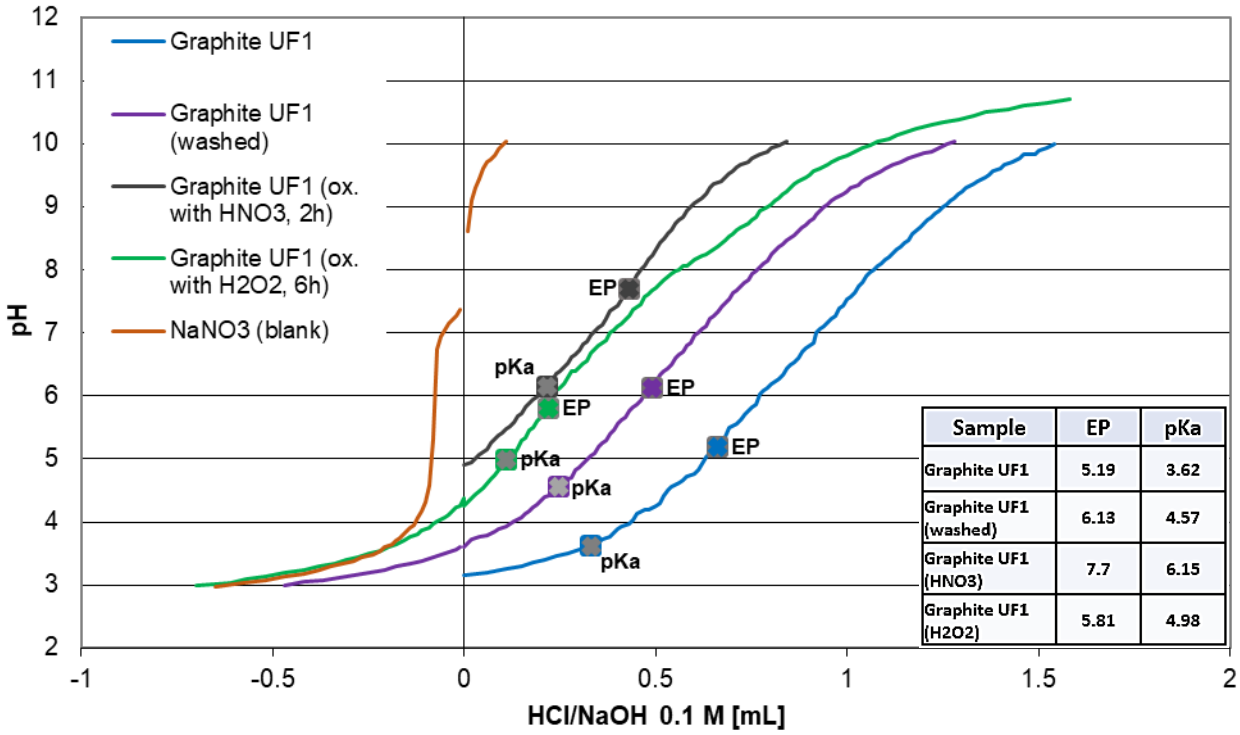

Figure 5.3: Potentiometric titration curves of differently treated graphite samples

When evaluating the results of the potentiometric titration, the difficulty was to interpret titration curves of the individual graphite samples. The method of potentiometric titration is particularly suitable for activated carbon samples due to their large specific surface area (300 – 1800 m^2 g^{-1}) according to the literature (Kümmel and Worch, 1990a). However, the investigated graphite UF1 99.5 species had a much lower surface area of about 20 m^2 g^{-1} as found by BET surface analysis. Therefore, it is generally difficult to detect inflection points that indicate the pK_a values of functional groups at the graphite surface. The titration curves from the graph are not meaningful enough to determine pK_a values indicative of certain functional surface groups in the graphite samples. For this assessment, the turning points are not strong enough, since the surface of graphite is generally too small. For more meaningful results, sample preparation would require a larger amount of graphite. When comparing the modified graphite samples with the untreated graphite samples, however, slight differences in the titration curves can be detected. In summary, the pK_a values of the modified graphite are slightly higher than those for the unmodified graphite. The washing of graphite UF1 99.5 also increases the pK_a value. Oxygen-containing functional groups (-COOH) react acidic, hence, the pK_a-values of modified graphite are assumed to be lower than that of unmodified graphite. Contrary to the expectations, the modification treatment, judging by the results, apparently reduced the number of acidic surface groups.

5.2.3 Measurements of the Laser Diffraction Size Analysis

For determination of the particle size of the graphite species a laser diffraction size analysis was executed. According to the results of the volume distribution (Figure 5.4), the particle size for pristin graphite UF1 99.5 is located in-between 0.4 and 2.75 µm and for modified graphite (treated with ozone) in-between 1 and 3 µm. The particle size analyser used is capable of measuring powder samples in the size range between 0.4 and 2000 µm (Beckman Coulter Inc., 2011b).

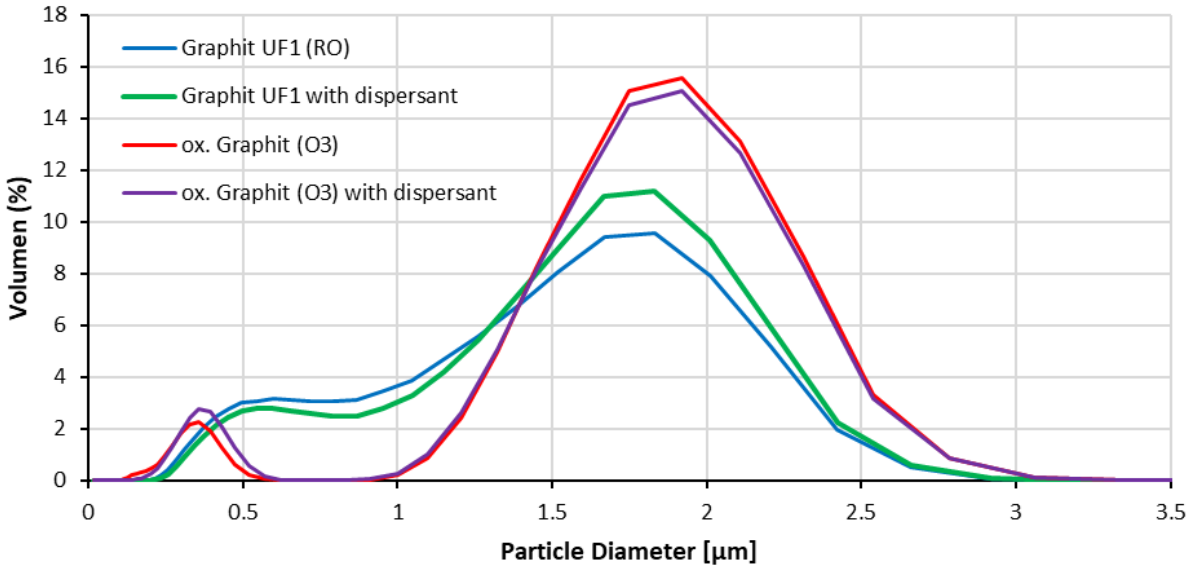

Figure 5.4: Volume distribution of graphite sample particles

The volume distributions in the graph are approximately the same for samples of the same graphite species, regardless whether the samples were prepared in reverse osmosis water with or without dispersant. All statistic values about the mean, median and mode are shown below (Table 5.3).

Table 5.3: Statistic data about the mean, median and mode of the particle size analysis of graphite samples

Particle Size	Mean [µm]	Median [µm]	Mode [µm]
Graphite UF1 99.5	1.33 ± 0.63	1.37	1.92
Graphite UF1 99.5 with dispersant	1.41 ± 0.62	1.51	1.92
Graphite (65 % HNO3, 2 h, 60 °C)	1.38 ± 0.67	1.51	1.92
Graph., dispersed (65 % HNO3, 2 h, 60 °C)	1.41 ± 0.64	1.53	1.92
Ozonised Graphite	1.61 ± 0.63	1.74	1.92
Ozonised Graphite with dispersant	1.58 ± 0.64	1.72	1.92

The modal value (mode) is defined as the value that occurs most frequently in a set of data and corresponds to the channel centre with the maximum volume percent (Beckman Coulter Inc., 2011a). The modification of graphite UF1 99.5 by ozonation treatment resulted in a change of the particle size distribution (Figure 5.4). The

statistical data (mean, median) have no significant alternation in the particle size, considering the standard deviation. The modal value remained the same for all samples.

Assuming that the particle particles correspond to an ideal spherical shape, the mass-specific surface of graphite UF 1 99.5 can be calculated via the graphite density of 2.26 g cm^{-3} and the particle diameter of 1.37 µm obtained from the median value from the particle size analysis (Table 5.3). The surface of a single graphite particle is calculated with the following equation (10):

$$S = \pi \cdot {d_p}^2 <=> S = 5.8965 \cdot 10^{-12}\, m^2 \quad (10)$$

S = single graphite particle surface

d_p = particle diameter

The volume V_p of the single graphite particle is calculated by the following equation (11):

$$V_p = \pi \cdot \frac{d_p^3}{6} <=> V_p = 1.3464 \cdot 10^{-18}\, m^3 \quad (11)$$

Using the equation (12) of density ρ, the mass of a single graphite particle can be calculated.

$$\rho = \frac{m}{V} <=> m = 3.0429\ 10^{-12}\, g \quad (12)$$

m = mass of single graphite particle

V = volume of single graphite particle

Finally, the equation (13) can be used to calculate the mass-specific surface area S_m of graphite per gram (Stieß, 2009).

$$S_m = \frac{S}{m} = 1.94\, \frac{m^2}{g} \quad (13)$$

The mass specific surface of graphite UF1 99.5 would be 1.94 $m^2\ g^{-1}$ according to this simplified calculation. However, the specific surface area after the BET surface analysis is 19.27 $m^2\ g^{-1}$. Thus, the result of the calculation would be only an approximate estimate, since the surface state of the graphite particles does not

correspond to an ideal spherical shape and only the median value was used as the particle diameter.

5.2.4 Zeta potential

The zeta potential of the graphite suspensions (20 mg/L) in water matrix was measured at different pH values (pH 1 to pH 10) for both sample series, graphite UF1 99.5 (washed) and oxidized graphite (Ozone treated). The graphics (Figure 5.5) shows the results of the zeta potential measurement with the including standard deviation.

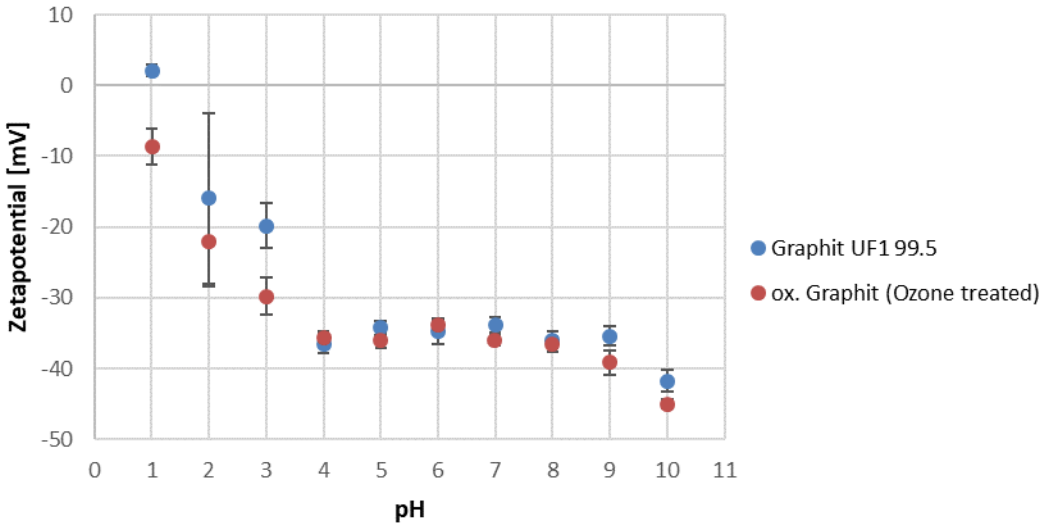

Figure 5.5: Zeta potential of sample suspensions for graphite UF1 99.5 and ox. graphite (Ozone treated).

The results of the zeta potential measurement series show that the zeta potential decreases with decreasing pH. The graph shows a tendency for the oxidation-modified graphite to have slightly larger zeta potentials in the acid range beginning from pH < 4. Higher zeta potentials indicate a higher Nernst potential (surface charge) at the particle surface (Müller and Hildebrand, 1996). Therefore, it can be assumed that the higher Nernst potential in the modified graphite is due to acidic functional surface groups formed by the oxidation treatment. However, a direct assignment of functional groups by the estimation of the Nernst potential via the zeta potential analysis is not possible. The isoelectric point (IEP) is located at the zero point of the zeta potential. The IEP could not be determined for the ozonised graphite sample but is assumed be below pH 1. For graphite UF1 99.5, the IEP is located between pH 1 and 2.

5.2.5 Point of Zero charge

The determination of point of zero charge according to the scientific paper of Noh & Schwarz (1988) was unsuccessful since the final pH values measured in the experiment (Figure 5.6) did not approximate a specific pH. The reason for this result may be explained by the low surface area of graphite, whereby no significant electrolyte balance could be established. In general, this experiment is carried out with activated carbon samples, which have a much larger surface area.

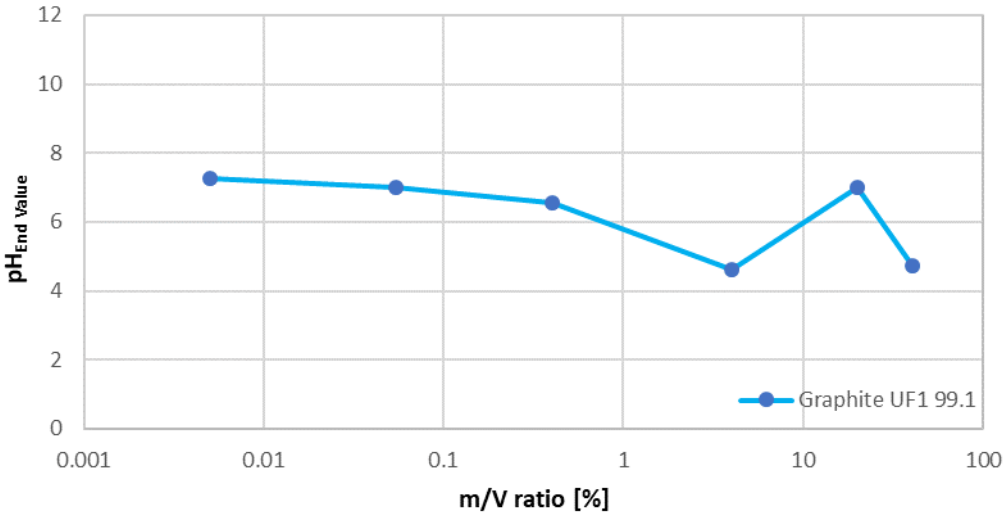

Figure 5.6: Plotted results from the experiment for the determination of the point of zero charge.

The 0.1 M NaCl reference samples, which did not contain graphite, both had a pH of 7.4. Tendentially, it can be observed that the pH in this experiment drops to 4.71 with increasing graphite mass in the samples. However, the pH of sample 5 deviates significantly, so the result of the measurement analysis is not very meaningful. In summary, however, it can be assumed that the point of zero charge for graphite UF1 99.5 is rather in the acidic range.

5.2.6 Element analysis of modified graphite species by EPS and XPS

All modified graphite samples subjected to EDX analysis have no detectable degree of oxidation (Table 5.4). It is believed that the EDX analysis is not sensitive enough at low element concentrations. In comparative studies with the EDX analysis method, the expected relative errors in the measurement results have to be considered. For samples with an element concentration higher than 50 %, a relative error of up to 5 % is expected. If the element concentration is less than 10%, the error may even be higher than 70 % (Schmidt, 1994). The graphite samples treated with nitric acid, hydrogen peroxide and ozone were measured in duplicate and their mean values are presented in the table below.

Table 5.4: EDX results of modified graphite samples, oxidized by chemical or thermal treatment

	Concentration [at. %]			Expected error [%]	
Graphite sample	**C**	**O**	**Total**	**C**	**O**
UF1 99.5	99.560	0.440	100	1 - 5	70 - 100
HNO_3 (2 h, 60 °C)	99.515	0.485	100	1 - 5	70 - 100
H_2O_2 (6 h)	99.415	0.585	100	1 - 5	70 - 100
350 °C (O_2/N_2 gas mix/2 h)	99.620	0.380	100	1 - 5	70 - 100
500 °C (O_2/N_2 gas mix/2 h)	99.510	0.490	100	1 - 5	70 – 100
O_3 (7 - 7.5 ppm, 1.5 h)	99.290	0.710	100	1 - 5	70 - 100

During the modification process a possible pore formation in the graphite material should be excluded. An electron-scanning microscopy (SEM) provided an insight into the graphite surface in the micrometre range. A pore formation in the ozonised graphite could not be detected visually (Figure 5.7).

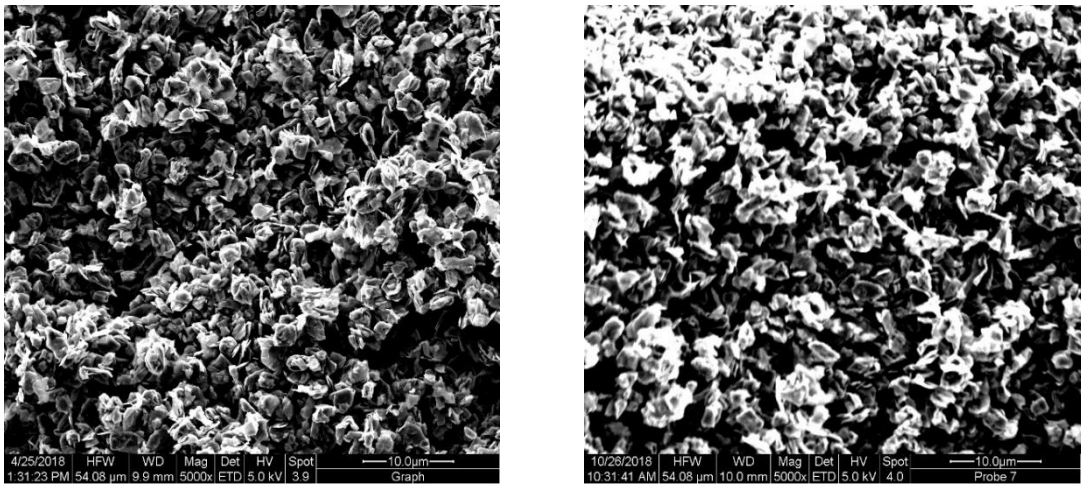

a) b)

Figure 5.7: SEM image in 5000x magnification of a) graphite UF1 99.5 and b) ozonized graphite

The XPS results of the graphite samples that were modified by chemical or thermal oxidation treatment are given in the table below (Table 5.5). All samples show a certain oxygen content in the range of about 3 to 6 %, even pristine graphite UF1 99.5. According to the statement of the operator, Dr. Ulrich Hagemann, the measurement error in the XPS analysis is about ± 3 % because of noise of the measurement signal, background noise, et cetera. Therefore, the measured values are only approximate results. However, the highest oxygen content of 5.2 at. % in the graphite surface was achieved in the sample treated with ozone gas. Also, the samples treated with ammonium peroxydisulfate or hydrogen peroxide for 48 h had round about 5 at. % oxygen in their sample surface. When considering the measurement error, it may be assumed that the modified samples have an increased oxidation degree of about 1 to 2 at. %, since the graphite UF1 99.5 sample already has a measured oxygen content

of about 4.1 % which is consistent with the XPS measurement results of natural graphite of a comparative study (Wu *et al.*, 2002). According to information from the manufacturer "Graphit Kropfmühl GmbH", the natural graphite "graphite UF1 99.5" was pre-treated first by a floatation and subsequently by a chemical cleaning with sulfuric acid and hydrofluoric acid to increase the purity, whereby the surface polarity on the graphite surface may be influenced by functional groups. Therefore, it is possible that functional oxygen surface groups have already been incorporated into the graphite UF1 99.5 material during the manufacturing process. According to an European patent "Process for the production of high-purity graphite", for the production of high-purity graphite (> 99%) from natural graphite, a pre-treatment via a pre-purification stage, a floating and subsequent chemical cleaning with certain acids is common (Lazar, Gerhard *et al.*, 1986).

The method to evaluate the sp^2/sp^3 content of the graphite samples is obtained by the C KLL spectra. The *D* parameter signifies the distance *D* between the most positive maximum and most negative minimum of the first derivative of C KLL spectrum. Moreover, is have been considered a linear approximation of the *D* value, starting from D = 13 eV for a total sp^3 hybridization up to D = 21 eV with 100 % of sp^2 hybridization (Mezzi and Kaciulis, 2010). The ideal graphite structure consists of 100 % sp^2-hybridized carbon atoms. Therefore, deviations from this value may indicate either proportionately present amorphous carbon, or bonds between the carbon atoms and heteroatoms, such as oxygen, which suggests acidic oxygen-containing surface groups.

Table 5.5: XPS results of modified graphite samples, oxidized by chemical or thermal treatment

	Concentration [at. %]		D parameter	sp^2 content
Graphite sample	**C**	**O**	**[eV]**	**[%]**
UF1 99.5	95.9	4.1 ± 0.12	~19	~75.0
H_2O_2 (6 h)	95.5	4.5 ± 0.14	~20	~87.5
500 °C (O_2/N_2 gas mix/2 h)	97.0	3.0 ± 0.09	~21	~100.0
$(NH_4)_2S_2O_8$ (48 h)	94.0	5.0 ± 0.15	~18	~62.5
H_2O_2 (48 h)	94.8	5.2 ± 0.17	~18	~62.5
IWW (500 °C/3 h)	96.8	3.2 ± 0.01	~19	~75.0
O_3 (7 - 7.5 ppm, 1.5 h)	94.1	5.9 ± 0.18	~17	~50.0

When evaluating the XPS spectrum of the ozonised graphite samples, indications for the presence of oxygen-containing functional surface groups were also found. The positions of the XPS peaks and the full width measured at the half of its maximum height (FWHM) were used to detect C-O, C = O and COOH groups. However, it was not clear to what extent these groups are present and whether they were within the confidence range or the limit of detection. When comparing the EDX results with the

XPS results, it is noticeable that in the XPS analysis significantly higher oxygen concentrations were detected in the modified graphite samples.

5.2.7 BET Specific surface data

The results (Table 5.6) show no crucial different in the BET Surface Area of graphite UF1 and Graphite, treated by ozone oxidation. The pore volume analysis also showed that the oxidation treatment of graphite UF1 99.5 did not produce any significant pore structure in the sample material. The measurements per graphite specimen were each carried out in duplicate.

Table 5.6: Results of the BET surface area analysis including the pore volume. All numbers indicating the standard deviation.

	BET Surface Area [m^2/g]	Pore volume [mL/g]
Graphite UF1 99.5	19.269 ± 0.050	0.0493 ± 0.000
Graphite (Ozone treated)	19.489 ± 0.541	0.0558 ± 0.002

Generally, graphite has a non-porous characteristic and in another scientific experiment titled with “What is the choice for supercapacitors: graphene or graphene oxide?” the BET surface is stated with 17.9 $m^2\ g^{-1}$ (Xu *et al.*, 2011). On average, in the experiment of this master’s work the BET surface area for pristine graphite UF1 99.5 was indicated with 19.27 ± 0.05 $m^2\ g^{-1}$. Thus, the result is largely consistent with the literature. For oxidized graphite the BET surface is 46.4 $m^2\ g^{-1}$ according to the scientific study “Structural evolution during annealing of thermally reduced graphene nanosheets for application in supercapacitors” (Chen *et al.*, 2012).

According to a calculation, assuming that a sample of ozonised graphite of 4 g was suspended in 15 ml of water, theoretically, with a BET surface area of 19.489 $m^2\ g^{-1}$, there would have to be $1.732 \cdot 10^{-10}$ mol m^{-2} dissociable functional groups onto the modified graphite surface to lower the solution pH from pH 7 to pH 6 compared with unmodified graphite.

5.3 Adsorption Batch Tests

In this master project, an initial list of substances (Benzene, Naphthalene, Anthracene, Phenol, Toluene, 1-Naphthol, 1-Anthrol, Aniline, Naphthylamine, Anisole, 2-Methoxy-naphthalene, 4-Chlorophenol, 4-Chloro-1-naphthole, L-Phenylalanine, L-Tyrosine and L-Tryptophan) for the experimental test series has been proposed. However, analytical method development revealed that some substances could not be tested. For example, benzene was too volatile for the technique used in the experiments, and anthracene is insoluble in water and could not be dissolved in the water matrix. For L-Phenylalanine and Toluene a fluorescence spectroscopic emission and excitation wavelength in the tested wavelength range could be found in the FEEM scan. Morevoer, for 4-Chlorophenol the fluorescence spectrometric measurement was not sensitive enough. Finally, an analytical method for the adsorption experiments (Table 5.7) could be developed for at least seven substances (Phenol, Anisole, 1-Naphtol, Naphthalene, 2-Methoxynaphthalene, L-Tyrosine and L-Tryptophan).

Table 5.7: UV/VIS Absorbance, Fluorescence Excitation/Emission wavelength, LOD/LOQ (DIN 32645), Degradation Stability and Calibration Range of substances for the adsorption batch tests

Substance	UV/VIS Absorbance (200 – 600 nm)	Fluorescence Excitation/Emission [nm]	LOD/LOQ (α = 0.02) [nM]	Degradation stability [h]	Calibration range [nM]
Benzene	too high volatility		-	-	-
Anthracene	too low solubility in water		-	-	-
Aniline	too high toxicity		-	-	-
Phenol	no signal	267/311	8.38/24.81	24	50 – 950
Anisole	no signal	270/303	9.33/27.6	24	50 – 950
4-Chlorophenol	no signal	too low sensitivity	65.13/178.84	48	50 – 950
1-Naphthol	no signal	233/500	21.89/63.56	24	50 – 950
Naphthalene	no signal	265/330	6.86/20.37	96 (at 8 °C)	50 – 950
2-Methoxynaphthalene	no signal	270/350	4.00/11.92	72	50 – 950
L-Tyrosine	no signal	274/325	24.57/71.07	2	50 – 950
L-Tryptophan	no signal	278/356	31.36/89.84	2	50 – 950
Phenylalanine	no signal	no useful signal	-	-	-
Toluene	no signal	no useful signal	-	-	-

5.3.1 Degradation experiment of the test substances

In order to check the concentration stability of the substances, a degradation test was carried out. The starting concentration of the substance solutions in the water matrix was 800 nM. The time-dependent concentration reduction of the solutions was investigated. The test solutions were prepared from fresh working solution (WS1 new) and a one-week older working solution WS1 (old). For phenol and anisole, a concentration stability at room temperature of at least 24 h could be ensured (Figure 5.8).

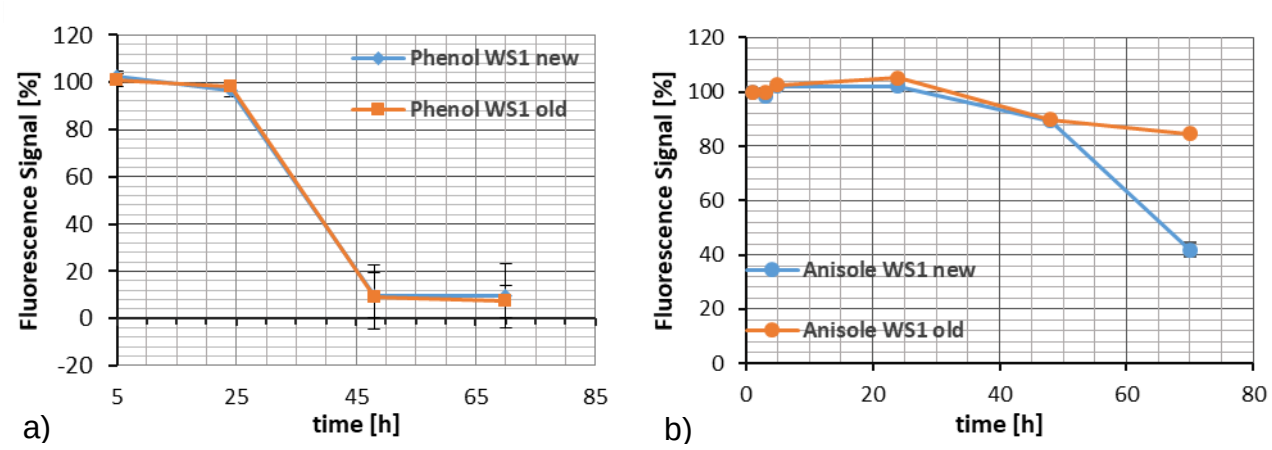

Figure 5.8: Time-dependent degradation of the concentration solution of a) Phenol and b) Anisole.

The relative standard deviation was taken into account for the plotted data in the diagrams.

For 4-chlorophenol, the concentration was stable for well over 48 hours and for naphthalene, 2-methoxynaphthalene, and 1-naphthol, a concentration stability of at least 24 h could be ensured (Figure 5.9).

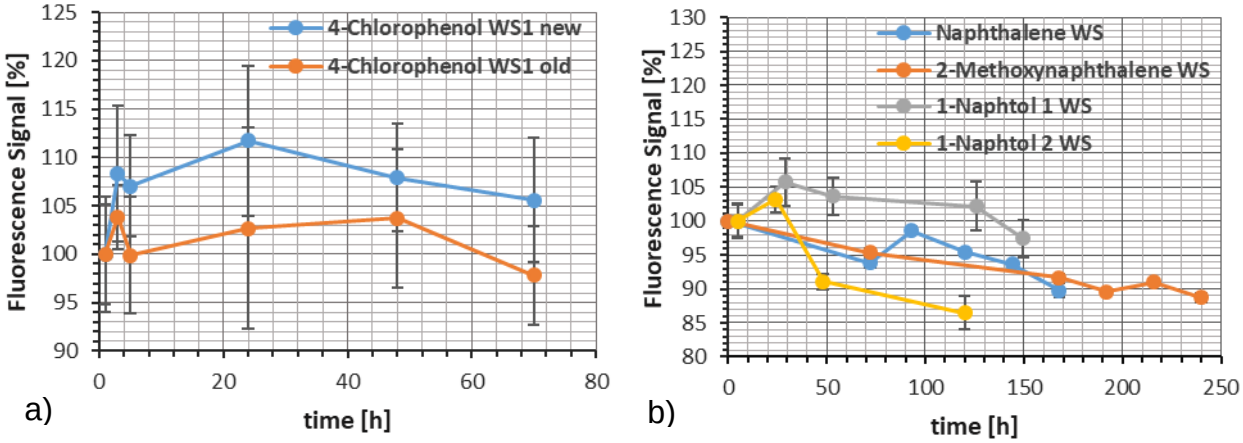

Figure 5.9: Time-dependent degradation of the concentration solution of a) 4-Chlorophenol and b) Naphthalene, 2-Methoxynaphthalene and 1-Naphthol.

The relative standard deviation was taken into account for the plotted data in the diagrams.

For the amino acid solutions L-tyrosine and L-tryptophan, it was found that the concentration stability only lasted about 2 hours (Figure 5.10). The degradation of these substances was rapid, so that adsorption batch tests over a period of 24 h were not possible to carry out.

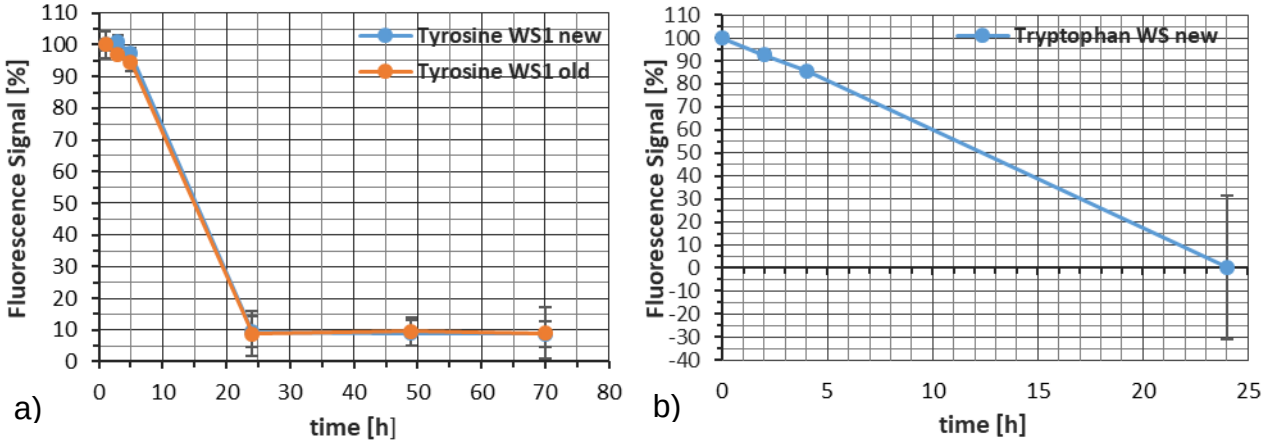

Figure 5.10: Time-dependent degradation of the concentration solution of a) L-Tyrosine and b) L-Tryptophan

The relative standard deviation was taken into account for the plotted data in the diagrams.

5.3.2 Background noise of adsorption batch test samples

The background noise measurements of the graphite UF1 99.5 suspensions yielded different results (Figure 5.11). It is noticeable that anisole has a negative deviation from the zero concentration of up to nearly 40 nM. A pseudo-concentration in the positive region of almost 55 nM was measured in the blank sample of 1-naphthol with 500 mg/L graphite UF1 99.5. Strong deviations from the zero point in the concentration measurement could also be observed with phenol and tyrosine at higher graphite concentrations. It is unclear where the measured concentrations come from, possibly by contaminants from the laboratory material (laboratory glassware, Ultra-Turrax etc.). However, a high standard deviation could be found in the measurements for all major deviations. For measurements in the low concentration range, the error is, according to experience, slightly larger. Each sample was prepared in duplicate. In addition, a seven-fold fluorescence spectrometric measurement repetition was performed for each of these samples.

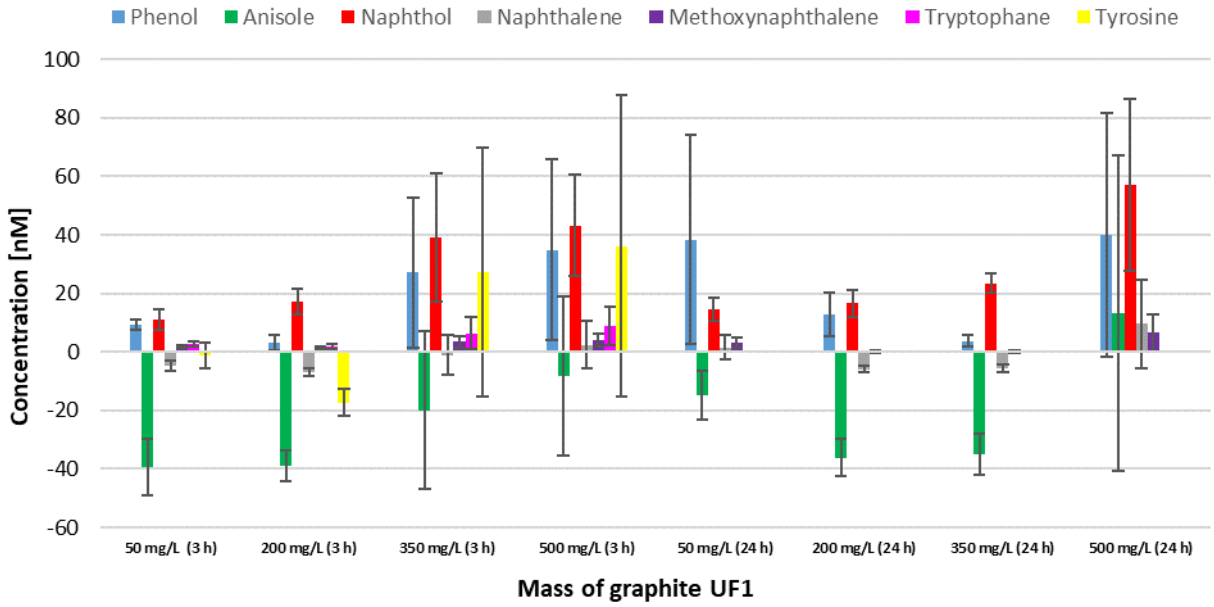

Figure 5.11: Measurement results of background noise from graphite UF 1 99.5 suspension in water matrix. The fluorescence spectrometric measurement was carried out at the maximum excitation and emission wavelengths of all test substances.

In the background noise measurements of the modified, ozone treated graphite also deviations from the zero concentration can be measured (Figure 5.12). This observation was also found in the water matrix blank sample with 0 mg/L modified graphite. The strongest deviation from anisole was up to 35 nM. The measured background noise distribution was approximately the same for each graphite sample batch of the corresponding test substances. Besides, the standard deviation for the phenol, anisole and 1-naphthol samples was also relatively high.

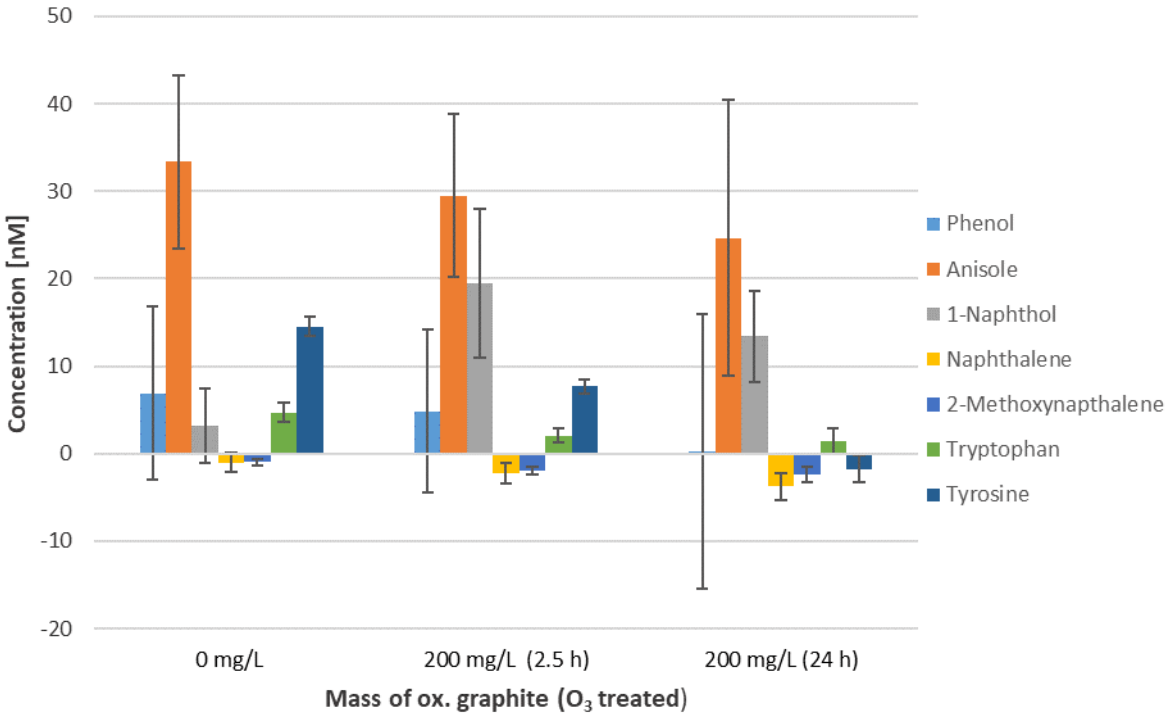

Figure 5.12: Measurement results of background noise from modified, ozone treated graphite suspension in water matrix.

The fluorescence spectrometric measurement was carried out at the maximum excitation and emission wavelengths of all test substances.

5.3.3 Adsorption Kinetics Tests

In the adsorption kinetics tests, it was to be shown after which shaking period (approx. 2.5 h or approx. 24 h) the adsorption equilibrium was reached. The initial concentration in the adsorption kinetics tests was 800 nM for all tested substances. The graphs below show the plot of adsorption loading versus time for all substances (phenol, anisole, 1-naphthol, naphthalene, 2-methoxynaphthalene, L-tryptophan and L-tyrosine). For each sample, the fluorescence spectrometric measurement was repeated seven times. The standard deviation was calculated from the measurement results and plotted in the graphics.

The adsorption kinetics tests have shown that for phenol and 1-naphthol the adsorption equilibrium appears to be adjusted after 24 hours for the graphite UF1 99.5 samples, since the equilibrium solid phase concentration q is the highest at this time (Figure 5.13). The modified, ozonised graphite samples for phenol is already at 2.5 h in adsorption equilibrium. On the other hand, with naphthol the modified, ozonised graphite sample seems to be in adsorption equilibrium after 24 h.

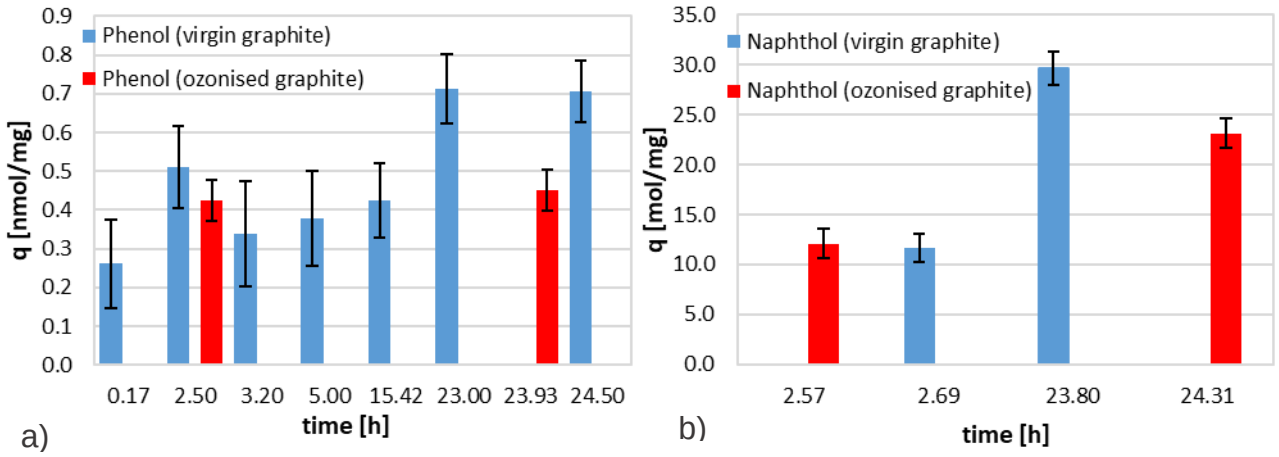

Figure 5.13: Adsorption kinetics tests of a) Phenol and b) 1-Naphthol.

In the case of anisole, the adsorption equilibrium solid phase concentrations *q* in the diagram indicate that an adsorption equilibrium has already set after 2.5 hours (Figure 5.14).

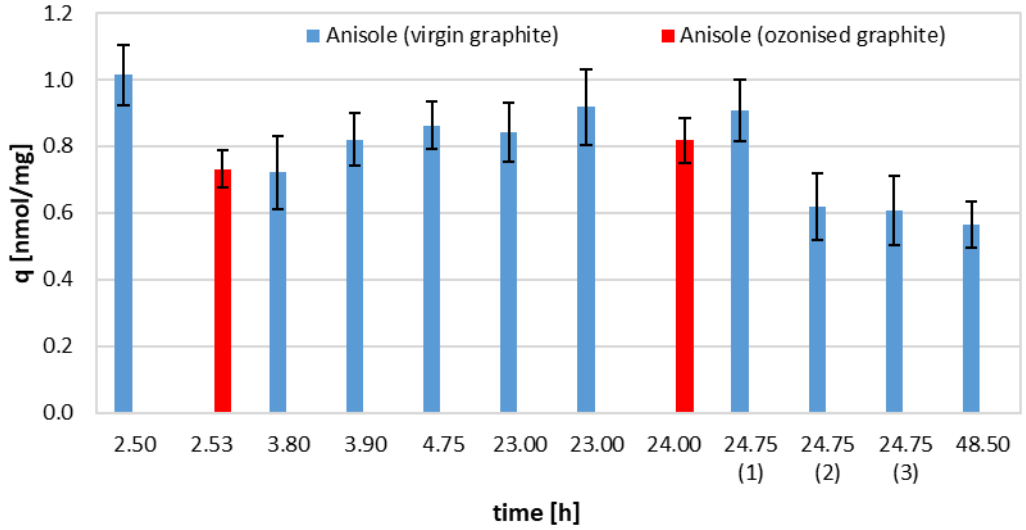

Figure 5.14: Adsorption kinetics test for Anisole

Naphthalene has a maximum adsorption solid phase concentration after 24 h for all virgin graphite UF1 99.5 samples. There is no significant difference in the ozonised graphite samples (Figure 5.15a). The derivative, 2-Methoxynapthalene has relatively uniform loading maxima for both virgin graphite UF1 99.5 and ozonised graphite samples in the time interval between 2.5 to 48 h, so it can be assumed that an adsorption equilibrium has set after 2.5 h (Figure 5.15b).

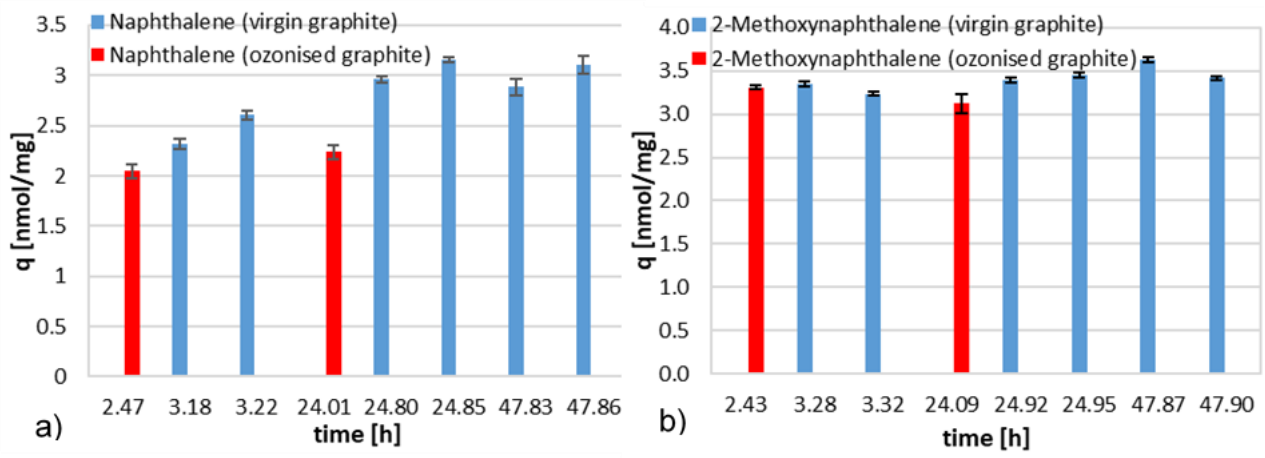

Figure 5.15: Adsorption kinetics tests of a) Naphthalene and b) 2-Methoxynaphthalene

For L-tyrosine and L-tryptophan, the tests could only be performed at 2.5 hours because of the low time-dependent concentration stability (Figure 5.16). The solid phase concentration levels of L-tryptophan are slightly higher than those of L-tyrosine, possibly due to the presence of the bicyclic aromatic system in the substance molecule of L-tryptophan. Both substances have higher solid phase concentration values in the ozonised graphite sample.

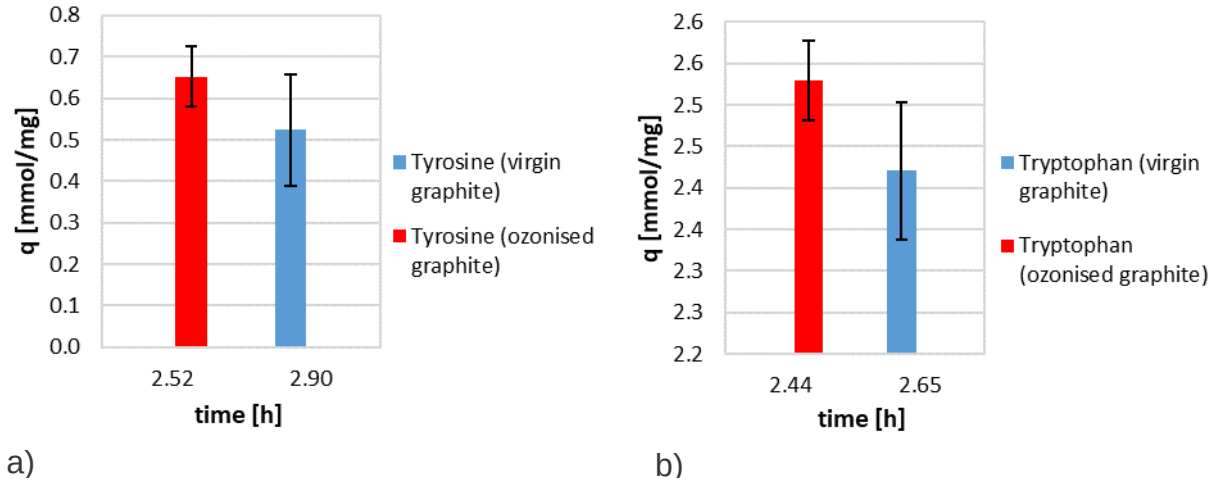

Figure 5.16: Adsorption kinetics tests of L-Tyrosine and L-Tryptophan.

The results of the adsorption kinetics tests show that the adsorption equilibrium tests precautionary should be carried out for 2.5 and 24 hours of shaking time for all test substances, except for L-Tyrosine and L-Tryptophan.

5.3.4 Adsorption Equilibrium Tests

The adsorption isotherms result from the measurements of the individual graphite substance suspensions after the respective shaking period (2.5 h or 24 h). The initial concentrations of the tested substances (phenol, anisole, 1-naphthol, naphthalene, 2-methoxynaphthalene, L-tryptophan and L-tyrosine) was 800 nM in all cases. Various graphite concentrations were used for the different samples (Table 4.2). There was a pH of about 8.0 to 8.2 in all sample solutions during the adsorption process. The corresponding averaged adsorption isotherm with the total error indication of the adsorption load *q* are attached to the appendix (Figure 8.32 - Figure 8.38)

Adsorption isotherms

Phenol

The plot of the adsorption isotherms for phenol shown in the graph indicates that slightly higher solid phase concentration values *q* have been established after a shaking time of 24 hours for both, virgin graphite and ozonised graphite samples (Figure 5.17). The adsorption isotherm for graphite UF1 is significantly higher after 24 h than after 3.5 h. Also, in the adsorption isotherms for anisole (Figure 5.18), 1-naphthol (Figure 5.19) and naphthalene (Figure 5.20), the adsorption equilibrium for both graphite UF1 99.5 and ozonised graphite set after 24 h.

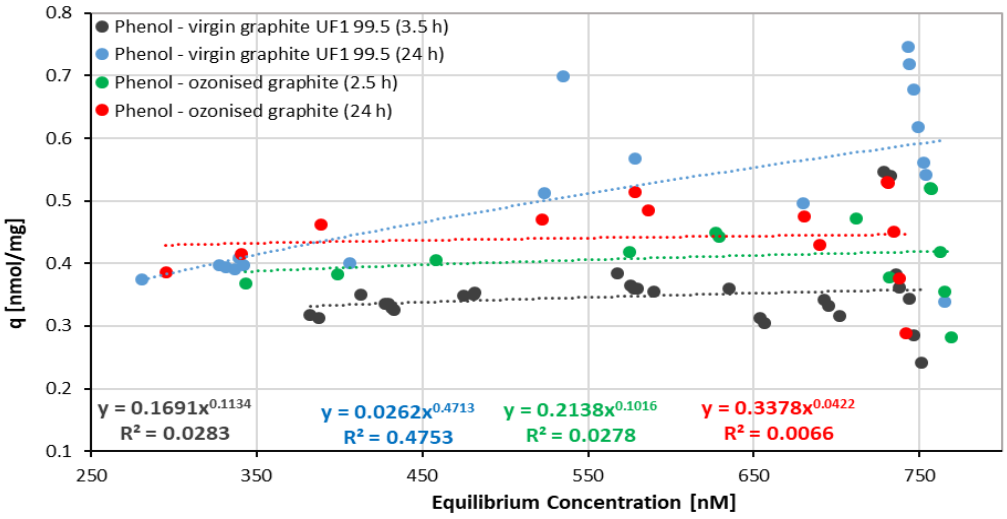

Figure 5.17: Time-dependent adsorption isotherms of Phenol in a single solute graphite species adsorption system

There is no significant difference in the adsorption properties of phenol with respect to graphite UF1 and ozonised graphite. At higher graphite concentrations in the sample suspensions (24 h), the equilibrium concentration is approximately equal for both graphite species. The following table (Table 5.8) lists the corresponding extrapolated Freundlich parameters K_F and *n* which were determined via equation (1) and equation (2).

Table 5.8: Freundlich constant K_f and Freundlich exponent *n* of Phenol measurement series

	Exponential regression		Linear regression	
Sample	**K_f (nmol/mg)/(µmol/L)^n**	***n***	**K_f (nmol/mg)/(µmol/L)^n**	***n***
graphite UF1 (3.5 h)	0.37	0.11	0.37	0.11
graphite UF1 (24 h)	0.68	0.47	0.68	0.47
ozonised graphite (2.5 h)	0.43	0.10	0.43	0.10
ozonised graphite (24 h)	0.45	0.04	0.45	0.04

Freundlich exponents n < 1 indicate high loading values *q* even at low concentrations. Such isotherms are indicated as favourable isotherms (Kümmel and Worch, 1990b).

Anisole

In the adsorption isotherms with the adsorption batch tests for anisole there is no significant difference in the values of the solid phase concentration of the individual measuring points. The difference between the solid phase concentration of all isotherms concerning the samples with the anisole solution is only about 0.2 nmol mg^{-1}. The modification of graphite UF1 has no particular influence on the adsorbent loading capacity. The reason may be the incomplete oxidation grade of graphite UF1. Apparently, not enough functional oxygen groups have formed on the graphite surface due to the ozonation method, or even too much of that functionalities have been existed at the pristine graphite UF1 99.5 samples due to the manufacture's chemical pre-treatment.

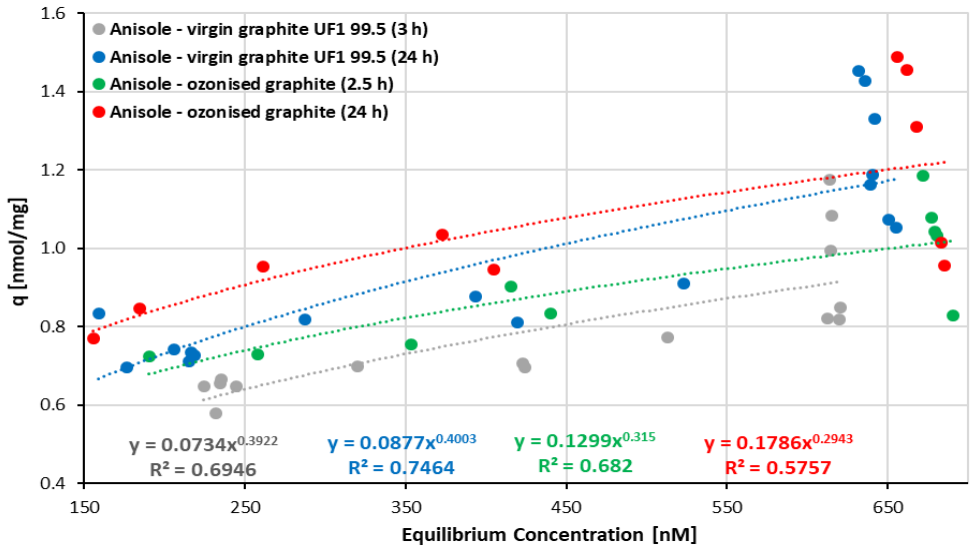

Figure 5.18: Time-dependent adsorption isotherms of Anisole in a single solute graphite species adsorption system

The following table lists the corresponding extrapolated Freundlich parameters K_F and *n* of the anisole test series (Table 5.9).

Table 5.9: Freundlich constant K_f and Freundlich exponent n of Anisole measurement series

	Exponential regression		Linear regression	
Sample	**K_f (nmol/mg)/(µmol/L)^n**	**n**	**K_f (nmol/mg)/(µmol/L)^n**	**n**
graphite UF1 (3 h)	1.10	0.39	1.13	0.44
graphite UF1 (24 h)	1.39	0.40	1.39	0.40
ozonised graphite (2.5 h)	1.14	0.32	1.06	0.27
ozonised graphite (24 h)	1.36	0.29	1.25	0.25

1-Naphthol

In the isotherms of the adsorption batch tests with an adsorption time of 24 h for 1-naphthol, a high difference were found in the loading capacities between both graphite species, graphite UF1 and ozonised graphite (Figure 5.19). Hereof, it can be observed that virgin graphite UF1 has a significantly higher solid phase concentration q as noticed for naphthalene (Figure 5.20) in the same way. However, for all adsorption batch tests for 1-naphthol, the isotherm graph increases with increasing graphite concentration in the samples, contrary to assumptions, indicating that the adsorption equilibrium probably may not have been reached after 24 hours.

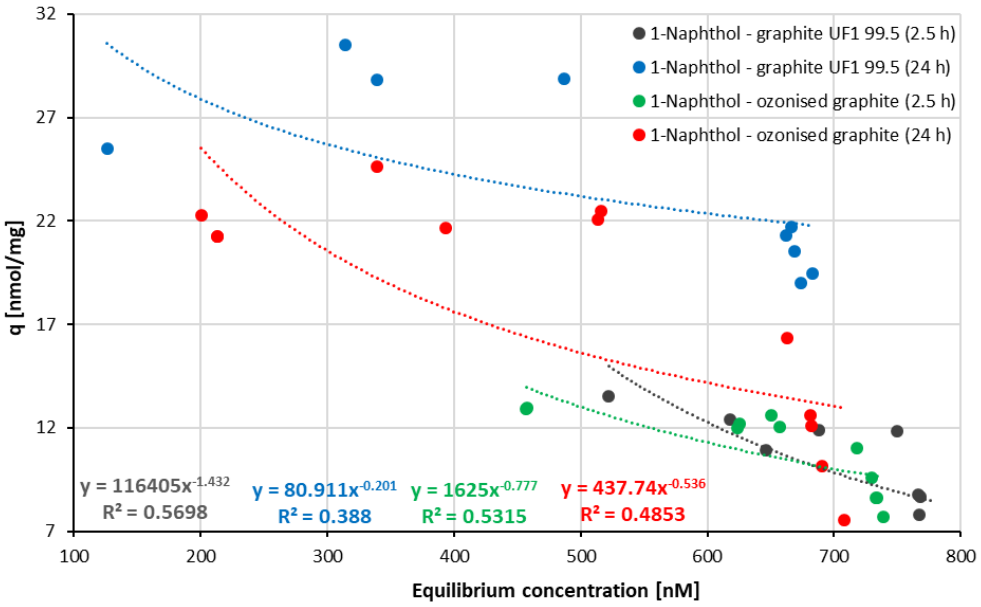

Figure 5.19: Time-dependent adsorption isotherms of 1-Naphthol in a single solute graphite species adsorption system

The following table lists the corresponding Freundlich parameters K_F (extrapolated) and n of the 1-naphthol test series (Table 5.10).

Table 5.10: Freundlich constant K_f and Freundlich exponent n of 1-Naphthol measurement series

	Exponential regression		Linear regression	
Sample	**K_f (nmol/mg)/(µmol/L)^n**	**n**	**K_f (nmol/mg)/(µmol/L)^n**	**n**
graphite UF1 (2.5 h)	5.89	-1.43	5.90	-1.43
graphite UF1 (24 h)	20.18	-0.20	20.17	-0.20
ozonised graphite (2.5 h)	7.58	-0.78	7.91	-0.77
ozonised graphite (24 h)	10.79	-0.54	10.78	-0.54

The reason that the Freundlich exponent n has negative values is due to the fact that the adsorption load q in the adsorption isotherms increases contrary to expectations with decreasing adsorptive equilibrium concentration. Isotherms of this kind are irreversible (Kümmel and Worch, 1990b).

Naphthalene

In general, when assessing the adsorption capacity of both graphite species, virgin graphite and ozonised graphite for the adsorption batch tests of naphthalene, no significant differences can be determined in the samples shaken for 2.5 h taking into account the total error for the individual measurement points (see Appendix, Figure 8.35). In the adsorption isotherm taken from the 24 h-samples, pristine graphite has the highest adsorption capacity. Possibly, hydrophilic oxygen groups at the modified graphite are account for the less well adsorption behaviour of naphthalene.

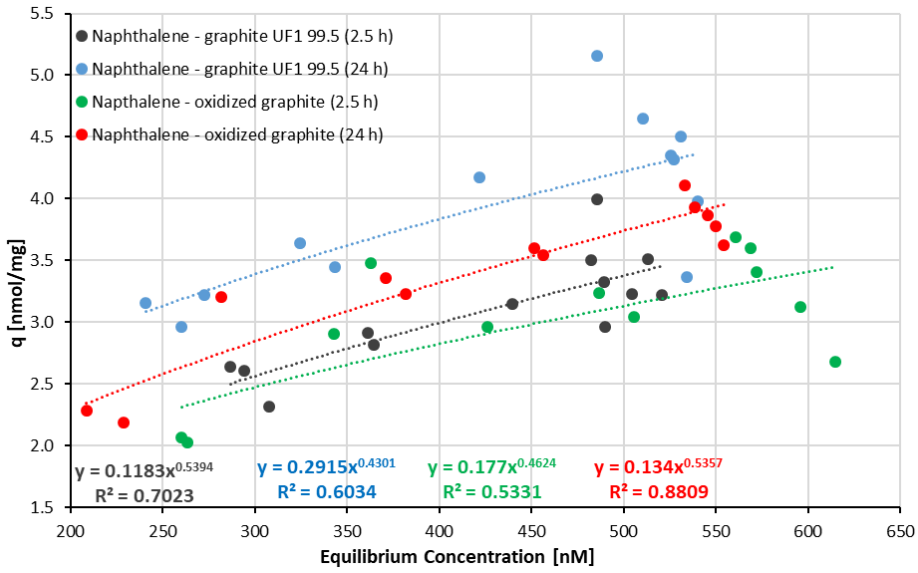

Figure 5.20: Time-dependent adsorption isotherms of Naphthalene in a single solute graphite species adsorption system

The following table lists the corresponding Freundlich parameters K_F (extrapolated) and n of the naphthalene test series (Table 5.11).

Table 5.11: Freundlich constant K_f and Freundlich exponent n of Naphthalene measurement series

	Exponential regression		Linear regression	
Sample	**K_f (nmol/mg)/(µmol/L)^n**	**n**	**K_f (nmol/mg)/(µmol/L)^n**	**n**
graphite UF1 (2.5 h)	4.91	0.54	4.91	0.54
graphite UF1 (24 h)	5.69	0.43	5.69	0.43
ozonised graphite (2.5 h)	4.32	0.46	4.32	0.46
ozonised graphite (24 h)	5.42	0.54	5.42	0.54

2-Methoxynaphthalene

The same conclusion drawn for the adsorption test series of naphthalene is valid for adsorption series experiments of 2-methoxynaphthalene without regarding the measurement results at the higher equilibrium concentration levels. In addition, there is no significant difference in the adsorption isotherms of all test series leading to the assumption that the adsorption equilibrium has set already after 2.5 h.

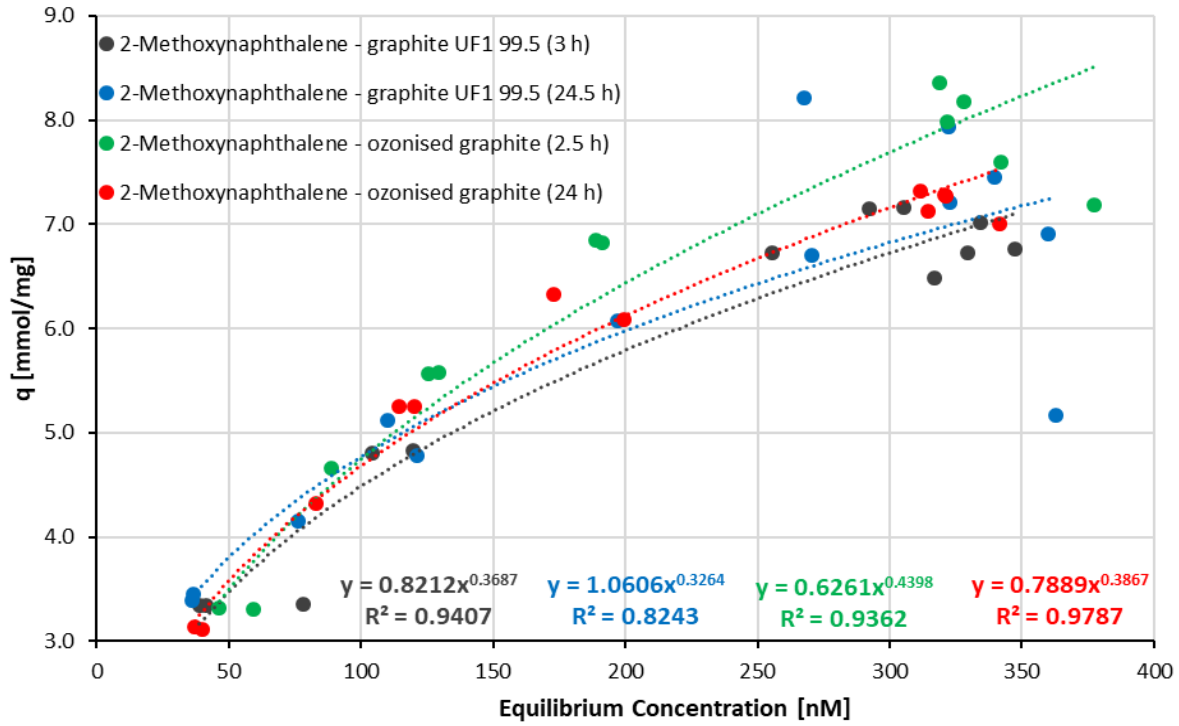

Figure 5.21: Time-dependent adsorption isotherms of 2-Methoxynaphthalene in a single solute graphite species adsorption system

The measurement points at the high equilibrium concentrations were relatively imprecise. When weighing small quantities of graphite, the laboratory balance occasionally showed fluctuating results, possibly caused by static electricity charge.

The corresponding Freundlich parameters K_F (extrapolated) and n are listed in the following table (Table 5.12).

Table 5.12: Freundlich constant K_f and Freundlich exponent n of 2-Methoxynaphthalene measurement series

	Exponential regression		Linear regression	
Sample	**K_f (nmol/mg)/(µmol/L)^n**	**n**	**K_f (nmol/mg)/(µmol/L)^n**	**n**
graphite UF1 (3 h)	10.48	0.37	10.36	0.35
graphite UF1 (24.5 h)	10.11	0.33	10.11	0.33
ozonised graphite (2.5 h)	13.06	0.44	13.06	0.44
ozonised graphite (24 h)	11.41	0.39	11.41	0.39

The adsorption isotherms of 2-methoxynaphthalene with a Freundlich Exponent of n < 1 have developed favourable as they are uniform and move toward the zero point in an exponentially decaying curve (Kümmel and Worch, 1990b).

L-Tryptophan

For the L-tryptophan adsorption batch tests, no significant differences in the adsorption capacities of both graphite species, virgin graphite and ozonised graphite are observed, disregarding the measurements at the high concentrations which are erroneous according to experience. The reason for this is the assumption that the graphite UF1 99.5 may already contain functional surface groups due to a chemical pre-treatment in the manufacturing process, as evidenced by the XPS results (Table 5.5). In addition, presumably no adsorption equilibrium could be established after 2.5 h, but since no adsorption isotherm after 24 h could be recorded due to the poor concentration stability of L-tryptophan, this cannot be proven. Therefore, the adsorption isotherms after 2.5 h are based on a pseudo-equilibrium.

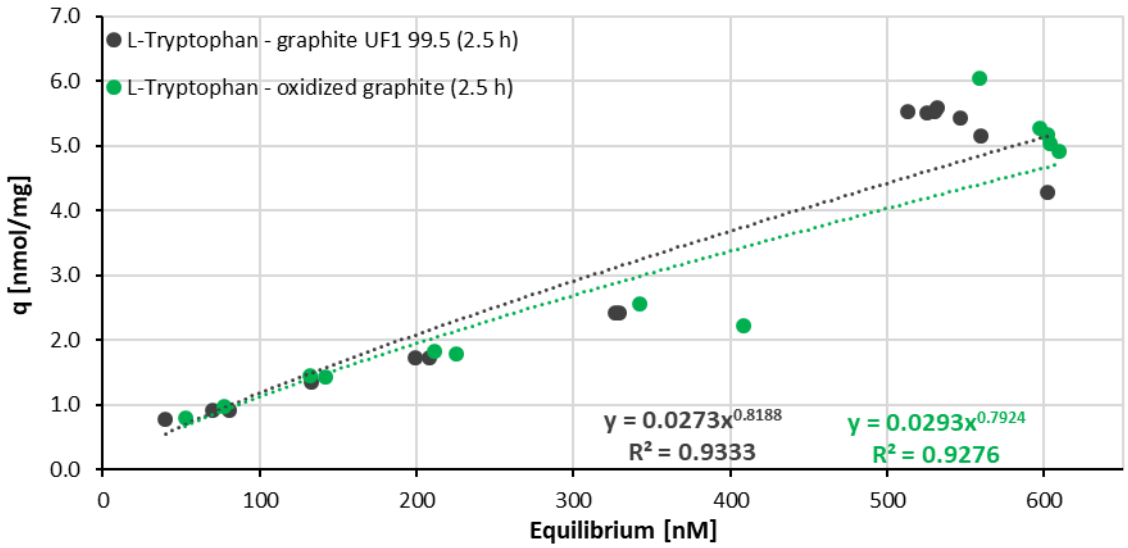

Figure 5.22: Time-dependent adsorption isotherms of L-Tryptophan in a single solute graphite species adsorption system

The corresponding Freundlich parameters K_F (extrapolated) and n are listed in the following table (Table 5.13).

Table 5.13: Freundlich constant K_f and Freundlich exponent n of L-Tryptophan measurement series

	Exponential regression		Linear regression	
Sample	**K_f (nmol/mg)/(µmol/L)^n**	**n**	**K_f (nmol/mg)/(µmol/L)^n**	**n**
graphite UF1 (2.5 h)	7.81	0.82	7.80	0.82
ozonised graphite (2.5 h)	6.98	0.79	6.99	0.79

L-Tyrosine

The adsorption isotherms of L-tyrosine are well developed without considering the measurements at the high equilibrium concentrations where a high deviation is indicated. However, slight differences indicating that the ozonised graphite has a higher solid-phase concentration after 2.5 h (Figure 5.23). Possibly, hydrogen bonds with the H-atoms of the functional groups at the modified graphite surface by the deprotonated carboxyl side group at the prevailing solution pH are established. Since the L-tryptophan and L-tyrosine solutions are rapidly degraded, as shown in the degradation tests (Figure 5.10), only an adsorption pseudo-equilibrium can be achieved in the corresponding adsorption isotherms from the adsorption batch tests conducted over a period of 2.5 h. Whether a different adsorption amount on the graphite samples after reaching the adsorption equilibrium was established after a test period of 24 h could therefore not be checked.

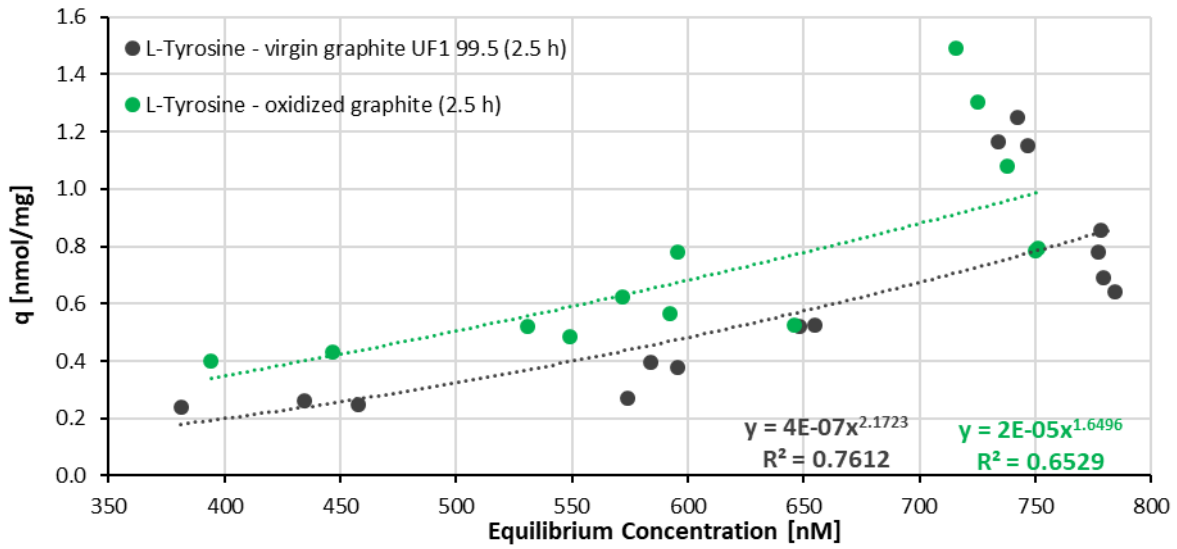

Figure 5.23: Time-dependent adsorption isotherms of L-Tyrosine in a single solute graphite species adsorption system

The corresponding Freundlich parameters K_F (extrapolated) and n are listed in the following table (Table 5.14).

Table 5.14: Freundlich constant K_f and Freundlich exponent *n* of L-Tyrosine measurement series

	Exponential regression		Linear regression	
Sample	**K_f (nmol/mg)/(µmol/L)^n**	***n***	**K_f (nmol/mg)/(µmol/L)^n**	***n***
graphite UF1 (2.5 h)	1.32	2.17	1.46	2.17
ozonised graphite (2.5 h)	1.78	1.65	1.59	1.65

Convex adsorption isotherms with a friendly exponent n > 1 are considered as unfavourable (Kümmel and Worch, 1990b).

Theoretical adsorption loading

An attempt was made to theoretically calculate the adsorption loading *q* on graphite of the individual solutes, assuming that the adsorptive agent is uniformly adsorbed onto the graphite surface in a monolayer (Table 5.15). For this calculation, the analysed BET surface area of 19.269 $m^2\ g^{-1}$ of graphite UF1 99.5, and the Avogadro constant were taken as a basis. The molecular surface area of the substances acting as adsorptive agents is roughly estimated using the software "Avogadro (Version 1.2.0)".

Table 5.15: Theoretically calculated adsorption loading *q* by the estimated molecular surface area

Adsorptive	molecular surface area [m^2]	molecules [g^{-1}]	q [nmol/mg]
Phenol	2.565×10^{-19}	7.51228×10^{19}	1.2×10^{-4}
Anisole	3.462×10^{-19}	5.56586×10^{19}	9.2×10^{-5}
1-Naphthol	3.492×10^{-19}	5.51804×10^{19}	9.2×10^{-5}
Naphthalene	3.328×10^{-19}	5.78996×10^{19}	9.6×10^{-5}
2-Methoxynaphthalene	4.481×10^{-19}	4.30016×10^{19}	7.1×10^{-5}
L-Tryptophan	6.505×10^{-19}	2.96218×10^{19}	4.9×10^{-5}
L-Tyrosine	4.228×10^{-19}	4.55747×10^{19}	7.6×10^{-5}

The theoretically calculated adsorption loading *q* of the individual substances is much lower than measured numbers under real conditions in the experimental procedure. However, the exact molecular surface could not be determined, which is why the calculation is rather inaccurate.

Gaussian error propagation

The calculation basis for the adsorption solid phase concentration q was calculated from the difference between the initial c_0 and equilibrium concentration c of the test substance, the graphite mass $m_{G,S}$ in the sample and the sample solution volume V_S according to the equation (14).

$$q = \frac{\overline{c_0} - \bar{c}}{m_{G,S}} \cdot V \qquad (14)$$

q amount of adsorption

$\overline{c_0}$ mean value of the initial concentration of the tested substance

$\bar{c}$ mean value of the concentration of the tested substance after absorption time

$m_{G,S}$ Mass of graphite in the sample

V_S Volume of the sample solution

During sample preparation, the volume of the graphite mass in the sample solution was small and has been neglected. The effect of the total error due to the measurement uncertainty was calculated using the Gaussian error propagation by the following equation (15):

$$\Delta q = \sqrt{(\frac{\Delta q}{\Delta V_S})^2 * (\Delta V_S)^2 + (\frac{\Delta q}{\Delta m_{G,S}})^2 * (\Delta m_{G,S})^2 + (\frac{\Delta q}{\Delta c_0})^2 * (\Delta c_0)^2 + (\frac{\Delta q}{\Delta c})^2 * (\Delta c)^2} \qquad (15)$$

Δq error of the amount of adsorption

ΔV_S error of the pipette volume (sample volume)

$\Delta m_{G,S}$ error of the analytical balance

Δc_0 Standard deviation of the fluorescence spectrometric initial concentration measurement

Δc Standard deviation of the fluorescence spectrometric concentration measurement after adsorption

The volume error ΔV_S of the 100 mL volumetric pipette (sample volume) was 0.08 mL and the weighing error $\Delta m_{G,S}$ of the analytical balance was 0.1 mg.

Comparison of adsorption isotherms

In the following section the different adsorption isotherms are compared. In this regard, differences in the loading capacity between the individual substances of the parent compound and its derivatives are to be determined. For this purpose, it should be clarified what influence the existing substituents of aromatics have on the adsorption properties of graphite UF1 99.5. Since there is no substantial difference in the solid

phase concentration in the case of ozonised graphite compared to graphite UF1 99.5, the following figures show examples of adsorption isotherms of the individual test substances in a simplified representation derived from the adsorption batch tests with graphite UF1 99.5. The isotherms were compiled from the mean values of the measurement points. The error bars represent the total error (see equation (15)) of the solid phase concentration *q*. All averaged adsorption isotherms from the adsorption equilibrium tests of the individual test substances with the respective error indications are shown in the appendix (Figure 8.32 - Figure 8.32).

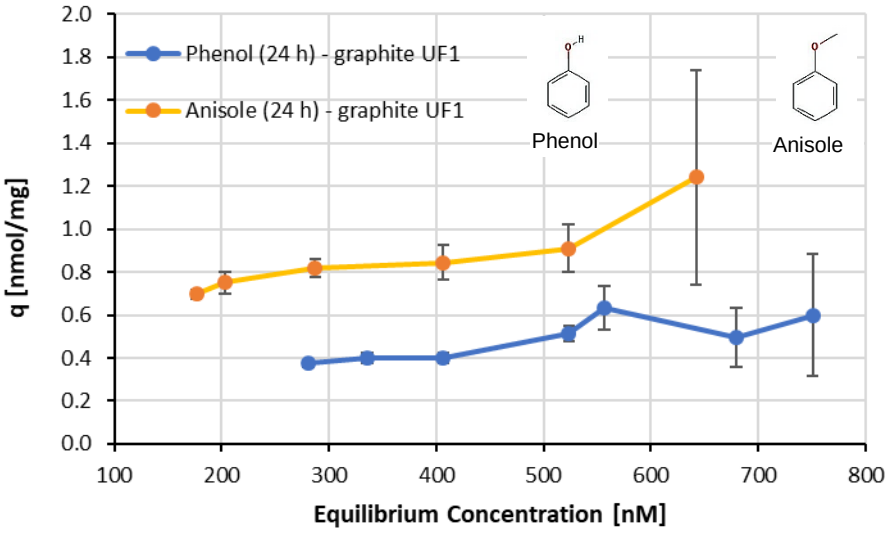

Figure 5.24: Adsorption isotherms of phenol and anisole from the graphite UF 1 99.5 adsorption batch tests

In the adsorption batch test, phenol (pK_a 9.99) was almost completely undissociated at the prevailing pH conditions of about 8.1. The hydroxy group at the aromatic cycle increases the electron density in the aromatic π-system by a positive mesomeric effect (+*M*) more than the methoxy group, meaning the hydroxy group acts more activating (Allinger *et al.*, 1980). This would increase the adsorption affinity of the aromatic system of the phenol molecule to the graphite surface by π-π interactions in contrast to anisole. However, the solid phase concentration at the graphite absorbent surface in the adsorption equilibrium for phenol is lower than for anisole. This is may be due to the fact that phenol is far more hydrophilic than anisole and thus more strongly retained in the aqueous phase. Also, the small fractional degree of dissociation of the OH-group in the phenol molecule at the prevailing solution pH may impair the adsorption behaviour (Figure 5.24).

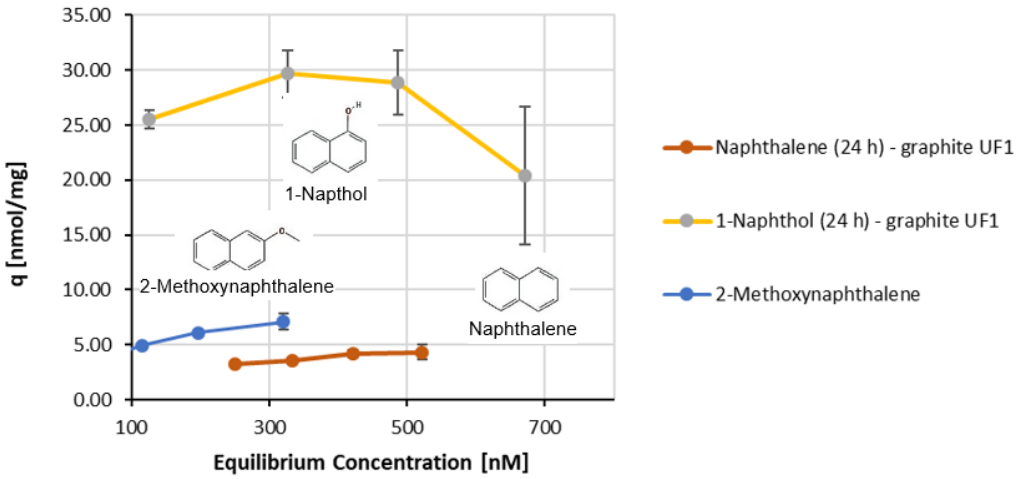

Figure 5.25: Adsorption isotherms of naphthalene, 1-naphthol and 2-methoxynaphthalene from the graphite UF 1 99.5 adsorption batch tests

In general, it may be assumed that the bicyclic aromatics adsorb better to the graphite surface than the monocyclic aromatics. This behaviour can be deduced from the Traube's rule, which states that the adsorption increases with the length of the hydrocarbons (Moreno-Castilla, 2003). When comparing the adsorption isotherms of the bicyclic aromatics (naphthalene, 1-naphthol, 2-methoxynaphthalene) from the test series, it is noticeable that naphthalene is the weakest of all these substances adsorbed onto the graphite UF1 99.5 surface, whereas a relatively strong adsorption is observed for 1-naphthol (Figure 5.25). The reason for this behaviour is obviously the electron density in the aromatic rings, which is higher in the substituted bicyclic aromatics, because of the predominating +*M*-effect of the hydroxy and methoxy group. In this regard, the same rule as for phenol and anisole can be used because the hydroxy group has a more activating effect on the aromatic system than the methoxy group, so that 1-naphthol is adsorbed better than the other derivates (Allinger *et al.*, 1980). The pK_a of 1-naphthol is at pH 9.3. Thus, 1-naphthol was prevailed in undissociated form during the adsorption experiments.

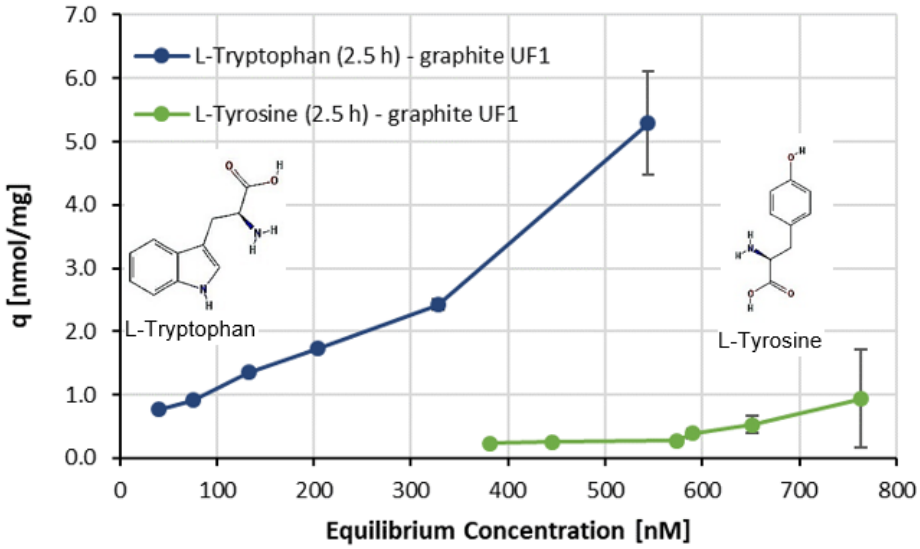

Figure 5.26: Adsorption isotherms of L-tryptophan and L-tyrosine from the graphite UF 1 99.5 adsorption batch tests

The backbone of L-tryptophan consists of a bicyclic aromatic system and thus has a larger π-electron system than tyrosine. As a result, the π-π interactions of L-tryptophan with the π-electrons of the basal planes at the graphite surface are more pronounced than with tyrosine, probably resulting in a stronger adsorption behaviour (Figure 5.26). The solution pH in the adsorption batch test samples of about 8.1 controlled the dissociation of tryptophan and tyrosine as the carboxylic side group of these molecules are deprotonated under these pH conditions (Figure 5.27). Hence, the adsorptive-adsorbent and adsorptive-adsorptive electrostatic interactions are influenced and thus the adsorption process may be profoundly affected, as it was proven for phenol when it was dissociated to phenolate at basic pH (Moreno-Castilla, 2003). Furthermore, the amino groups in L-tryptophan (pK_a 9.34) and L-tyrosine (pK_a 9.04) are in protonated form at a solution pH of 8.1 and may cause a cation-π bond with the π-electrons at the graphite surface (Ji *et al.*, 2009).

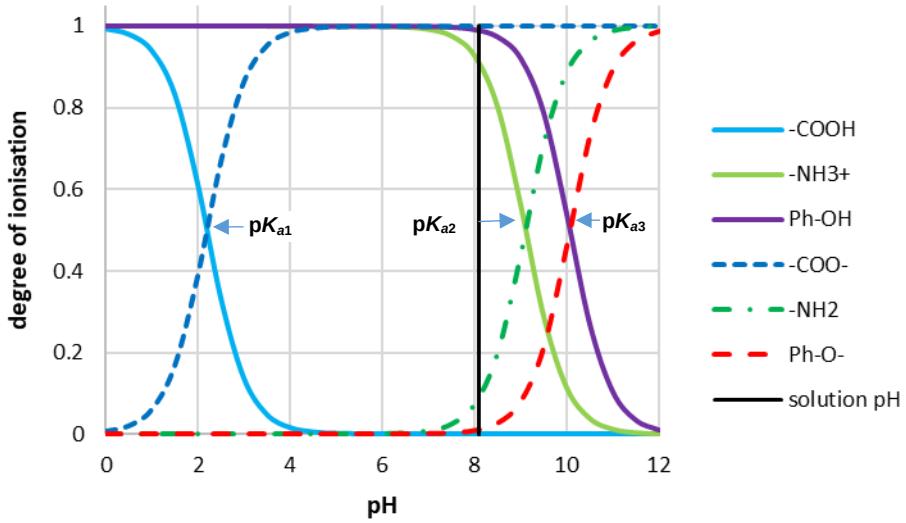

Figure 5.27: Degree of ionisation at the different pK_a values of L-tyrosine

The degree of ionisation α corresponding to the three different pK_a's of L-tyrosine was determined by the following equation (16) and equation (17).

$$\alpha \text{ for weak acids} = \frac{10^{(pH-pKa)}}{1+ 10^{(pH-pKa)}} \qquad (16)$$

$$\alpha \text{ for weak bases} = \frac{10^{(pKa-pH)}}{1+ 10^{(pKa-pH)}} \qquad (17)$$

5.3.5 Filter uptake test of the absorptive substances

After the adsorption experiments, the graphite suspension was separated from the sample solution by filtration. In the experiment, it was found that the membrane filter used for this purpose partly adsorbs the dissolved sample substance. In order to investigate the relative uptake of these substances in the filtration process, the filter uptake test was carried out. The results with the corresponding standard deviation are shown in the following graphics (Figure 5.28 and Figure 5.29).

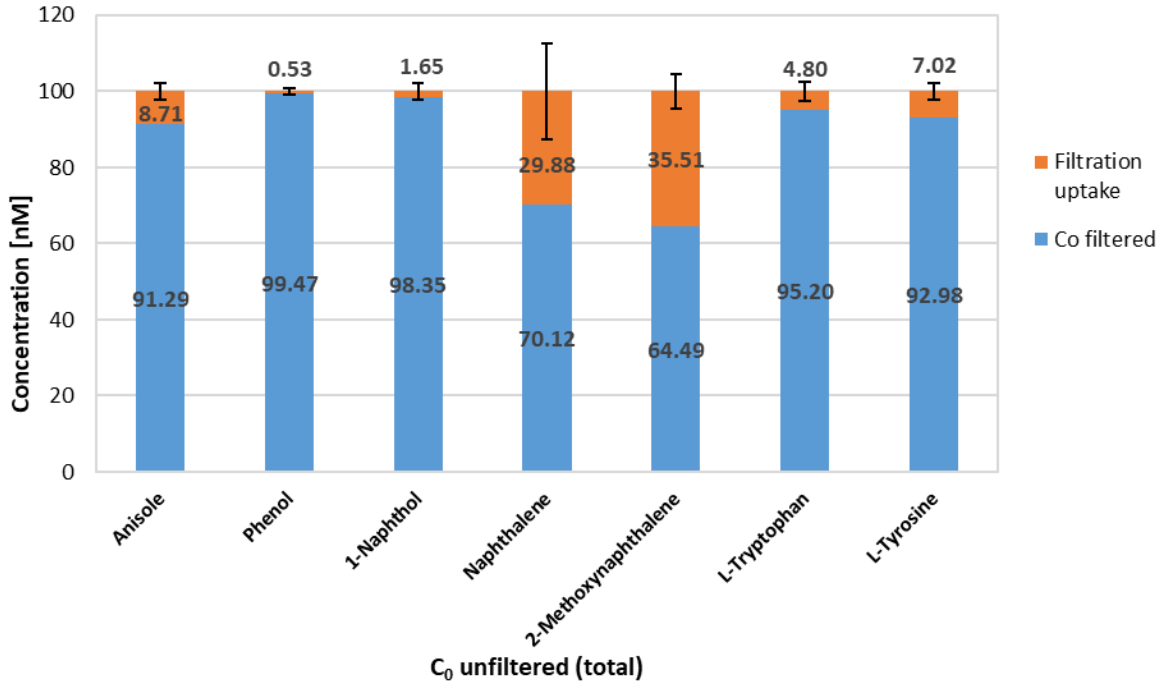

Figure 5.28: Relative filter uptake of the adsorbing substances at few suspension volume

The filter apparatus was washed with 15 ml of substance suspension and then 15 ml of substance suspension were filtered for the sample analysis.

The relative absorption of the dissolved substances from the graphite suspension during the filtering process by the membrane filter is lower when a suspension volume of 50 ml is used for the washing process of the filter apparatus and for the actual filtering for analysis purposes. Therefore, it was decided to use the higher amount of 50 ml of suspension for the filtration process in the experiments.

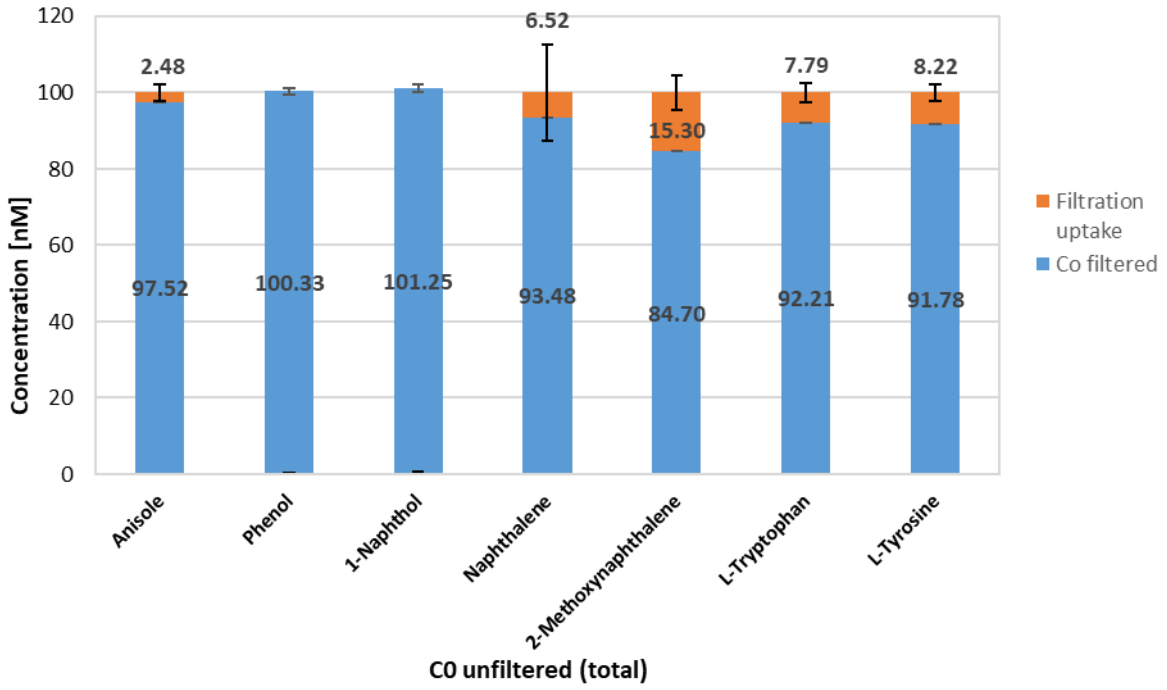

Figure 5.29: Relative filter uptake of the adsorbing substances at much suspension volume

The filter apparatus was washed with 50 ml of substance suspension and then 50 ml of substance suspension were filtered for the sample analysis.

Significant substance losses during filtration were found in naphthalene (6.5 %), 2-methoxynaphthalene (15.3 %), L-tryptophan (7.8 %) and L-tyrosine (8.2 %). For reliable results, it is important to use equal volumes for all samples during the filtration process.

6. Conclusion

Generally, RO-Water has a low ion concentration due to semipermeable membrane filtration (Table 5.1). Therefore, the measured electrical conductivity of 20.1 µS cm^{-1} is low. An ionic concentration due to the self-dissociation of water is still present. The preparation of the water matrix based on RO water was achieved by the addition of $NaHCO_3$ and $MgSO_4$. With increasing ion concentration, the electrical conductivity increases in an aqueous medium, which could be confirmed in an experiment (Table 5.2). The buffer capacity of the water matrix containing the salts $NHCO_3$ (1.5 mM) and $MgSO_4$ (1.5 mM) met the requirements of the experimental procedure because the pH had a relatively stable pH of 8.1 in the adsorption batch tests (Figure 5.1). For the comparison of the adsorption properties of the adsorbents, in addition to graphite UF1 99.5 a modified by oxidation graphite variant was used. The oxygen-containing functional groups introduced by oxidation onto the graphite surface should influence the adsorption affinity of the aromatic test substances in order to be able to investigate the occurring adsorption mechanisms. The various graphite modifications carried out

by means of chemical or thermal oxidation were in part only moderately successful, as found by elemental analysis using EDX and XPS. In the EDX analysis, no reliable results could be achieved on the degree of oxidation of variously modified graphite samples. In all samples an elemental oxygen concentration of less than 1 at. % was measured (Table 5.4). The determination limit for the oxygen detection, which indicates oxygen-containing functional groups, has been undershot due to the expected high measurement error for measurement values below 10 at. % of the total elemental content in the sample (Schmidt, 1994). For this reason, an additional XPS analysis was performed in order to obtain possibly more revealing results. In fact, higher oxygen concentrations were measured in the modified graphite samples via the XPS procedure (Table 5.5). The ozonised graphite sample contained the highest oxygen surface concentration at 5.9 at. %. Also, via a chemical oxidation with hydrogen peroxide (30 %), the oxygen concentration was 5.2 at. %. Hence, the ozonised graphite sample was used for the experimental performance of the adsorption batch tests. The oxygen concentration at the ozonised graphite surface was calculated by the data from the gas adsorption experiment. Theoretically, the oxygen content is 1.3125×10^{-5} mol m^{-2}. In a comparative study on the ozonation of graphite by (Razumovskii *et al.*, 2007), a similar value could be determined. To investigate possible functional oxygen groups onto the modified graphite samples treated with hydrogen peroxide and nitric acid, a potentiometric titration was applied (Figure 5.3). From the results, however, no accurate assessment of the degree of oxidation could take place. The resulting pK_a values are slightly higher for the modified graphite samples compared to untreated graphite. Incorporated functional oxygen groups at the graphite surface are acidic, so the pK_a values would have to be lower. According to the results of the zeta potential measurement, the zeta potentials of virgin graphite and ozonised graphite differ in the acidic pH range of 1 to 3 (Figure 5.5). The ozonised graphite has a higher zeta potential, suggesting a higher Nernst potential (Müller and Hildebrand, 1996). Incorporated acidic functional oxygen groups at the surface of the graphite particles have presumably increased the surface charge, indicating to at least for a small extent a successful oxidation of the graphite surface by acidic functional surface groups. The isoelectric point can also be determined via the zeta potential measurement, which is at the zero point of the zeta potential (Noh and Schwarz, 1989). The isoelectric point is apparently between pH 1 and 2 for graphite UF1 99.5 and at a pH above 1 for the ozonised graphite. The point of the zero charge could not be determined according to the implementation of Noh & Schwarz (1989), since graphite powder, compared to activated carbon, has an insufficient surface area (Figure 5.6). The BET surface area of both samples, virgin graphite (19.27 m^2 g^{-1}) and ozonised graphite (19.49 m^2 g^{-1}), differed only slightly (Table 5.6). A pore formation by the modification process could therefore not be determined. In addition, also no pores in the ozonised graphite were visually detected from the SEM images (Figure 5.7). The BET surface area results were largely consistent with comparative studies of Xu *et al.* (2011) and Chen *et al.* (2012). For the graphite species characterization, finally, a particle size analysis was carried out (Figure 5.4). In summary, the statistical values for the mean value and the median for all graphite species have no significant alternation (Table 5.3). The mode value has remained the same for both species. From

the measured data the surface of graphite UF1 99.5 could be theoretically calculated, which resulted in 1.94 $m^2 g^{-1}$. Thus, the theoretical value is lower than the experimentally determined value obtained by the BET surface area analysis.

The adsorption batch tests were carried out with seven chosen aromatic test substances (Phenol, Anisole, 1-Naphthol, Naphthalene, 2-Methoxynaphthalene, L-Tryptophan and L-Tyrosine). First, the concentration stability of all substances were tested. The results yielded to a concentration stability for at least 24 h for all substances. Exceptionally, the amino acids L-Tryptophan und L-Tyrosine were less stable and began to degrade already after 2.5 h, since they are biomolecules which may be degrades readily by natural processes (Figure 5.10). In another experiment, the background noise of the test substances was measured by fluorescence spectrometry. Only the filtered sample solution without test substances after incubation with the adsorbents, graphite UF1 and ozonised graphite, was investigated (Figure 5.11). For 1-naphthol, anisole, and L-tyrosine, a background noise of up to 55 nM could be detected. For remaining substances, the pseudo-concentration that could influence the results in the adsorption batch test were low. The background noise with the sample solutions incubated in ozonised graphite had critical values of 20 to 35 nM for anisole and 1-naphthol (Figure 5.12). This also applies to the blank samples which were not incubated with graphite, whereby L-tyrosine also having a conspicuous value of 15 nM. The adsorption kinetics tests were used to check after which time an approximately ideal adsorption equilibrium sets in. According to the results, it was decided to carry out the adsorption equilibrium batch tests for a duration of 2.5 h and 24 h for all test substances. Due to the short concentration stability of the aromatic amino acids, the respective adsorption isotherms could only be recorded after 2.5 h, hence only an adsorption pseudo-equilibrium can be reached in these adsorption experiments. It is generally assumed that the graphite was only moderately oxidised via ozonation and only a few functional oxygen groups were formed additionally at the graphite surface. However, due to the pre-treatment of the natural graphite UF1 99.5 in the manufacturing process by sulfuric and fluoric acid possibly originally functional oxygenic surface groups were existing already in the virgin graphite (Table 5.5). In the adsorption batch tests, therefore, only minor deviations in the individual adsorption isotherms of the test substances were found in comparison with the samples of virgin graphite except for 1-napthol and naphthalene. Presumably, there were not enough sets of samples for the individual graphite concentrations to obtain more meaningful results. In the evaluation of the Gaussian error propagation it has been shown that the total error for the loading q is on average higher in the samples with the lower graphite concentrations. Significant deviations in the position of the adsorption isotherms were observed for 1-naphthol, where higher loading concentrations q were reached after 24 h for graphite UF1. For Naphthalene, this observation applies as well. It is possible that the hydrophilic oxygen groups at the modified graphite surface make the bicyclic hydrophobic aromatic compounds less well adsorbed. However, in the adsorption equilibrium for L-tyrosine, higher loading levels were found for the ozonised adsorbent. Possibly, L-tyrosine formed hydrogen bonds with the functional oxygen groups at the modified graphite surface by the deprotonated carboxyl side group at the prevailing

solution pH. In the adsorption process, the electron density in the aromatic rings of the test substances plays an important role which promotes the π-π interaction between the electron rich regions of the basal planes of the graphite surface and the aromatic system of the adsorptive compound. Also, steric hindrance by large side groups may possibly influence the adsorption properties. Anisole is more hydrophobic compared to phenol and is therefore believed to be better adsorbed by the hydrophobic graphite surface. In addition to 2-methoxynaphthalene and naphthalene, 1-naphthol has the highest electron density in the aromatic system due to the predominant +*M* effect of the OH-substituent and is therefore believed to be adsorbed better to graphite UF1 99.5 (Allinger *et al.*, 1980). Due to the dominant +*M* effect of the methoxy group in 2-methoxynaphthalene, the electron density is higher than in naphthalene, which could be reflected in the better adsorption property (Klein, 2015). In general, molecules with many hydrocarbon units are better adsorbed according to the Traube's rule, thus the double-cyclic aromatics could have higher loading values (Moreno-Castilla, 2003). For the bicyclic aromatic compound L-tryptophan, this rule applies also, as opposed to L-tyrosine which has only an aromatic monocycle in the molecular backbone. Furthermore, a cation-π bond with the π-electrons on the graphite surface and the protonated amino groups in L-tryptophan (pK_{aNH3+} 9.34) and L-tyrosine (pK_{aNH3+} 9.04) may have taken place (Ji *et al.*, 2009). Finally, a filter uptake test was executed to measure the loss of substance in the sample solutions of the adsorption batch tests by the membrane filter during the filtration process. In summary, it is recommended to use at least 50 mL sample volume for the washing and filtering process, as the volume loss is higher with less volume. Significant filtration reductions could be observed with naphthalene (6.5 %), 2-methoxynaphthalene (15.3 %), L-tryptophan (7.8 %) and L-tyrosine (8.2 %) even with the higher sample volume.

The method development for the adsorption batch tests with graphite as an adsorbent has taken a lot of time. For the modification of graphite UF1 99.5, in which functional oxygen groups were to be introduced onto the graphite surface via oxidation, a promising method was to be found. In this case, oxidation with potassium permanganate was not carried out. In future scientific studies on this topic, it would therefore be advisable to use potassium permanganate for graphite oxidation in order to possibly obtain a higher functional oxygen surface group concentration according to the scientific study of " A new structural model of graphite oxide" (He *et al.*, 1998). Also, the ozonation of graphite was successful in this regard. However, functional oxygen-containing surface groups may have been incorporated onto the natural graphite UF1 99.5 surface during the manufacturing process (Graphit Kropfmühl GmbH) by a chemical pre-treatment process with sulfuric and fluoric acid. In this regard, it would be useful to remove these possibly present functional surface groups by a thermal treatment at high temperatures in a nitrogen atmosphere. Finally, it is recommended to prepare several sets of samples in the adsorption batch tests for the individual graphite concentrations, even if this takes more time in the experimental procedure. With this measure definitively more precise results can be achieved.

7. References

Allinger, N. L. *et al.* (1980) 'Die aromatische Substitution', in Koßmehl, G. (ed.) *Organische Chemie*. Berlin (Germany): Walter de Gruyter & Co., p. 570. Available at: https://www.degruyter.com/downloadpdf/books/9783110829709/9783110829709.548/9783110829709.548.pdf (Accessed: 15 December 2018).

Bandosz, T. J. *et al.* (1993) 'Characterization of the surfaces of activated carbons in terms of their acidity constant distributions', *Carbon*. Pergamon, 31(7), pp. 1193–1202. doi: 10.1016/0008-6223(93)90072-I.

Bandosz, T. J. and Ania, C. O. (2006) 'Surface chemistry of activated carbons and its characterization', in Bandosz, T. J. (ed.) *Activated Carbon Surfaces in Environmental Remediation*. 1st edn. New York (USA): ELSEVIER, p. 159 ff.

Beckman Coulter Inc. (2001) *COULTER SA 3100 Series Surface Area und Pore Analyzers - Product Manual*. Brea, California (USA).

Beckman Coulter Inc. (2011a) 'Median and Mode', in *LS 13 320 Laser Diffraction Particle Size Analyzer Instructions For Use*. 1st edn. Brea, CA (USA), p. C-6.

Beckman Coulter Inc. (2011b) 'Tornado Dry Powder System', in *LS 13 320 Laser Diffraction Particle Size Analyzer Instructions For Use*. 1st edn. Brea, CA (USA), pp. 6–48.

Bhatnagar, A. *et al.* (2013) 'An overview of the modification methods of activated carbon for its water treatment applications', *Chemical Engineering Journal*. Elsevier, 219, pp. 499–511. doi: 10.1016/J.CEJ.2012.12.038.

Borlinghaus, R. T. (2016) 'Fluoreszenz', in *Konfokale Mikroskopie in Weiß*. Berlin, Heidelberg: Springer Berlin Heidelberg, pp. 29–53. doi: 10.1007/978-3-662-49359-5_2.

Brodie, B. C. (1859) 'On the Atomic Weight of Graphite', *Philosophical Transactions of the Royal Society of London*. The Royal Society, 149(0), pp. 249–259. doi: 10.1098/rstl.1859.0013.

Brunauer, S., Emmett, P. H. and Teller, E. (1938) *Adsorption of Gases in Multimolecular Layers*. Available at: https://pubs.acs.org/sharingguidelines (Accessed: 28 October 2018).

Çeçen, F. and Aktaş, O. (2012a) 'Activated carbon for water and wastewater treatment : integration of adsorption and biological treatment', in *Historical Appraisal of Activated Carbon*. Weinheim (Germany): Wiley-VCH, pp. 1–3.

Çeçen, F. and Aktaş, O. (2012b) 'Temperature', in *Activated carbon for water and wastewater treatment : integration of adsorption and biological treatment*. Weinheim (Germany): Wiley-VCH, p. 20.

Chen, C.-M. *et al.* (2012) 'Structural evolution during annealing of thermally reduced graphene nanosheets for application in supercapacitors', *Carbon*. ELSEVIER, 50(10), pp. 3572–3584. Available at: https://doi.org/10.1016/j.carbon.2012.03.029 (Accessed: 11 November 2018).

Chung, D. D. L. (2002) 'Review: Graphite', *Journal of Materials Science*, pp. 1475–1489. doi: 10.1023/A:1014915307738.

Coughlin, R. V. and Ezra, F. S. (1968) *Role of Surface Acidity in the Adsorption of Organic Pollutants on the Surface of Carbon*. UTC. Available at: https://pubs.acs.org/sharingguidelines (Accessed: 27 October 2018).

Eggert, F. (2005) 'Anregung der charakteristischen Strahlung', in *Standardfreie Elektronenstrahlmikroanalyse mit dem EDX im Rasterelektronenmikroskop*. Norderstedt (Germany): Books on Demand GmbH, p. 19 ff. Available at: http://www.mikroanalytik.de/Download/ESMA-Leseprobe.pdf (Accessed: 15 October 2018).

Electrical Conductivity (EC) (2015) *aqion.de*. Available at: http://www.aqion.de/site/130 (Accessed: 5 November 2018).

Franz, M., Arafat, H. A. and Pinto, N. G. (2000) 'Effect of chemical surface heterogeneity on the adsorption mechanism of dissolved aromatics on activated carbon', *Carbon*. Pergamon, 38(13), pp. 1807–1819. doi: 10.1016/S0008-6223(00)00012-9.

Gupta, V. *et al.* (2017) 'Higher oxidation level in graphene oxide', *Optik*. Urban & Fischer, 143, pp. 115–124. doi: 10.1016/J.IJLEO.2017.05.100.

Haasch, R. T. (2014) 'X-Ray Photoelectron Spectroscopy (XPS) and Auger Electron Spectroscopy (AES)', in Sardela, M. (ed.) *Practical materials characterization*. New York: Springer, p. 93 ff. Available at: https://books.google.de/books?id=umEgBAAAQBAJ&pg=PA93&dq=isbn:1461492807&hl=de&source=gbs_toc_r&cad=3#v=onepage&q&f=false (Accessed: 16 October 2018).

Haydar, S. *et al.* (2003) 'Adsorption of p-nitrophenol on an activated carbon with different oxidations', *Carbon*. Pergamon, 41(3), pp. 387–395. doi: 10.1016/S0008-6223(02)00344-5.

He, H. *et al.* (1998) 'A new structural model for graphite oxide', *Chemical Physics Letters*. North-Holland, 287(1–2), pp. 53–56. doi: 10.1016/S0009-2614(98)00144-4.

Ivančev-Tumbas, I. (2014) 'The fate and importance of organics in drinking water treatment: a review', *Environmental Science and Pollution Research*. Springer Berlin Heidelberg, 21(20), pp. 11794–11810. doi: 10.1007/s11356-014-2894-8.

Jander, G. and Jahr, K. F. (1989) *Maßanalyse: Theorie und Praxis der Titration mit chemischen u. physikalischen Indikationen*. De Gruyter.

Ji, L. *et al.* (2009) 'Mechanisms for strong adsorption of tetracycline to carbon nanotubes: A comparative study using activated carbon and graphite as adsorbents', *ENVIRONMENTAL SCIENCE & TECHNOLOGY*, 43, pp. 2322–2327. doi: 10.1021/es803268b.

Kanda, K. (1991) 'Energy dispersive X-ray spectrometer'. Available at: https://patentimages.storage.googleapis.com/57/77/03/f02cb9f2384bf0/US5065020.pdf (Accessed: 16 October 2018).

Kienle, H. von and Bäder, E. (1980a) 'Methoden zur Charakterisierung von Aktivkohlen', in *Aktivkohle und ihre industrielle Anwendung*. Stuttgart (Germany): Ferdinand Enke Verlag, pp. 56–57.

Kienle, H. von and Bäder, E. (1980b) 'Wasserreinigung', in *Aktivkohle und ihre*

industrielle Anwendung. Stuttgart (Germany): Ferdinand Enke Verlag, p. 143.

Klein, D. R. (2015) 'Aktivierung und Desaktivierung', in *Wiley Schnellkurs Organische Chemie Synthese*. 1. Weinheim: Wiley-VCH, pp. 43–45. Available at: https://books.google.de/books?id=_7ZNCAAAQBAJ&printsec=frontcover&hl=de&source=gbs_ge_summary_r&cad=0#v=onepage&q&f=false (Accessed: 27 November 2018).

Kümmel, R. and Worch, E. (1990a) 'Adsorberpolymere', in *Adsorption aus wässrigen Lösungen*. Leipzig (Germany): VEB Deutscher Verlag für Grundstoffindustrie, p. 28.

Kümmel, R. and Worch, E. (1990b) 'Adsorptionsgleichgewichte', in *Adsorption aus wässrigen Lösungen*. 1st edn. Leipzig (Germany): VEB Deutscher Verlag für Grundstoffindustrie, p. 54.

Kümmel, R. and Worch, E. (1990c) 'Grundbegriffe der Adsorption', in *Adsorption aus wässrigen Lösungen*. Leipzig (Germany): VEB Deutscher Verlag für Grundstoffindustrie, pp. 17–21.

Lakowicz, J. R. (2006) *Principles of fluorescence spectroscopy*. 3rd Editio. Boston (USA): Springer Science+Business Media, LLC.

Latscha, H. P., Kazmaier, U. and Klein, H. A. (2016) 'Substituenten-Effekte', in *Organische Chemie - Chemie-Basiswissen II*. 7. Berlin Heidelberg (Germany): Springer Spektrum, pp. 29–30.

Lazar, Gerhard, M. D. *et al.* (1986) 'Verfahren zur Gewinnung von hochreinem Graphit aus Naturgraphit'. European Patent Office.

Lee, D. W. *et al.* (2010) 'The Structure of Graphite Oxide: Investigation of Its Surface Chemical Groups', *The Journal of Physical Chemistry B*. American Chemical Society, 114(17), pp. 5723–5728. doi: 10.1021/jp1002275.

Lide, D. R. *et al.* (2005) *CRC Handbook of Chemistry and Physics Editor-in-Chief*. Version 20. Boca Ranton (USA): CRC Press LLC. Available at: https://s3.amazonaws.com/academia.edu.documents/49221189/CRC_Handbook_of_Chemistry_and_Physics_85th_ed_-_David_R._Lide.pdf?AWSAccessKeyId=AKIAIWOWYYGZ2Y53UL3A&Expires=1540989278&Signature=FwDJ33wHq4HVczB8W8%2BkIUaxSwU%3D&response-content-disposition=inlin (Accessed: 31 October 2018).

Loveland, P. J. and Whalley, W. R. (2000) 'Particle Size Analysis', in Smith, K. A. and Mullins, C. E. (eds) *Soil and Environmental Analysis: Physical Methods, Revised, and Expanded*. 2nd edn. New York (USA): Marcel Dekker, Inc., pp. 281–308.

Mahajan, O. P., Moreno-Castilla, C. and Walker, P. L. (1980) 'Surface-Treated Activated Carbon for Removal of Phenol from Water', *Separation Science and Technology*. Taylor & Francis Group, 15(10), pp. 1733–1752. doi: 10.1080/01496398008055619.

Marcano, D. C. *et al.* (2010) 'Improved Synthesis of Graphene Oxide', *ACS Nano*, 4(8), pp. 4806–4814. doi: 10.1021/nn1006368.

Mattson, J. A. *et al.* (1969) 'Surface chemistry of active carbon: Specific adsorption of phenols', *Journal of Colloid and Interface Science*. Academic Press, 31(1), pp. 116–130. doi: 10.1016/0021-9797(69)90089-7.

Mazumder, M. *et al.* (2018) ‘SEM and ESEM techniques used for analysis of asphalt binder and mixture: A state of the art review’, *Construction and Building Materials*, 186, pp. 313–329. doi: 10.1016/j.conbuildmat.2018.07.126.

McCelland, A. and Mankin, M. (2018) ‘Fluorescence Spectroscopy’, in *Optical Measurements for Scientists and Engineers: A Practical Guide*. Cambridge (United Kingdom): Cambridge University Press, pp. 118–120. Available at: https://books.google.de/books?id=N7pQDwAAQBAJ&pg=PR3&hl=de&source=gbs_selected_pages&cad=2#v=onepage&q&f=false (Accessed: 21 October 2018).

Menéndez-Díaz, J. A. and Martín-Gullón, I. (2006) ‘Types of carbon adsorbents and their production’, in Bandosz, T. J. (ed.) *Activated carbon surfaces in environmental remediation: Volume 7*. 1st edn. San Diego (USA): Elsevier Science Publishing Co Inc, pp. 1–48. Available at: http://digital.csic.es/bitstream/10261/95477/1/Types of carbon adsorbents and their producton.pdf (Accessed: 2 December 2018).

Mezzi, A. and Kaciulis, S. (2010) ‘Surface investigation of carbon films: from diamond to graphite’, *SURFACE and INTERFACE ANALYSIS (John Wiley & Sons Ltd)*, 50(11), pp. 1082–1084. doi: DOI 10.1002/sia.3348.

Mizokawa, Y. *et al.* (1987) ‘Comparison of the CKLL first-derivative auger spectra from XPS and AES using diamond, graphite, SiC and diamond-like-carbon films’, *Surface Science*. North-Holland, 182(3), pp. 431–438. doi: 10.1016/0039-6028(87)90011-2.

Moreno-Castilla, C. *et al.* (1995) *Activated Carbon Surface Modifications by Nitric Acid, Hydrogen Peroxide, and Ammonium Peroxydisulfate Treatments*, *Langmuir*. Available at: https://pubs.acs.org/sharingguidelines (Accessed: 5 October 2018).

Moreno-Castilla, C. (2003) ‘Adsorption of organic molecules from aqueous solutions on carbon materials’, *ELSEVIER*. doi: 10.1016/j.carbon.2003.09.022.

Müller, R. H. and Hildebrand, G. E. (1996) *Zetapotential und Partikelladung in der Laborpraxis*. Stuttgart (Germany): Wissenschaftliche Verlagsgesellschaft mbH.

Murphy, K. R. *et al.* (2010) ‘Measurement of Dissolved Organic Matter Fluorescence in Aquatic Environments: An Interlaboratory Comparison’, *Environmental Science & Technology*. American Chemical Society, 44(24), pp. 9405–9412. doi: 10.1021/es102362t.

Nikam, K. and Hydarali (2018) ‘A Scientometric Analysis of Graphite Research in India: 1989–2014’, *Journal of Advancements in Library Sciences*, 3(1), pp. 6–12. Available at: http://sciencejournals.stmjournals.in/index.php/JoALS/article/view/355/182 (Accessed: 2 November 2018).

Noh, J. S. and Schwarz, J. A. (1989) ‘Estimation of the point of zero charge of simple oxides by mass titration’, *Journal of Colloid and Interface Science*. Academic Press, 130(1), pp. 157–164. doi: 10.1016/0021-9797(89)90086-6.

Orrit, M. (2016) *SINGLE MOLECULE OPTICS-2016*. Leiden (Netherlands). Available at: https://pdfs.semanticscholar.org/de20/723bfa9f3bd686dee1511145466f0542e00a.pdf (Accessed: 3 November 2018).

Pierson, H. O. (1993a) ‘Graphite Structure and Poperties’, in *HANDBOOK OF CARBON, GRAPHITE, DIAMOND AND FULLERENES: Properties, Processing and Applications*. New Jersey (USA): Noyes Publications, pp. 43–68.

Pierson, H. O. (1993b) ‘THE GRAPHITIZATION PROCESS’, in *HANDBOOK OF CARBON, GRAPHITE, DIAMOND AND FULLERENES: Properties, Processing and Applications*. New Jersey (USA): Noyes Publications, pp. 81–82.

Polansky, O. E. (1963) ‘Bestimmung des Parameters der Methylgruppe und M-Effekt der Methylgruppe’, *Monatshefte für Chemie*. Springer-Verlag, 94(1), pp. 43–50. doi: 10.1007/BF00900218.

Pollard, S. J. T. *et al.* (1992) ‘Low-cost adsorbents for waste and wastewater treatment: a review’, *Science of The Total Environment*. Elsevier, 116(1–2), pp. 31–52. doi: 10.1016/0048-9697(92)90363-W.

Pratt, A. R., Muir, I. J. and Nesbitt, H. W. (1993) ‘X-ray photoelectron and Auger electron spectroscopic studies of pyrrhotite and mechanism of air oxidation’, *Pergamon*, 58, p. 829. Available at: https://ac.els-cdn.com/0016703794905088/1-s2.0-0016703794905088-main.pdf?_tid=9d24aa12-1bb7-446d-9020-58c17d38f57b&acdnat=1539865090_2e613b4823305cbea542d41d82b836c7 (Accessed: 18 October 2018).

PubChem Substance and Compound databases (2018) *Phenol, Anisole, 1-Naphthalene, 2-Methoxynaphthalene, L-Tyrosine, L-Tryptophan*. Available at: https://pubchem.ncbi.nlm.nih.gov (Accessed: 31 October 2018).

Radovic, L. R., Morena-Castilla, C. and Rivera-Utrilla, J. (2001) ‘CARBON MATERIALS AS ADSORBENTS IN AQEOUS SOLUTIONS’, in Radovic, L. R. (ed.) *Chemistry and Physics of Carbon : A series of advances (VOLUME 27)*. New York (USA): Marcel Dekker, Inc, pp. 228–241.

Razumovskii, S. D. *et al.* (2007) ‘Carbon Nanostructure Reactivity: Reactions of Graphite Powders with Ozone’, *Fullerenes, Nanotubes and Carbon Nanostructures*. Taylor & Francis Group , 15(1), pp. 53–63. doi: 10.1080/15363830600812423.

Rivera-Utrilla, J. *et al.* (2011) ‘Activated carbon modifications to enhance its water treatment applications. An overview’, *Journal of Hazardous Materials*. Elsevier, 187(1–3), pp. 1–23. doi: 10.1016/J.JHAZMAT.2011.01.033.

Sablinskas, V. (2003) ‘Fluorescence Spectrometers’, in Gauglitz, G. and Vo-Dinh, T. (eds) *Handbook of Spectroscopy*. Weinheim: WILEY-VCH Verlag GmbH & Co. KGaA, pp. 66–68.

Salame, I. I. and Bandosz, T. J. (2001) ‘Surface Chemistry of Activated Carbons: Combining the Results of Temperature-Programmed Desorption, Boehm, and Potentiometric Titrations.’, *Journal of colloid and interface science*, 240(1), pp. 252–258. doi: 10.1006/jcis.2001.7596.

Schirmer, U. (2018) *Die Adsorption von Dispersionspartikeln und Schutzkolloiden an Oberflächen von Zementphasen und Phasen der Zusatzstoffe*. Weimar. Available at: https://e-pub.uni-weimar.de/opus4/frontdoor/deliver/index/docId/3738/file/Ulrike_Schirmer_Dissertation.pdf (Accessed: 30 November 2018).

Schmidt, P. F. (1994) ‘Zu erwartende Genauigkeiten und Nachweisgrenzen’, in *Praxis der Rasterelektronenmikroskopie und Mikrobereichsanalyse*. Renningen-Malmsheim (Germany): expert verlag, pp. 434–435.

Shindo, D. and Oikawa, T. (2002a) ‘Basic Principles of Analytical Electron Microscopy’,

in *Analytical Electron Microscopy for Materials Science*. Tokyo: Springer Japan, pp. 1–11. Available at: http://link.springer.com/10.1007/978-4-431-66988-3_1 (Accessed: 15 October 2018).

Shindo, D. and Oikawa, T. (2002b) 'Energy Dispersive X-ray Spectroscopy', in *Analytical Electron Microscopy for Materials Science*. Tokyo: Springer Japan, p. 81. Available at: http://link.springer.com/10.1007/978-4-431-66988-3_4 (Accessed: 15 October 2018).

Smeljansky, M. (2006) *Synthese der mikro- und mesoporösen zeolithartigen Gerüstalumosilikate und Untersuchung ihres katalytischen Einflusses auf die Friedel-Crafts-Reaktion und die Kolbe-Schmidt-Carboxylierung*. Diplomica Verlag GmbH.

Sontheimer, H., Frick, B. R., Fettig Joachim, *et al.* (1985) 'Beziehungen zwischen den einzelnen Dichten und Bestimmungsmethoden', in *Adsorptionsverfahren zur Wasserreinigung*. Karlsruhe (Germany): DVGW-Forschungsstelle am Engler-Bunte Institut der Universität Karlsruhe (TH), pp. 80–84.

Sontheimer, H., Frick, B. R., Fettig, J., *et al.* (1985) 'Die FREUNDLICH-Isotherme', in *Adsorptionsverfahren zur Wasserreinigung*. Karlsruhe (Germany): Engler-Bunte-Institut der Universität Karlsruhe (TH), p. 131.

Stieß, M. (2009) 'Spezifische Oberfläche', in *Particle Size Analysis*. 3. Berlin Heidelberg: Springer-Verlag, pp. 16–17. doi: 10.1007/978/3-540-32552-9.

Subrahmanyam, C., Bulushev, D. A. and Kiwi-Minsker, L. (2005) 'Dynamic behaviour of activated carbon catalysts during ozone decomposition at room temperature', *Applied Catalysis B: Environmental*. Elsevier, 61(1–2), pp. 98–106. doi: 10.1016/J.APCATB.2005.04.013.

Szabó, T. *et al.* (2006) 'Evolution of Surface Functional Groups in a Series of Progressively Oxidized Graphite Oxides', *CHEMISTRY OF MATERIALS*. American Chemical Society, 18(11), pp. 2740–2749. doi: 10.1021/CM060258+.

Terzyk, A. P. *et al.* (2003) 'New correlations between the composition of the surface layer of carbon and its physicochemical properties exposed while paracetamol is adsorbed at different temperatures and pH', *Journal of Colloid and Interface Science*. Academic Press, 257(1), pp. 13–30. doi: 10.1016/S0021-9797(02)00032-2.

Verliefde, A. *et al.* (2007) 'Priority organic micropollutants in water sources in Flanders and the Netherlands and assessment of removal possibilities with nanofiltration', *Environmental Pollution*. Elsevier, 146(1), pp. 281–289. doi: 10.1016/J.ENVPOL.2006.01.051.

Verma, H. R. (2007) 'X-Ray Photoelectron Spectroscopy', in *Atomic and Nuclear Analytical Methods*. Patiala (India): Springer Berlin Heidelberg, pp. 213–241. Available at: http://link.springer.com/10.1007/978-3-540-30279-7_5 (Accessed: 18 October 2018).

Wollrab, A. (2014) 'Aromatische Verbindungen', in *Organische Chemie*. 4th edn. Berlin Heidelberg (Germany): Springer Spektrum, p. 246.

Worch, E. (2012) 'Adsorption as a surface process', in *Adsorption Technology in Water Treatment - Fundamentals, Processes, and Modeling*. Berlin (Germany): Walter de Gruyter GmbH & Co, p. 1.

Wu, Y. . *et al.* (2002) ‘Modified natural graphite as anode material for lithium ion batteries’, *Journal of Power Sources*. Elsevier, 111(2), pp. 329–334. doi: 10.1016/S0378-7753(02)00349-X.

Xu, B. *et al.* (2011) ‘What is the choice for supercapacitors: graphene or graphene oxide?’, *Energy & Environmental Science*. Royal Society of Chemistry, 4(8), pp. 2826–2830. doi: 10.1039/c1ee01198g.

Yaya, A. *et al.* (2012) *Layered Nanomaterials-A Review Valorisation of Local Materials for Sustainable Structural Applications View project LAYERED NANOMATERIALS-A REVIEW*. Available at: https://www.researchgate.net/publication/269035537 (Accessed: 13 August 2018).

Yin, C. Y., Aroua, M. K. and Daud, W. M. A. W. (2007) ‘Review of modifications of activated carbon for enhancing contaminant uptakes from aqueous solutions’, *Separation and Purification Technology*. Elsevier, 52(3), pp. 403–415. doi: 10.1016/J.SEPPUR.2006.06.009.

Yong, A. *et al.* (2015) ‘Refinements to the structure of graphite oxide: absolute quantification of functional groups via selective labelling †’, 7, p. 20256. doi: 10.1039/c5nr05891k.

Zawadzki, M. *et al.* (2012) ‘Vapor−Liquid Equilibrium Data for Binary Systems of 1H-Pyrrole with Butan-1-ol, Propan-1-ol, or Pentan-1-ol’. doi: 10.1021/je3004194.

8. Appendix

8.1 3D-fluorescence-excitation-emission-matrix (FEEM)

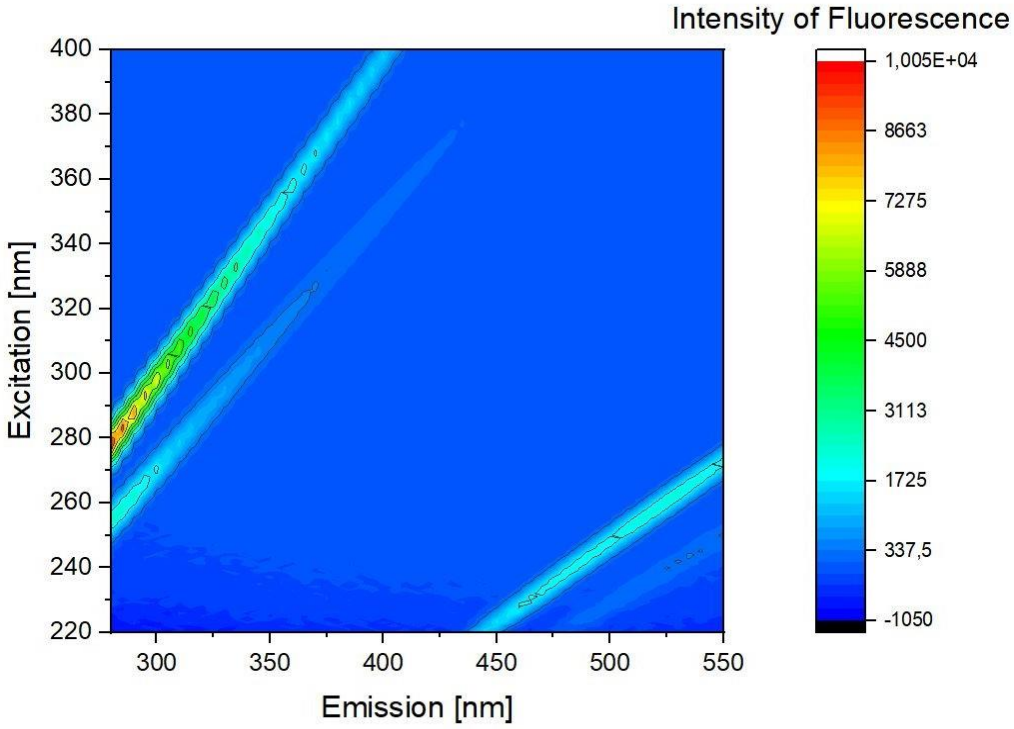

Figure 8.1: 3D-fluorescence-excitation-emission matrix of water matrix

Without IHU 310 UV transmitting filter

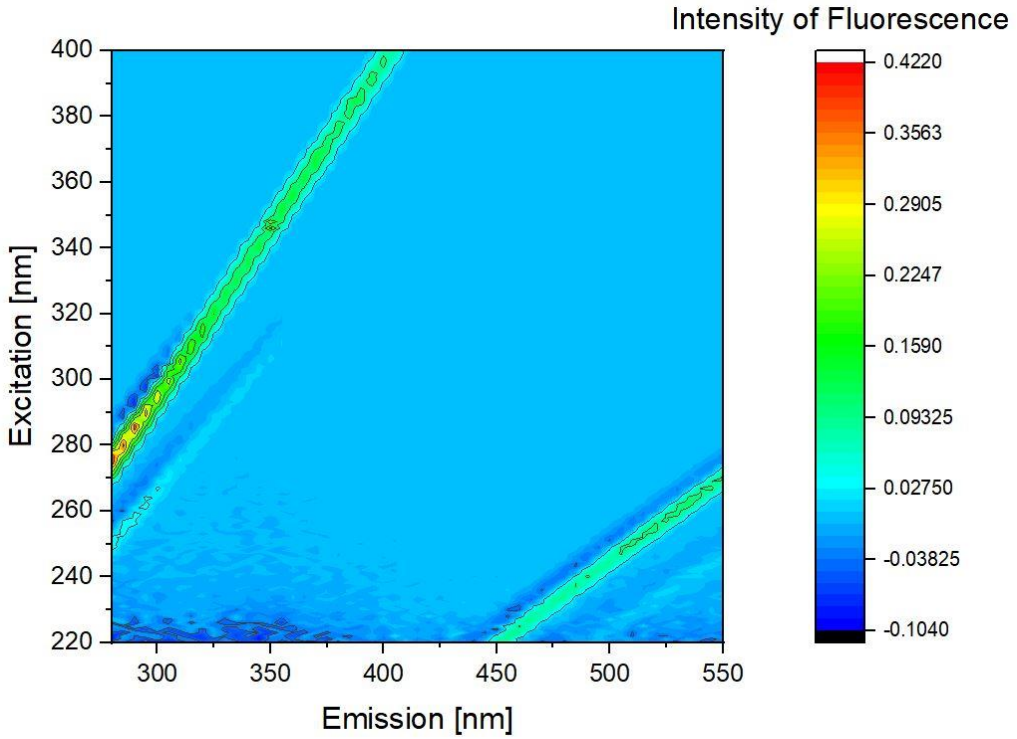

Figure 8.2: 3D-fluorescence-excitation-emission matrix of water matrix incubated in virgin graphite

Without IHU 310 UV transmitting filter

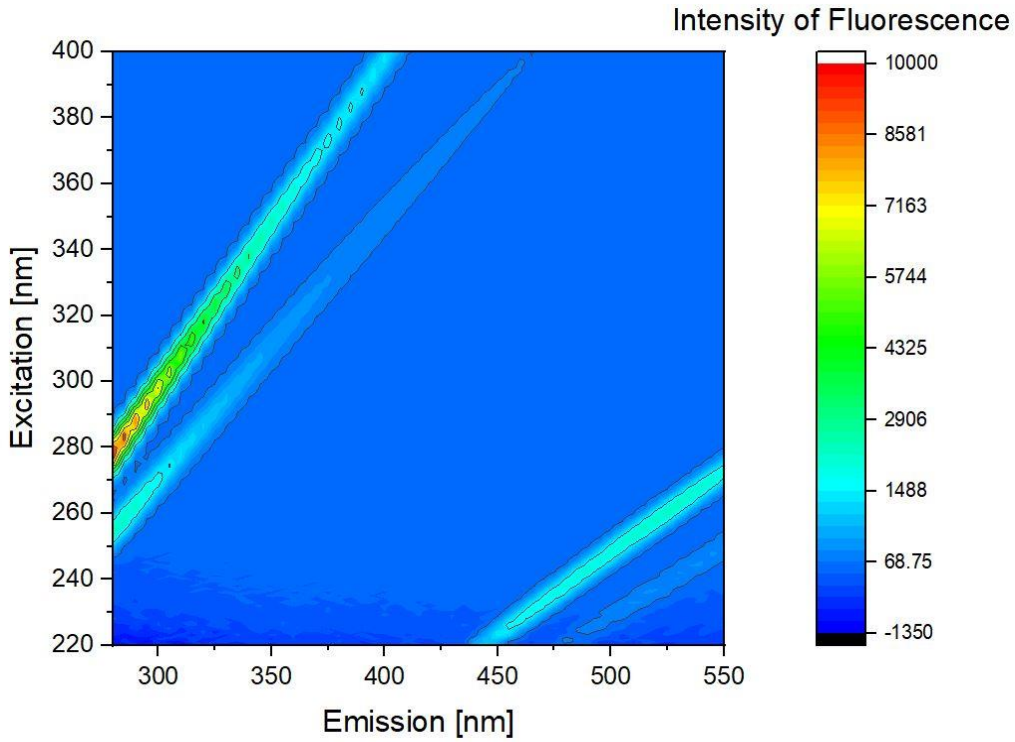

Figure 8.3: 3D-fluorescence-excitation-emission matrix of water matrix incubated in ozonised graphite

Without IHU 310 UV transmitting filter

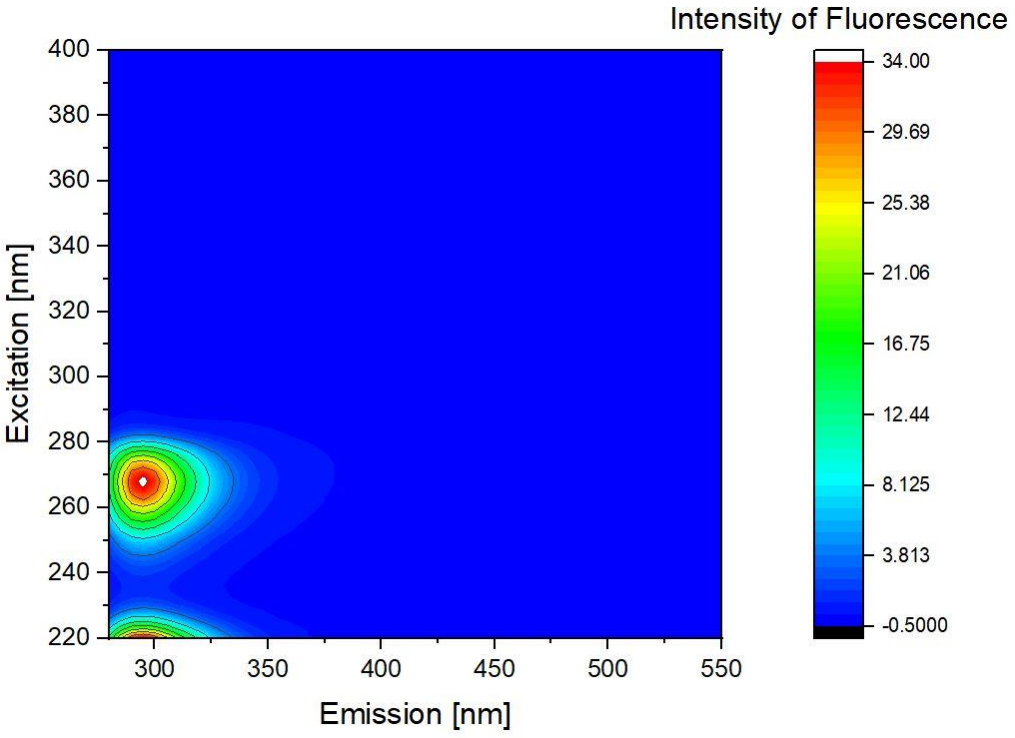

Figure 8.4: 3D-fluorescence-excitation-emission matrix of Phenol

With IHU 310 UV transmitting filter

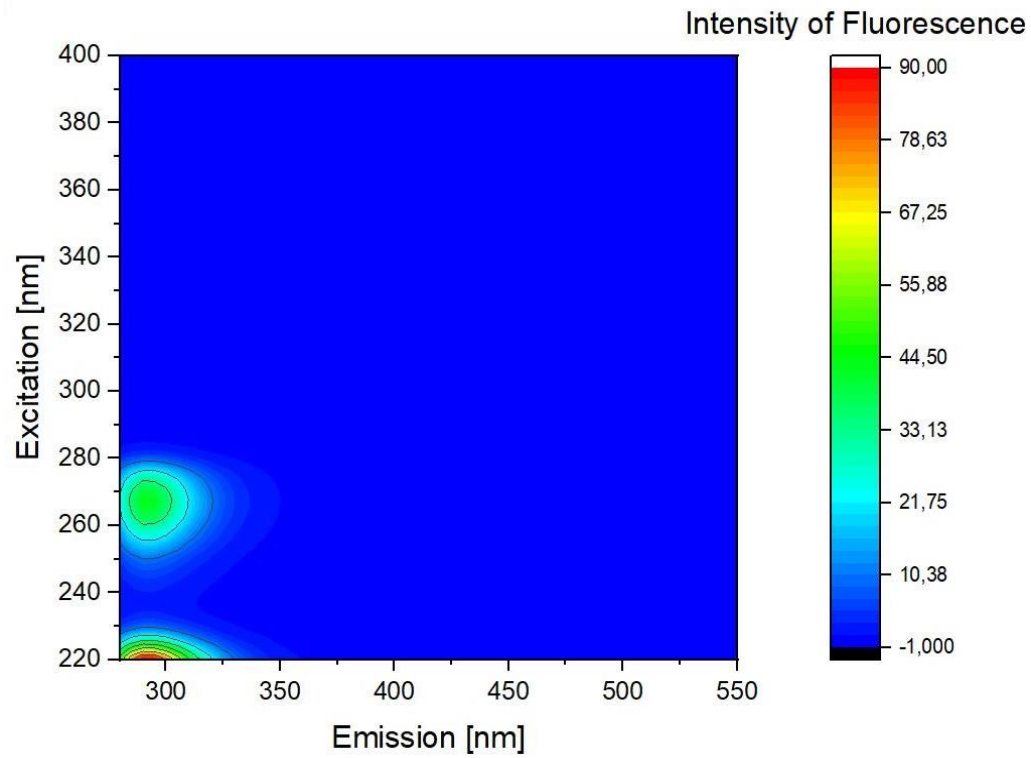

Figure 8.5: 3D-fluorescence-excitation-emission matrix of Anisole

With IHU 310 UV transmitting filter

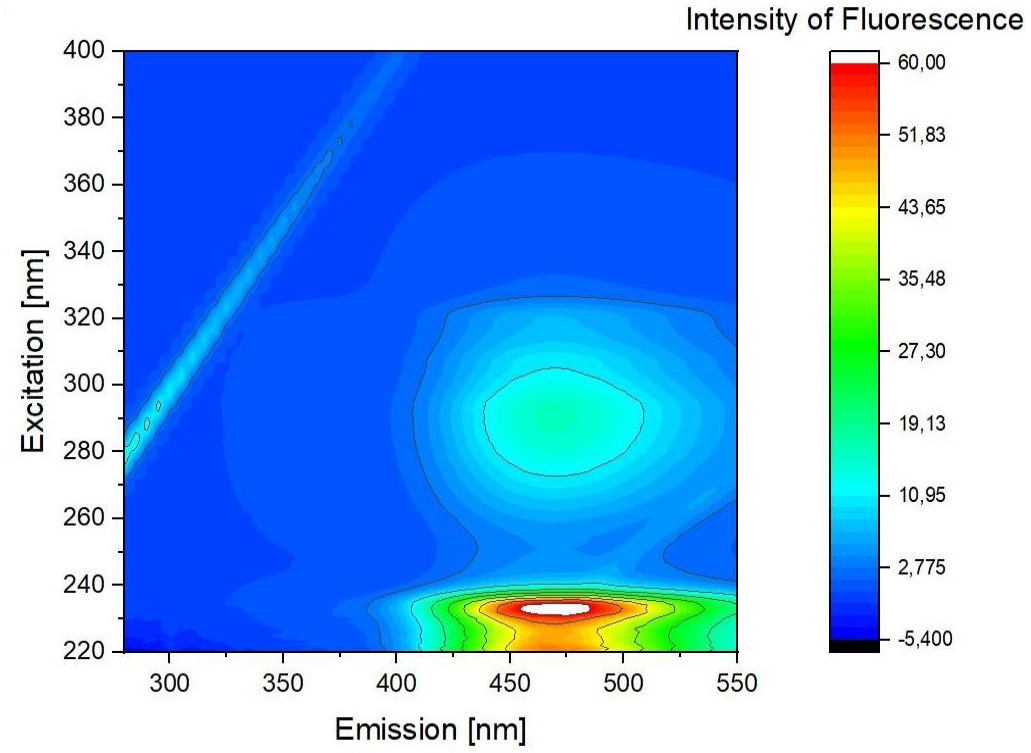

Figure 8.6: 3D-fluorescence-excitation-emission matrix of 1-Naphthol

Without IHU 310 UV transmitting filter

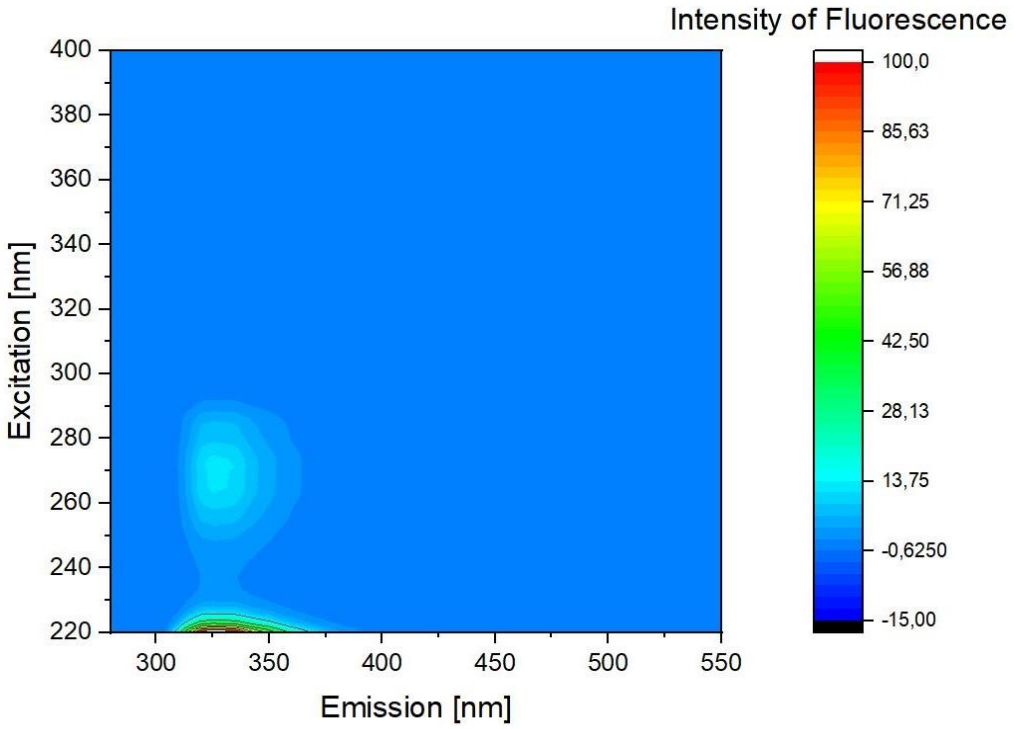

Figure 8.7: 3D-fluorescence-excitation-emission matrix of Naphthalene

With IHU 310 UV transmitting filter

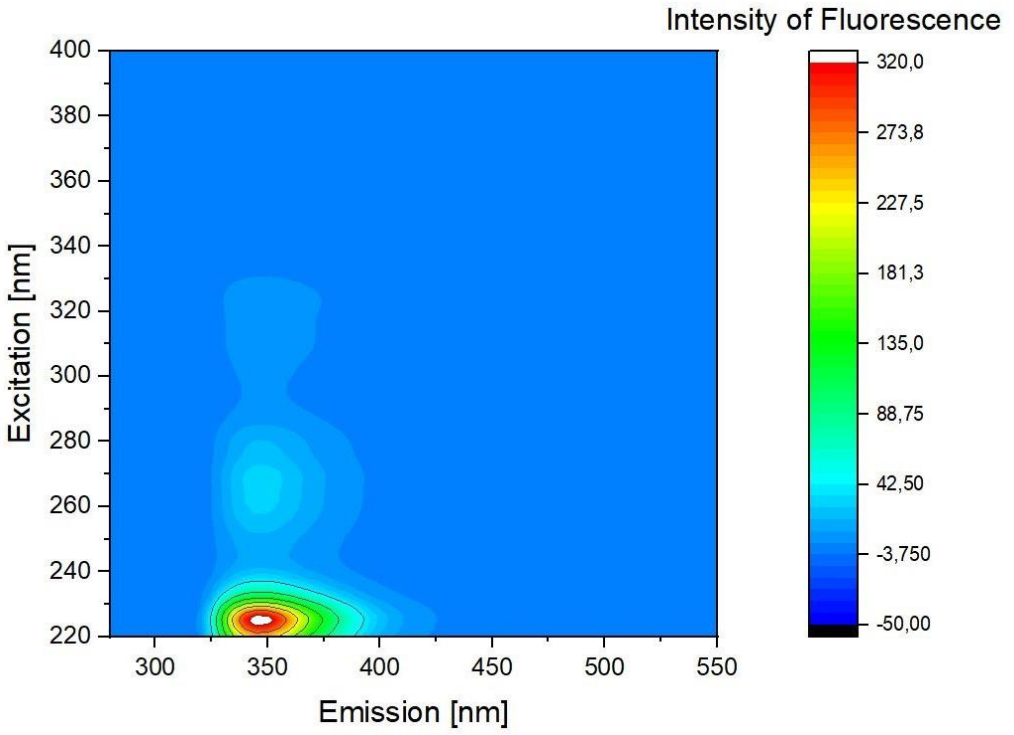

Figure 8.8: 3D-fluorescence-excitation-emission matrix of 2-Methoxynaphthalene

With IHU 310 UV transmitting filter

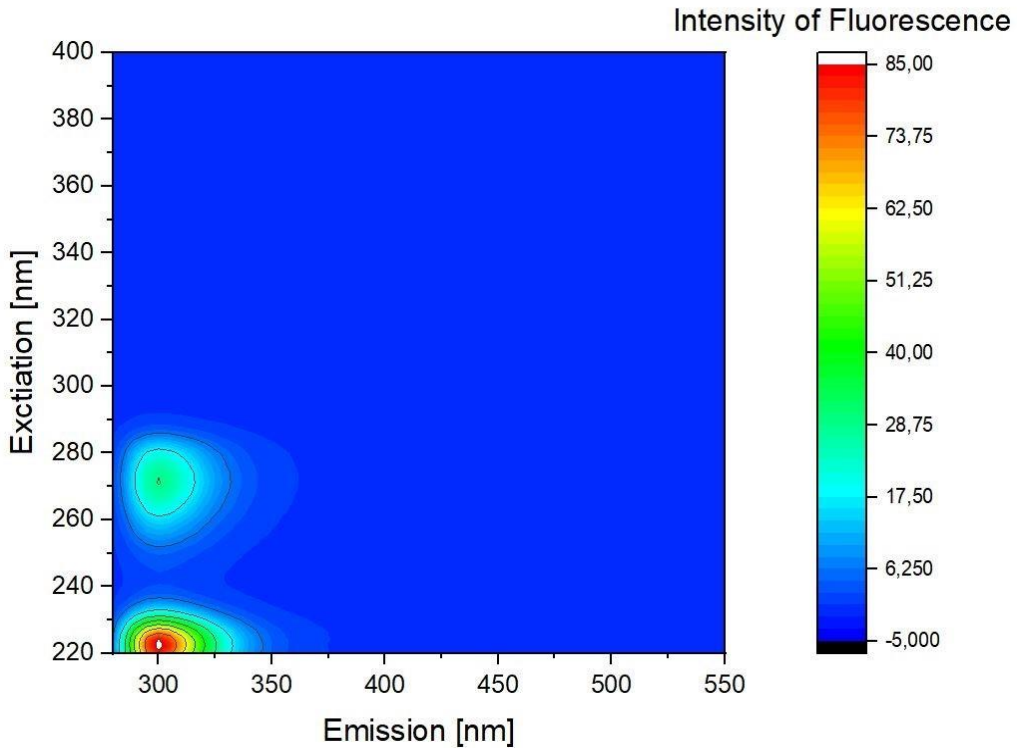

Figure 8.9: 3D-fluorescence-excitation-emission matrix of L-Tyrosine

With IHU 310 UV transmitting filter

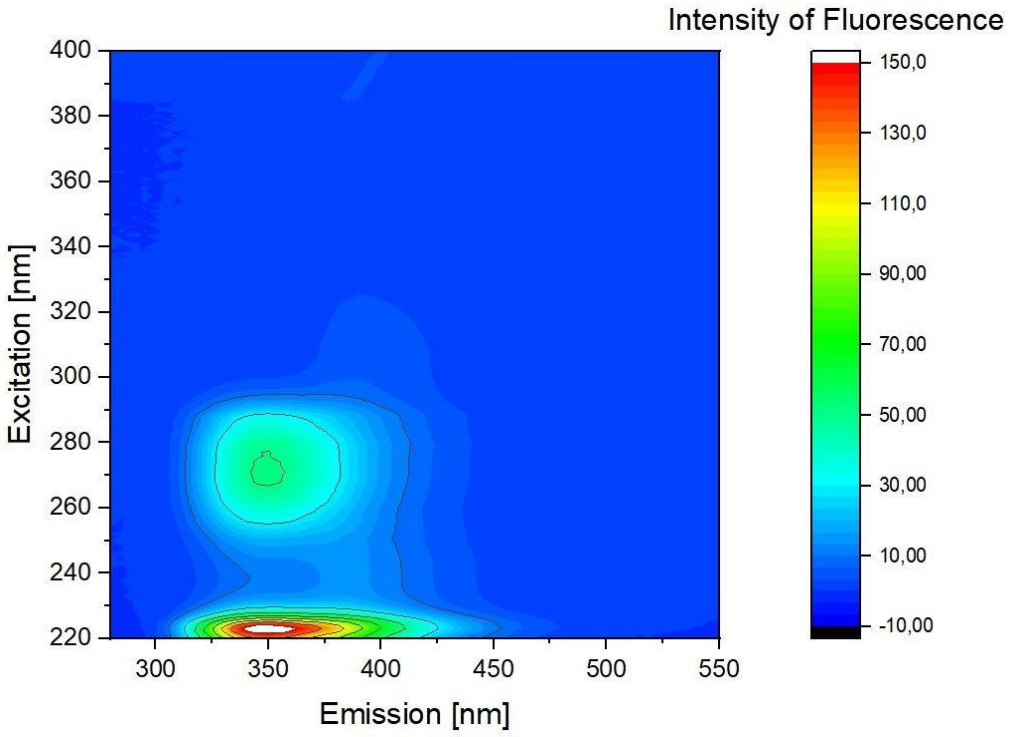

Figure 8.10: 3D-fluorescence-excitation-emission matrix of L-Tryptophan

With IHU 310 UV transmitting filter

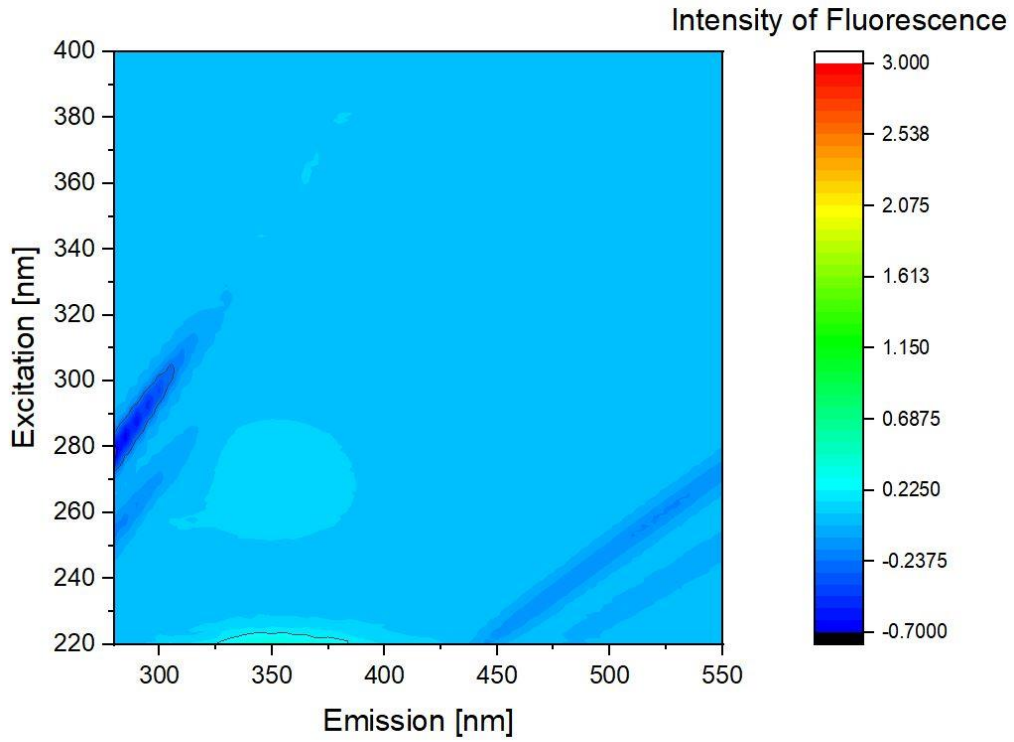

Figure 8.11: 3D-fluorescence-excitation-emission matrix of L-Phenylalanine

Without IHU 310 UV transmitting filter

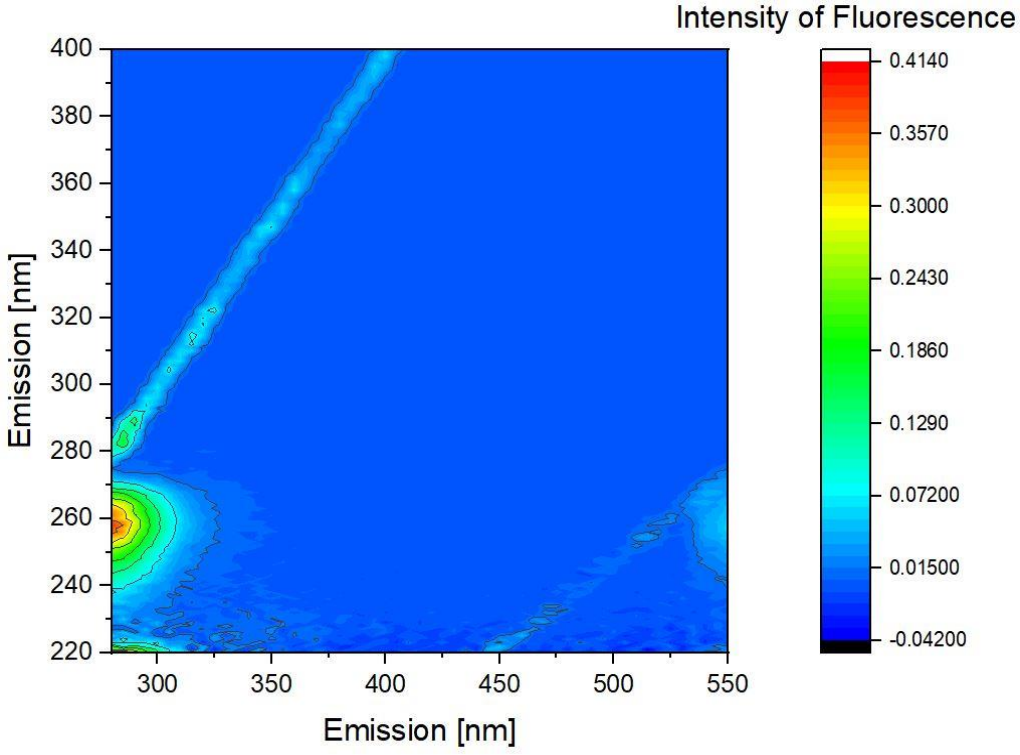

Figure 8.12: 3D-fluorescence-excitation-emission matrix of Toluene

Without IHU 310 UV transmitting filter

8.2 Scanning electron microscopy

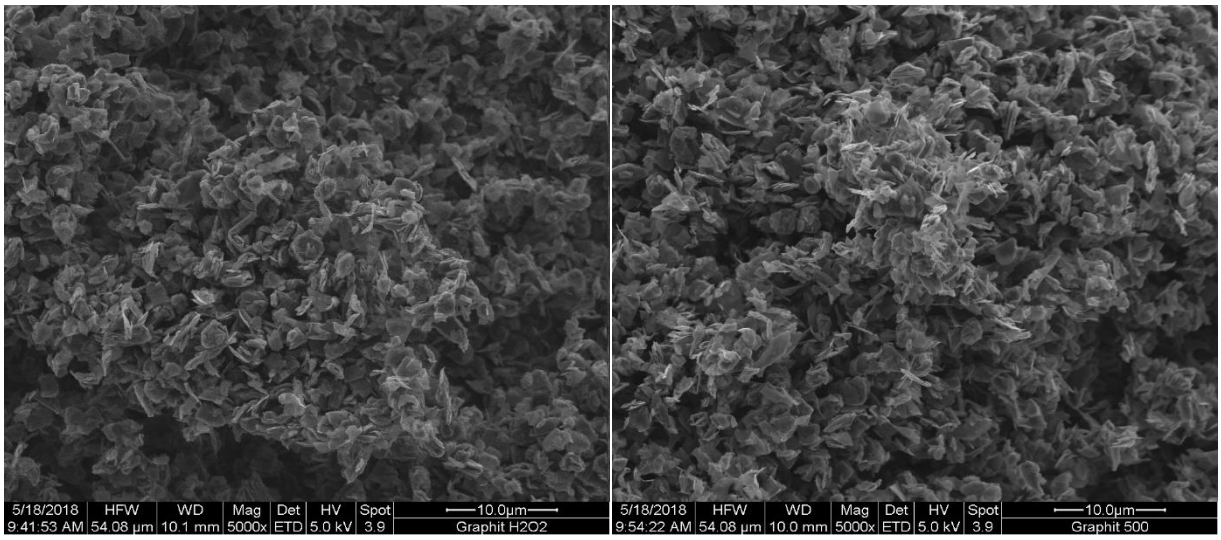

a) b)

Figure 8.13: SEM image in 5000x magnification of a) H_2O_2 treated graphite (30 %, 6 h) and b) thermal treated graphite (500 °C, 2 h, O_2/N_2 atmosphere)

8.3 Calibration curves for substance analysis

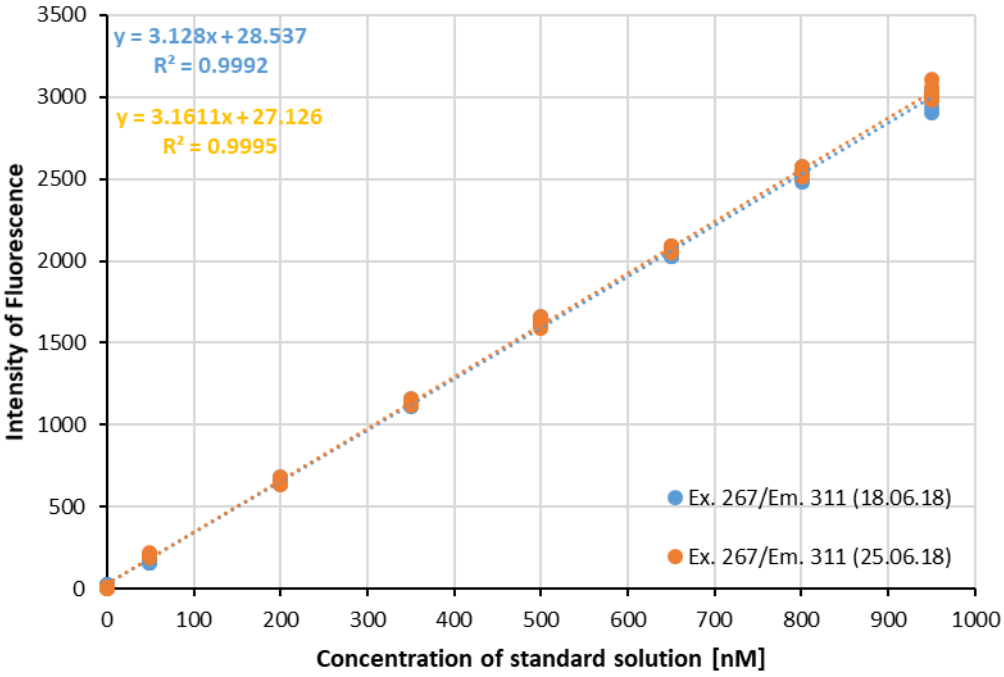

Figure 8.14: Calibration curve of phenol solution in water matrix

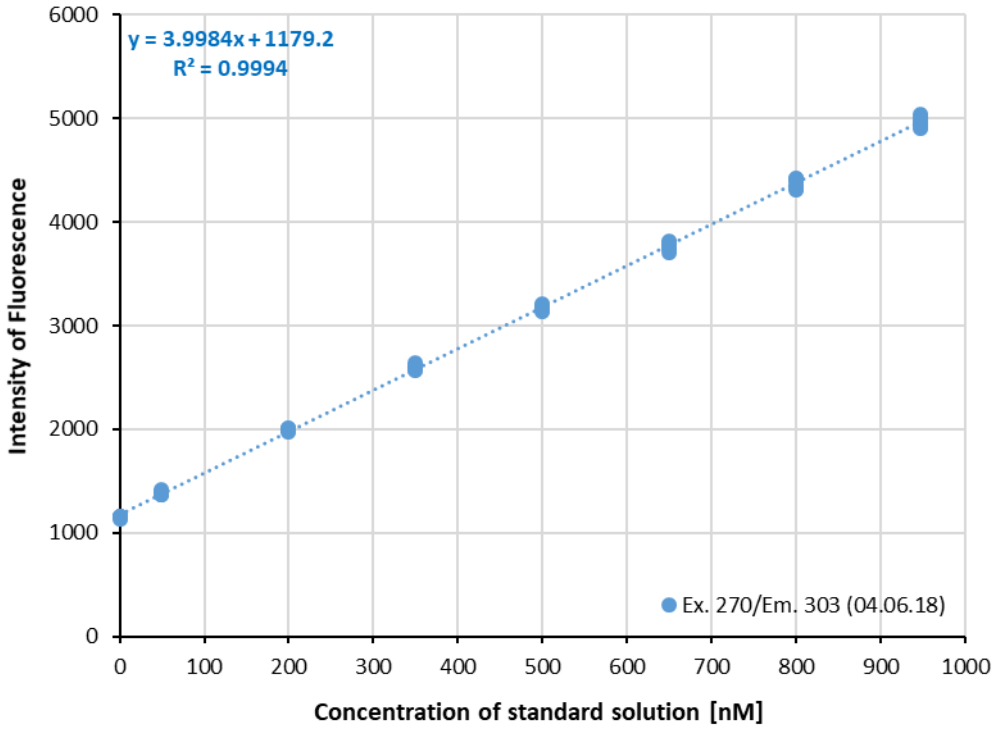

Figure 8.15: Calibration curve of anisole solution in water matrix

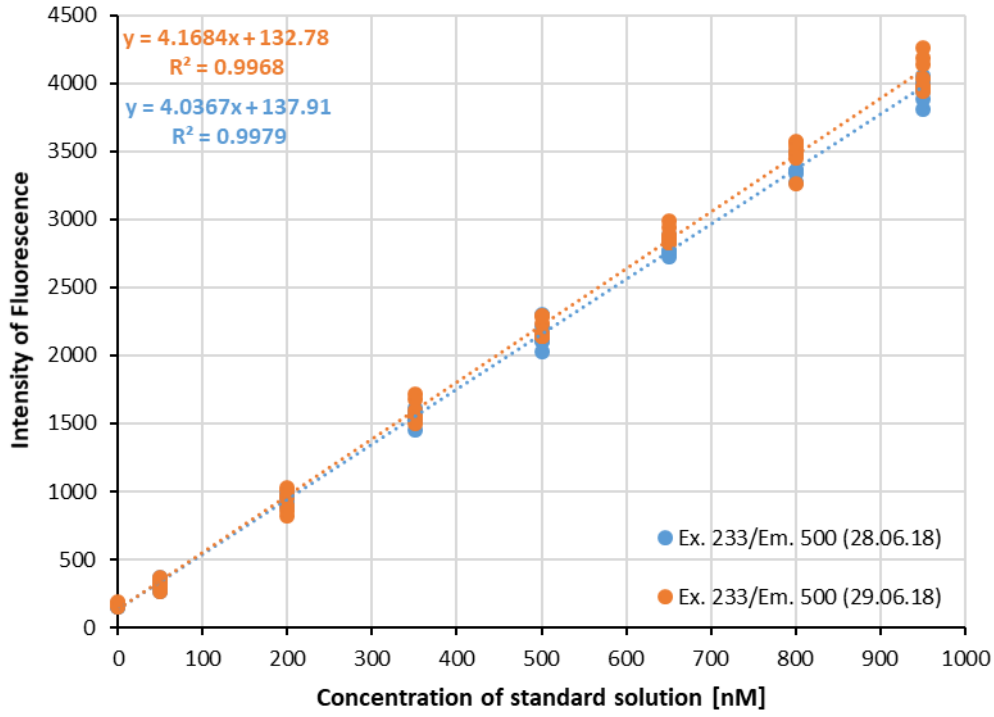

Figure 8.16: Calibration curve of 1-naphthol solution in water matrix

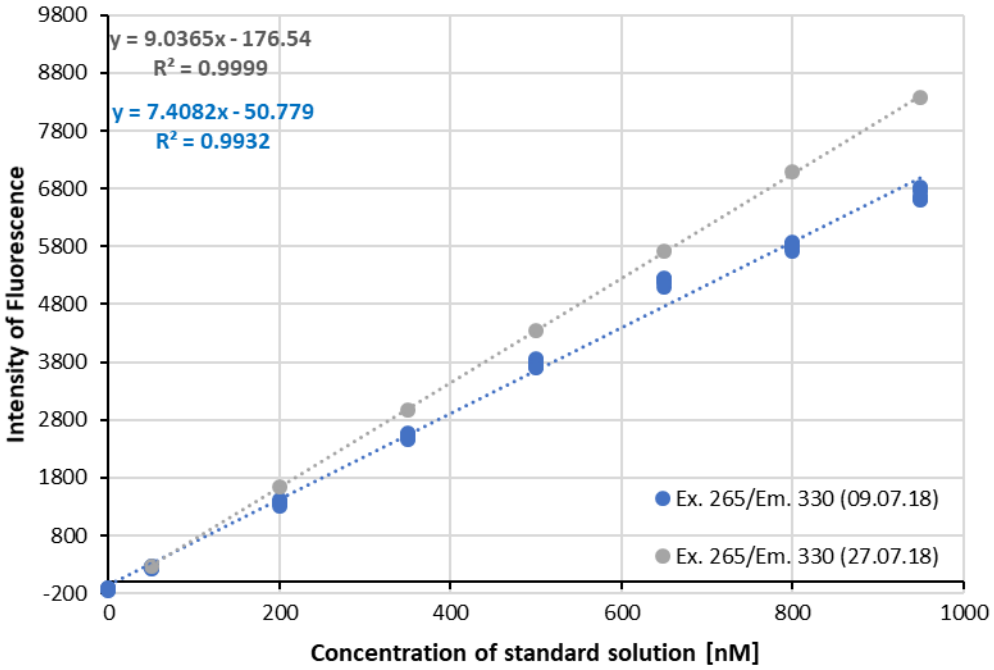

Figure 8.17: Calibration curve of naphthalene solution in water matrix

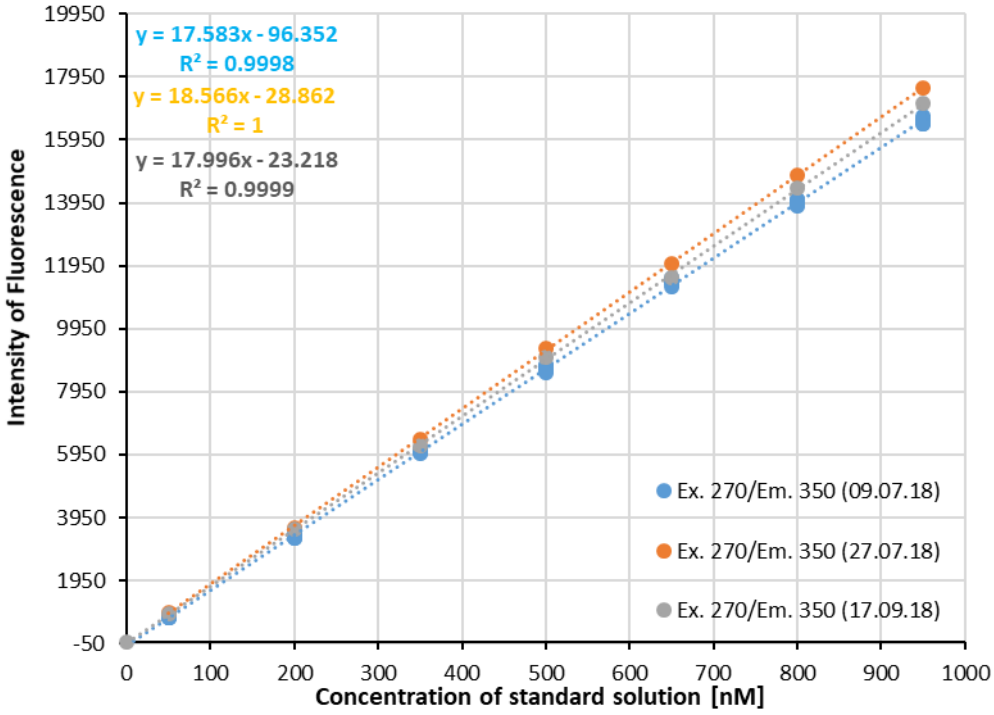

Figure 8.18: Calibration curve of 2-methoxynaphthalene solution in water matrix

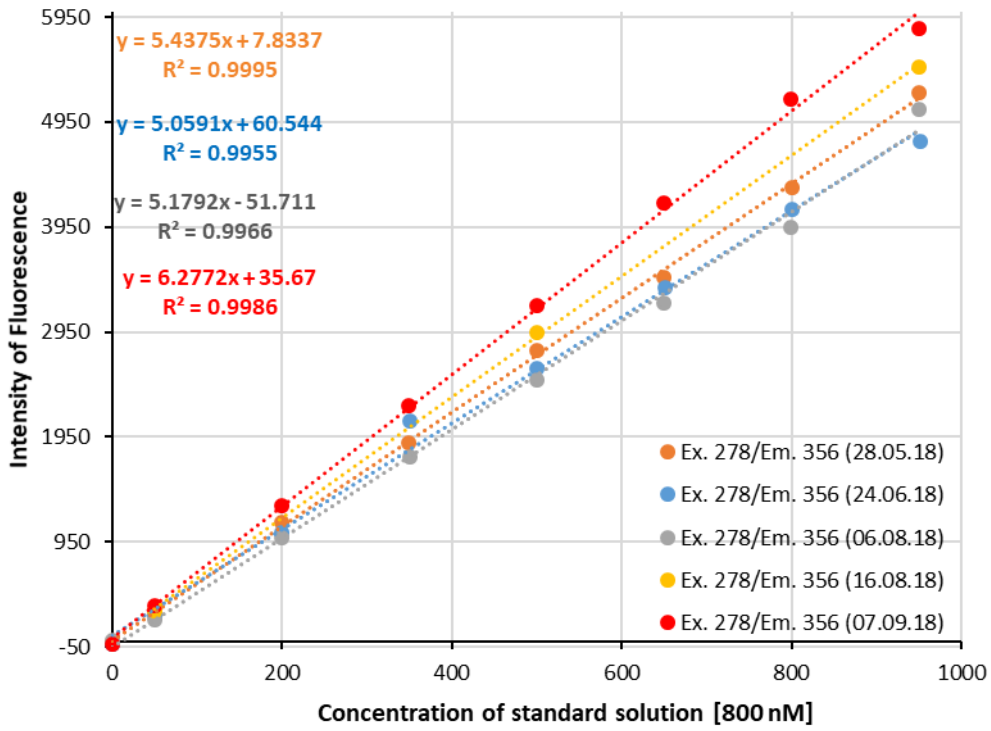

Figure 8.19: Calibration curve of L-tryptophan solution in water matrix

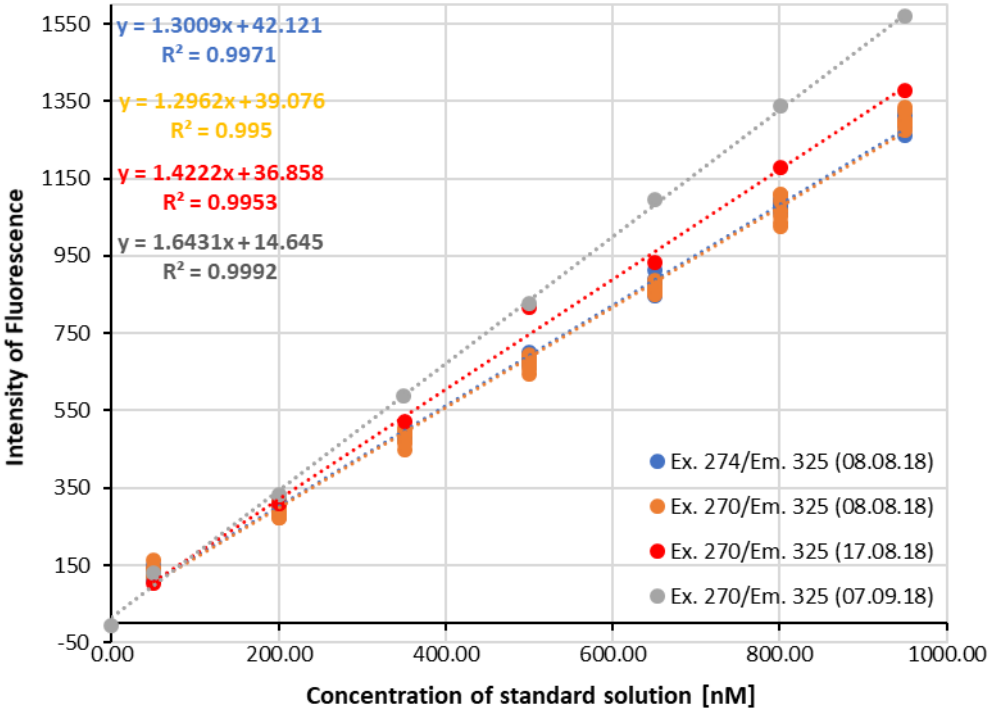

Figure 8.20: Calibration curve of L-tyrosine solution in water matrix

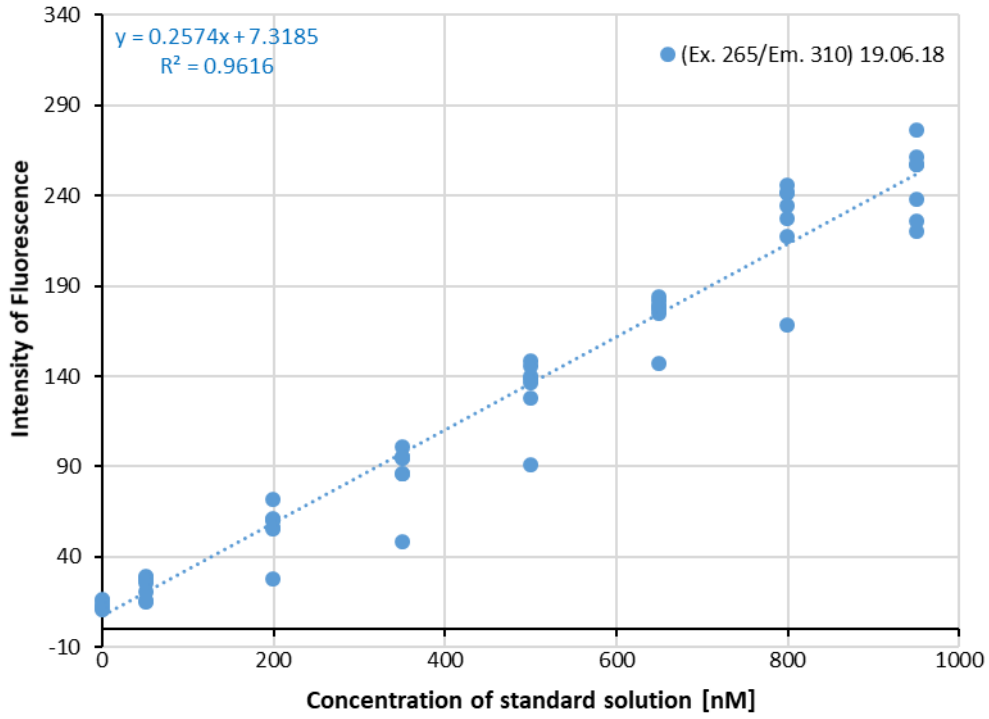

Figure 8.21: Calibration curve of 4-chlorophenol solution in water matrix

8.4 Adsorption kinetics tests

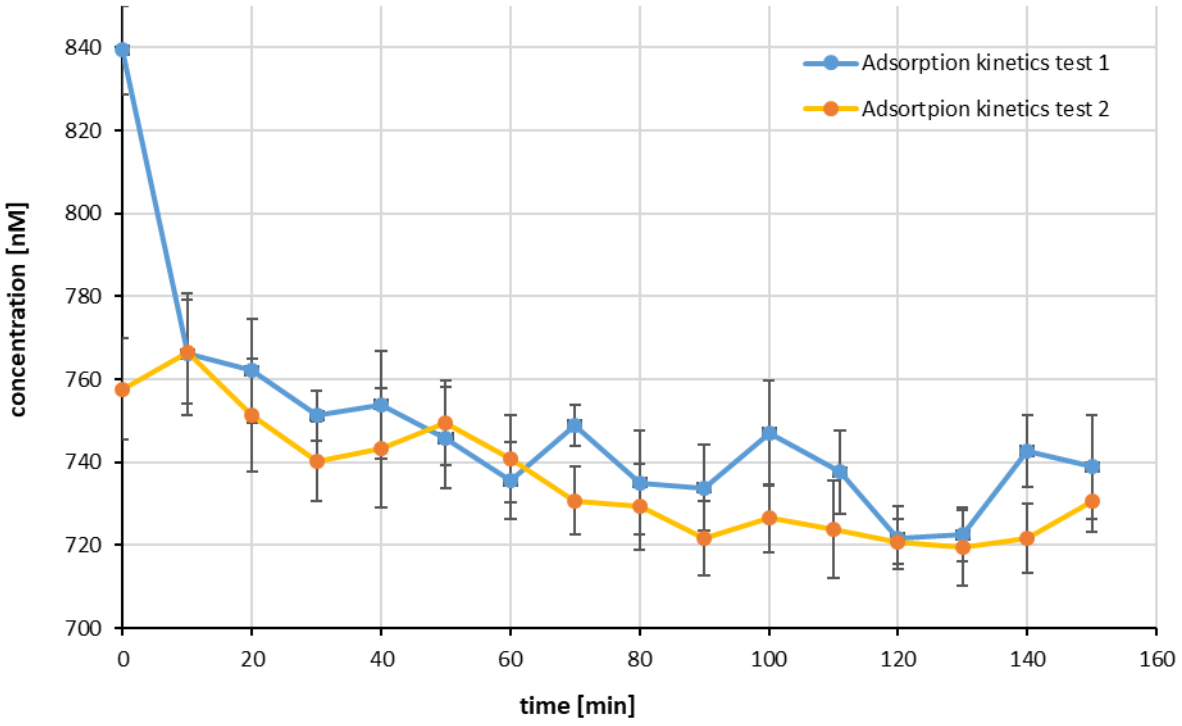

Figure 8.22: Adsorption kinetics test of phenol

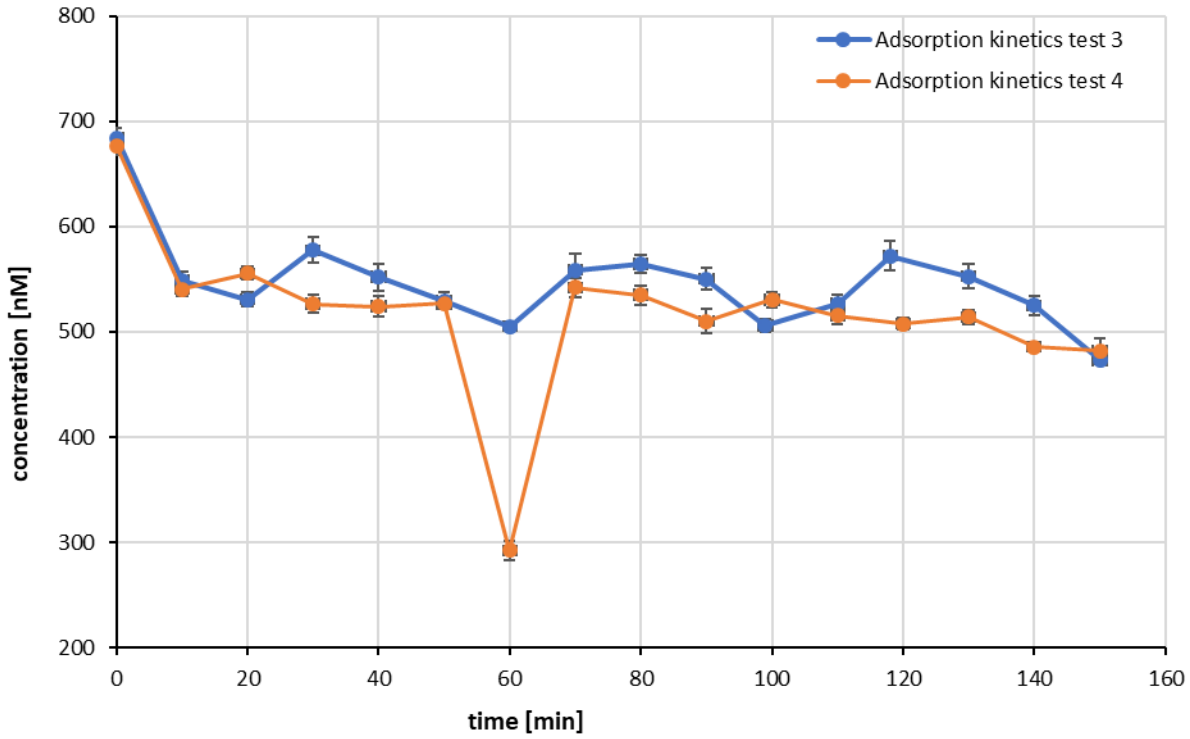

Figure 8.23: Adsorption kinetics test for anisole

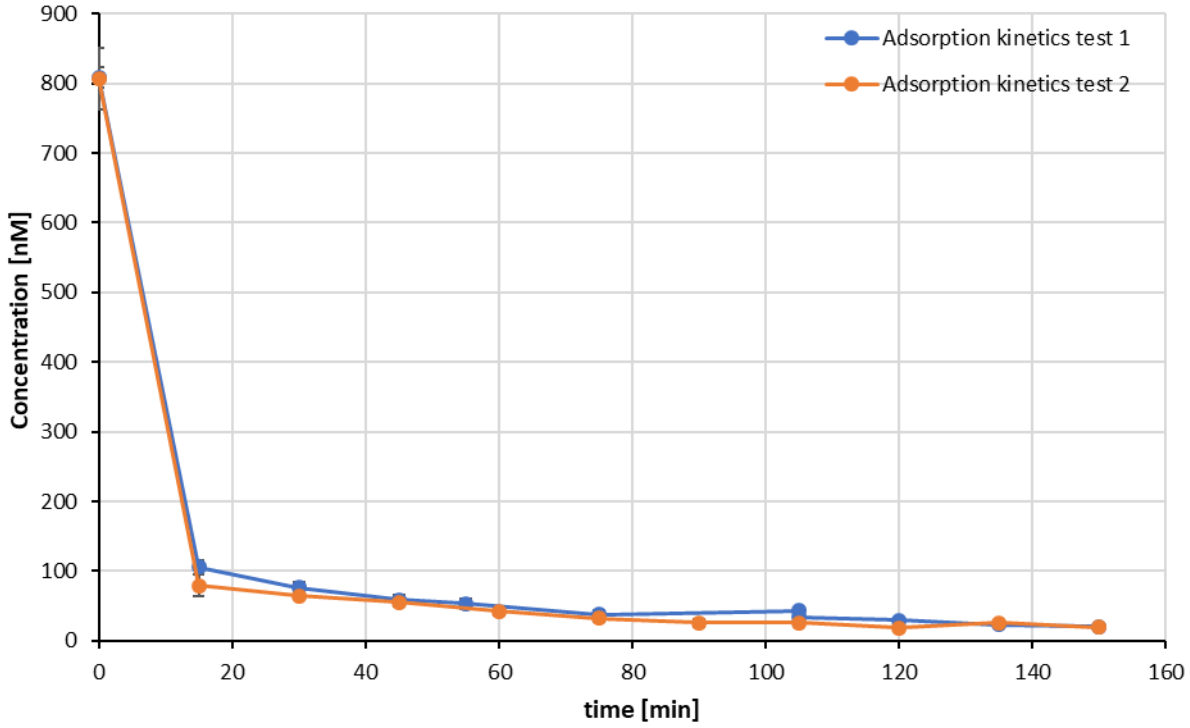

Figure 8.24: Adsorption kinetics test for 1-naphthol

8.5 Logarithmic Adsorption isotherms

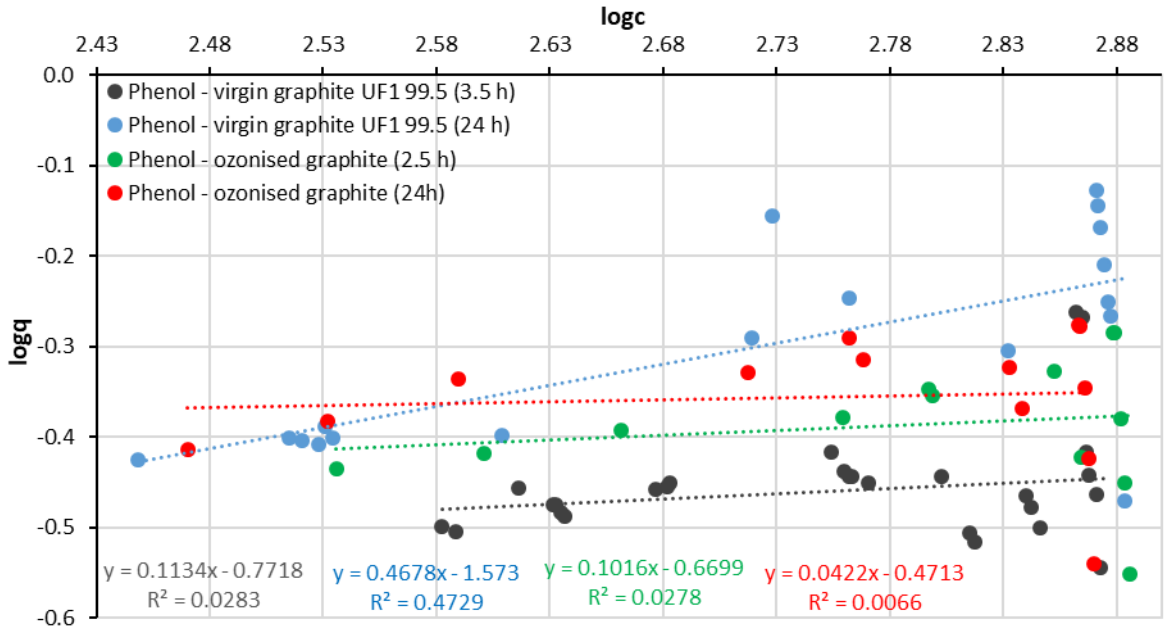

Figure 8.25: Double decadic logarithmic adsorption isotherm of phenol adsorption batch tests

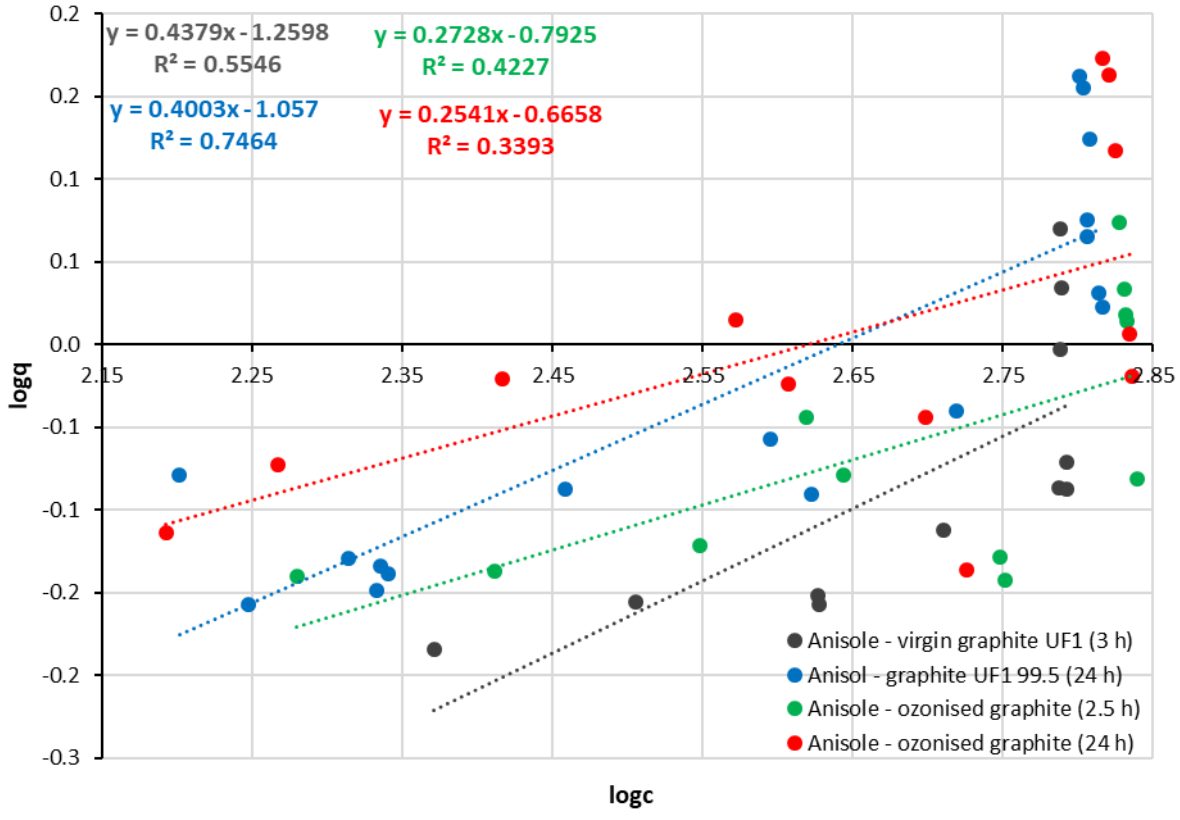

Figure 8.26: Double decadic logarithmic adsorption isotherm of anisole adsorption batch tests

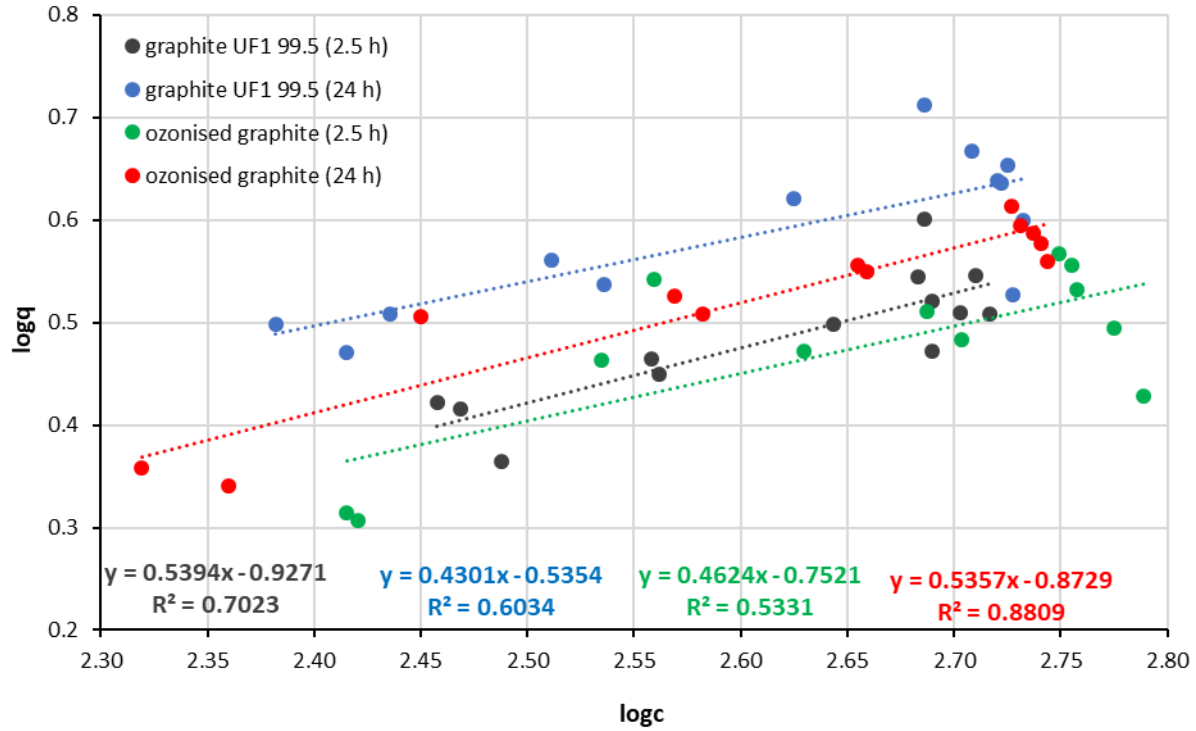

Figure 8.27: Double decadic logarithmic adsorption isotherm of 1-naphthol adsorption batch tests

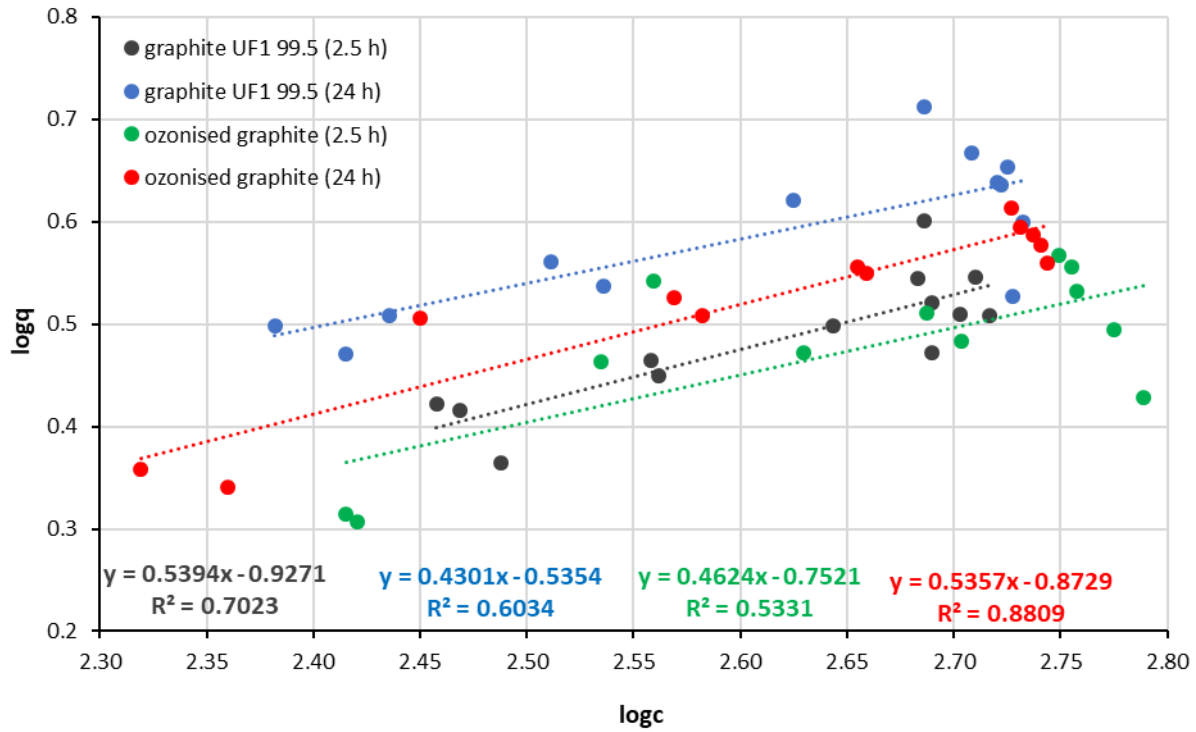

Figure 8.28: Double decadic logarithmic adsorption isotherm of naphthalene adsorption batch tests

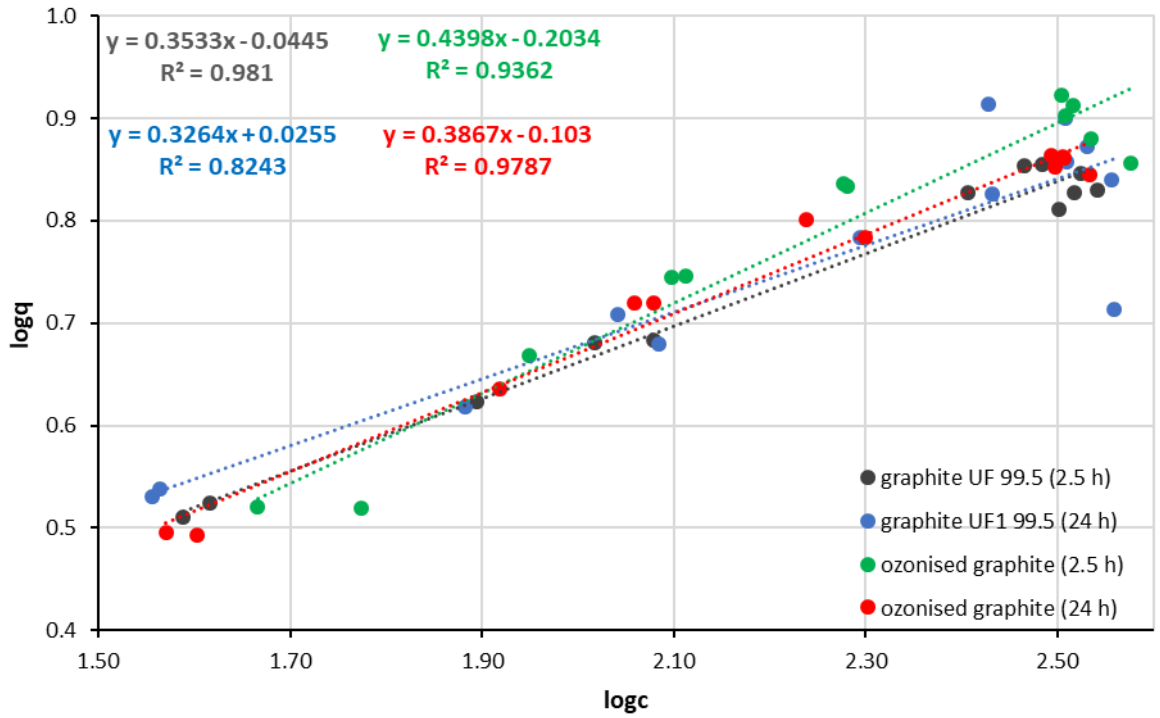

Figure 8.29: Double decadic logarithmic adsorption isotherm of 2-methoxynaphthalene adsorption batch tests

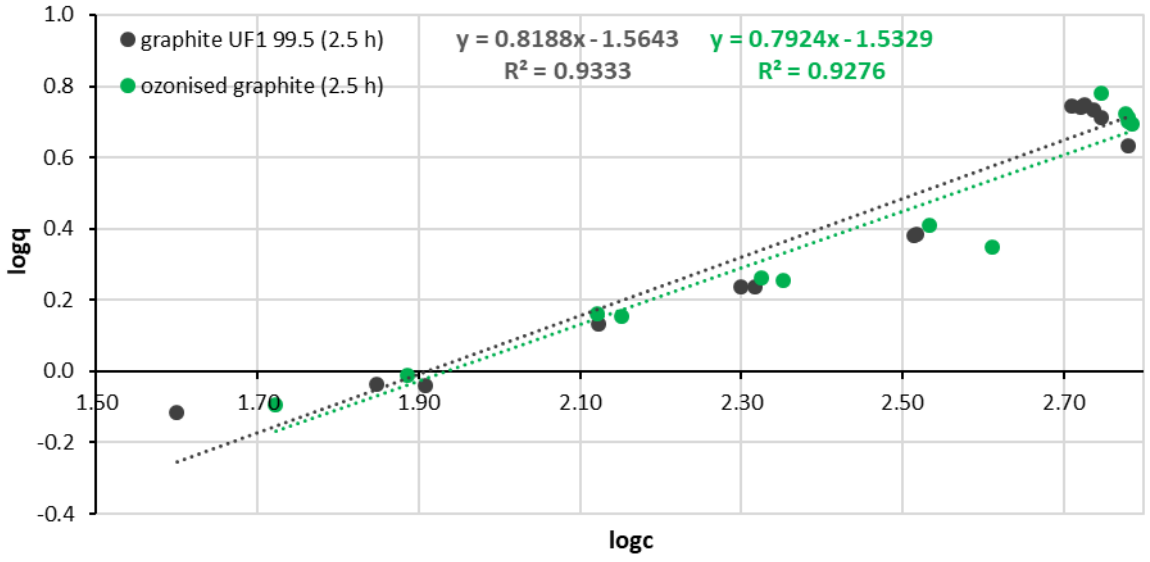

Figure 8.30: Double decadic logarithmic adsorption isotherm of L-tryptophan adsorption batch tests

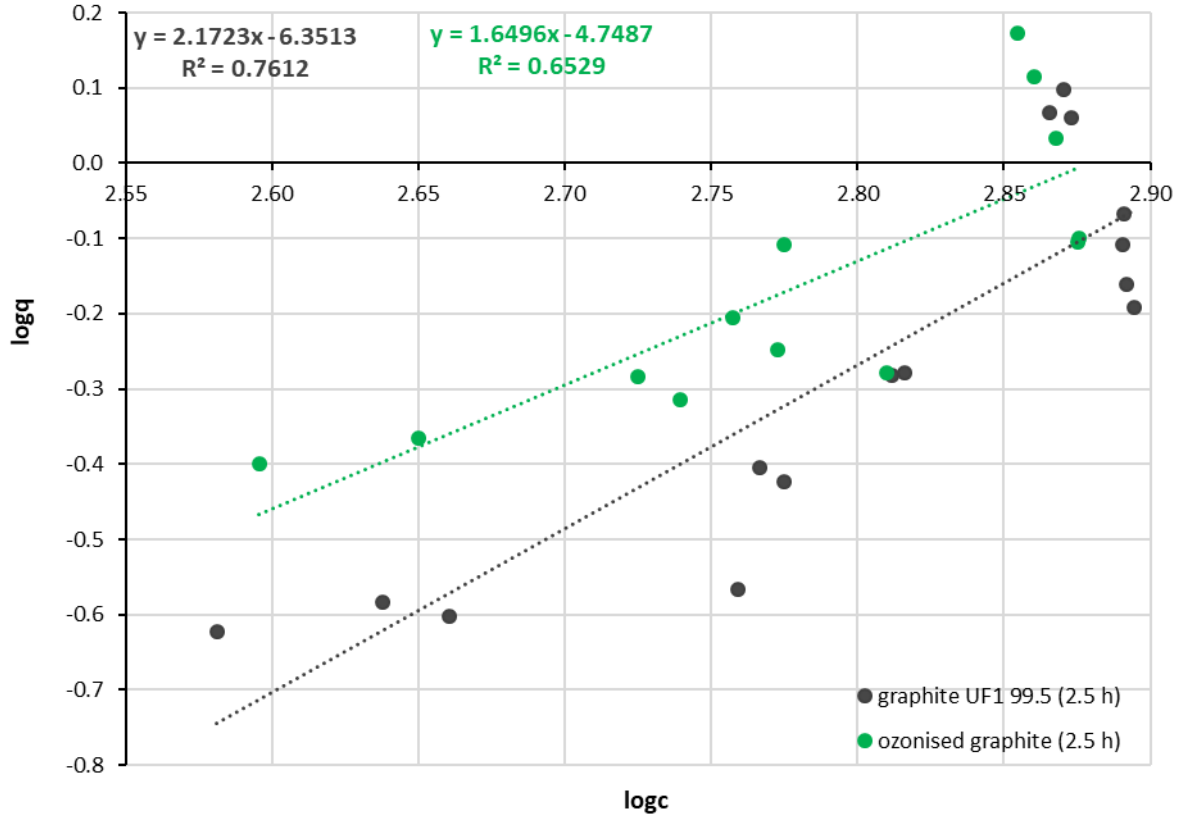

Figure 8.31: Double decadic logarithmic adsorption isotherm of L-tyrosine adsorption batch tests

8.6 Averaged Adsorption Isotherms

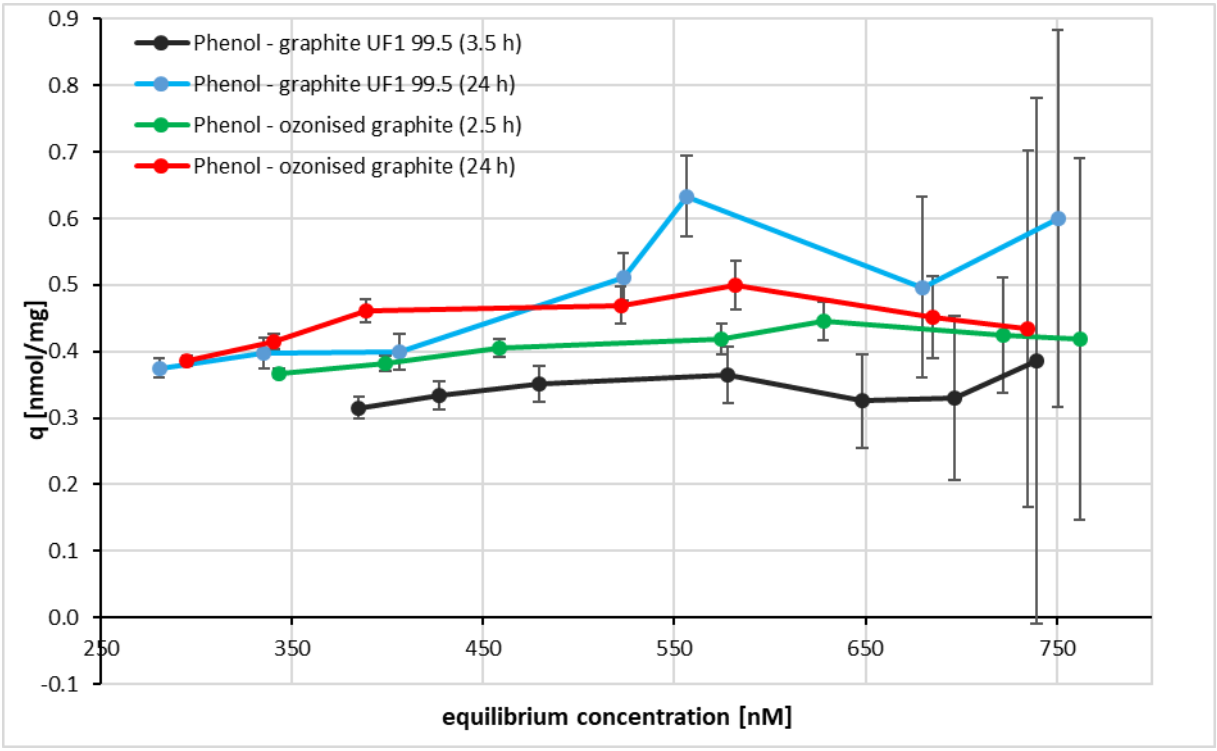

Figure 8.32: Averaged adsorption isotherms of phenol batch tests with the total error indication of *q*

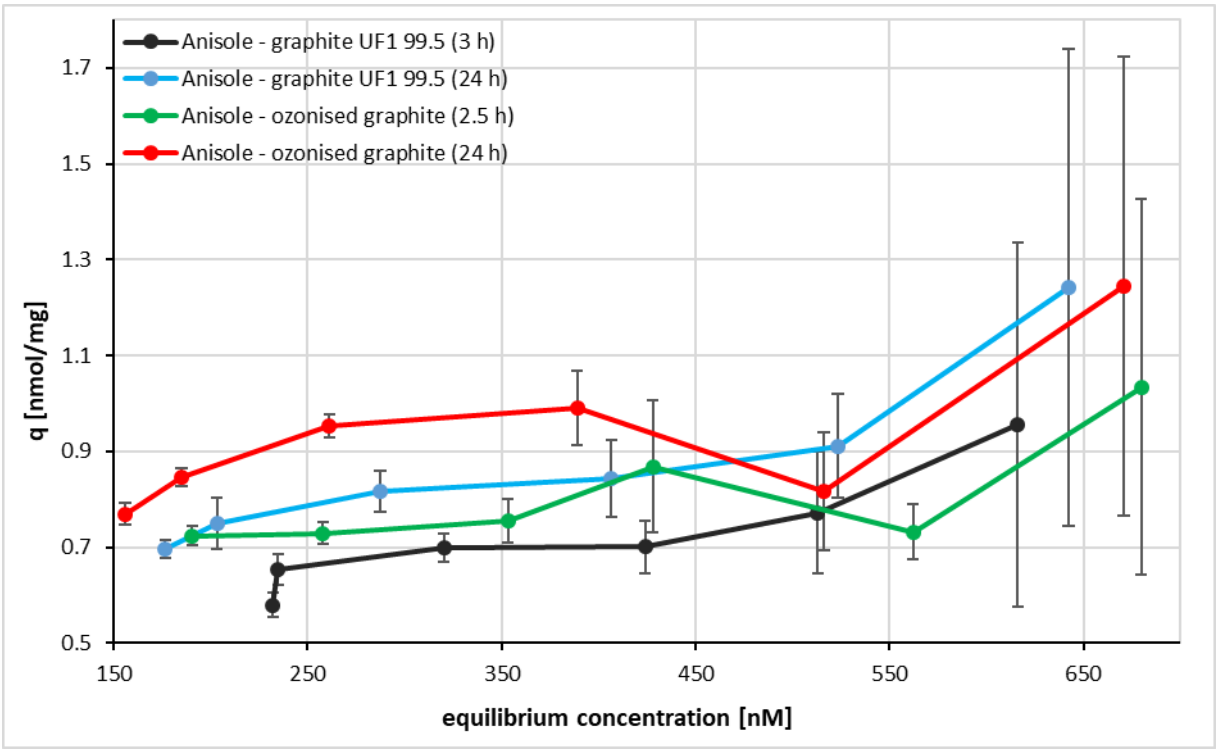

Figure 8.33: Averaged adsorption isotherms of anisole batch tests with the total error indication of *q*

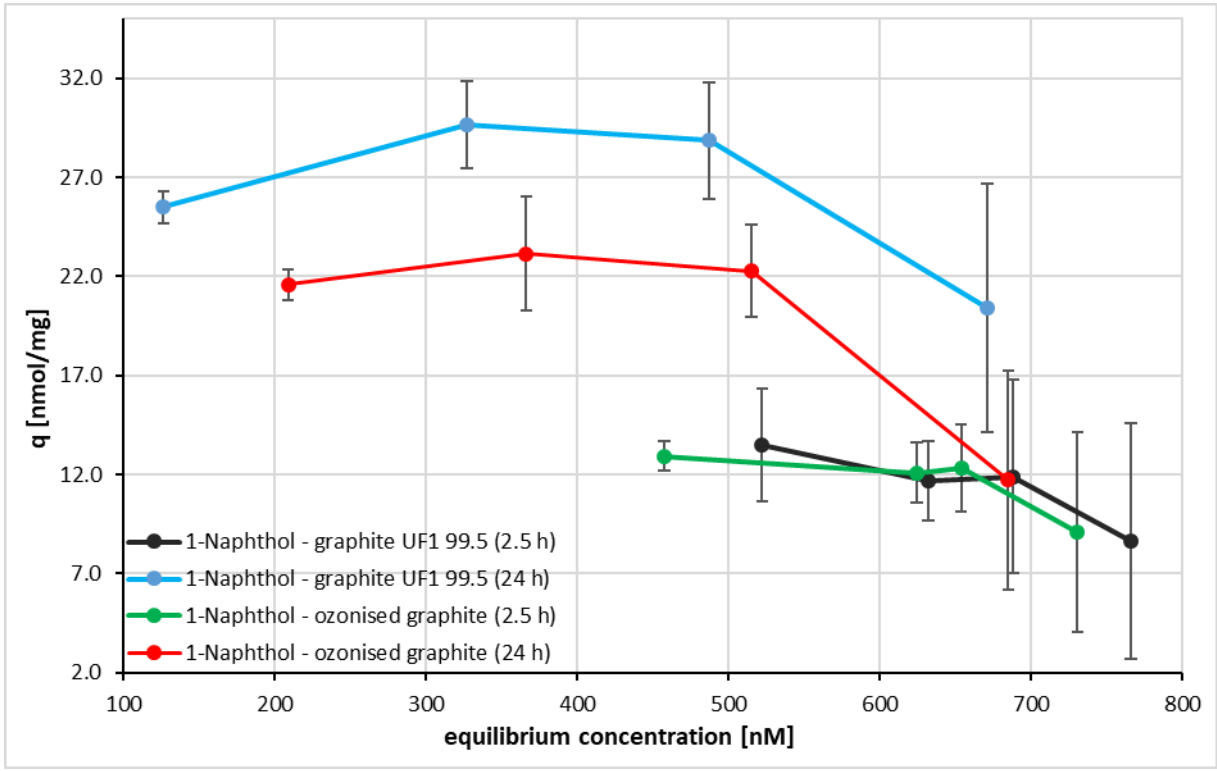

Figure 8.34: Averaged adsorption isotherms of 1-naphthol batch tests with the total error indication of *q*

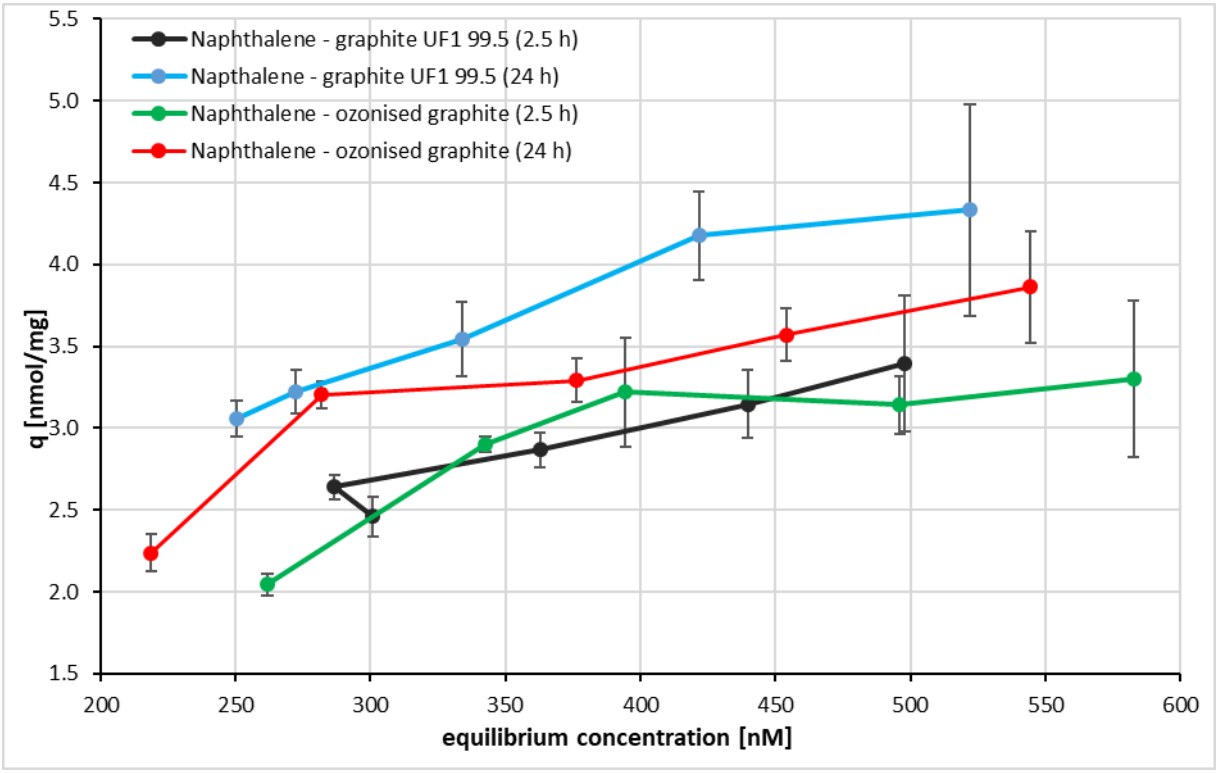

Figure 8.35: Averaged adsorption isotherms of naphthalene batch tests with the total error indication of *q*

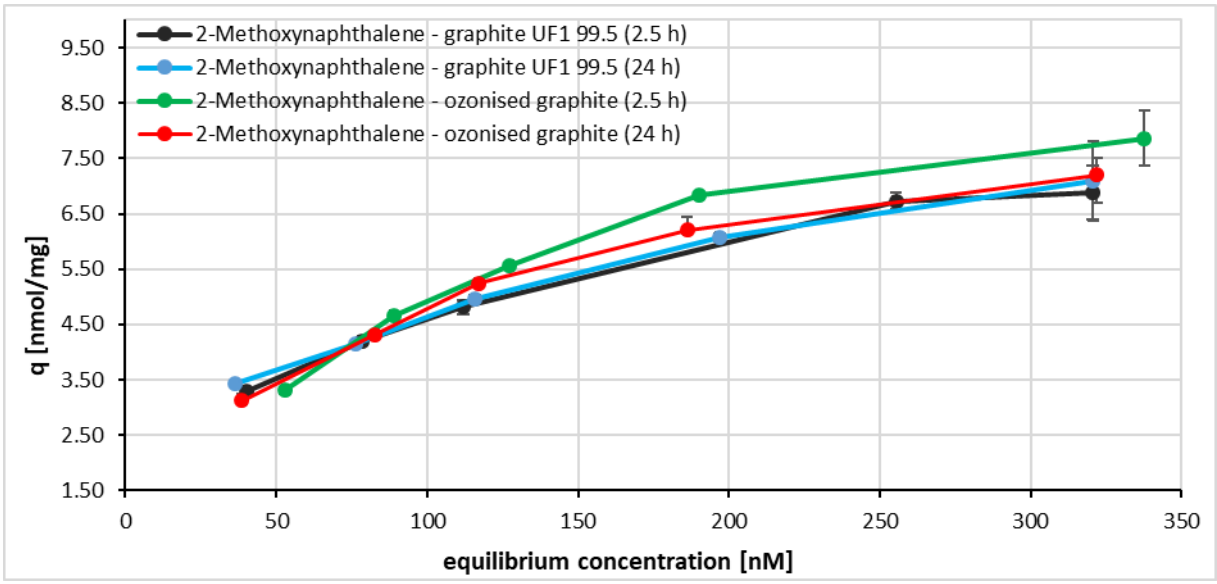

Figure 8.36: Averaged adsorption isotherms of 2-methoxynaphthalene batch tests with the total error indication of *q*

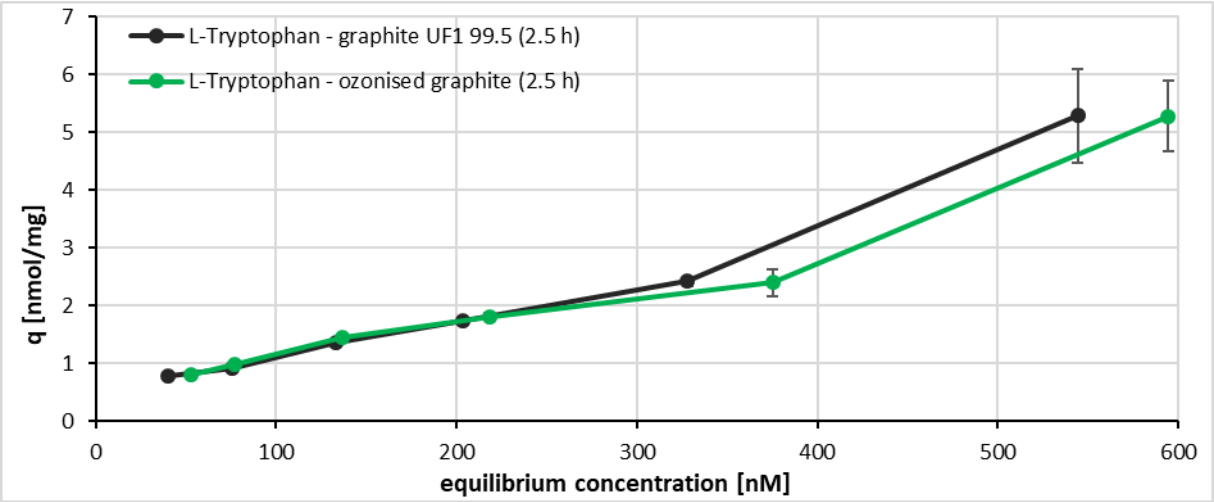

Figure 8.37: Averaged adsorption isotherms of L-tryptophan batch tests with the total error indication of *q*

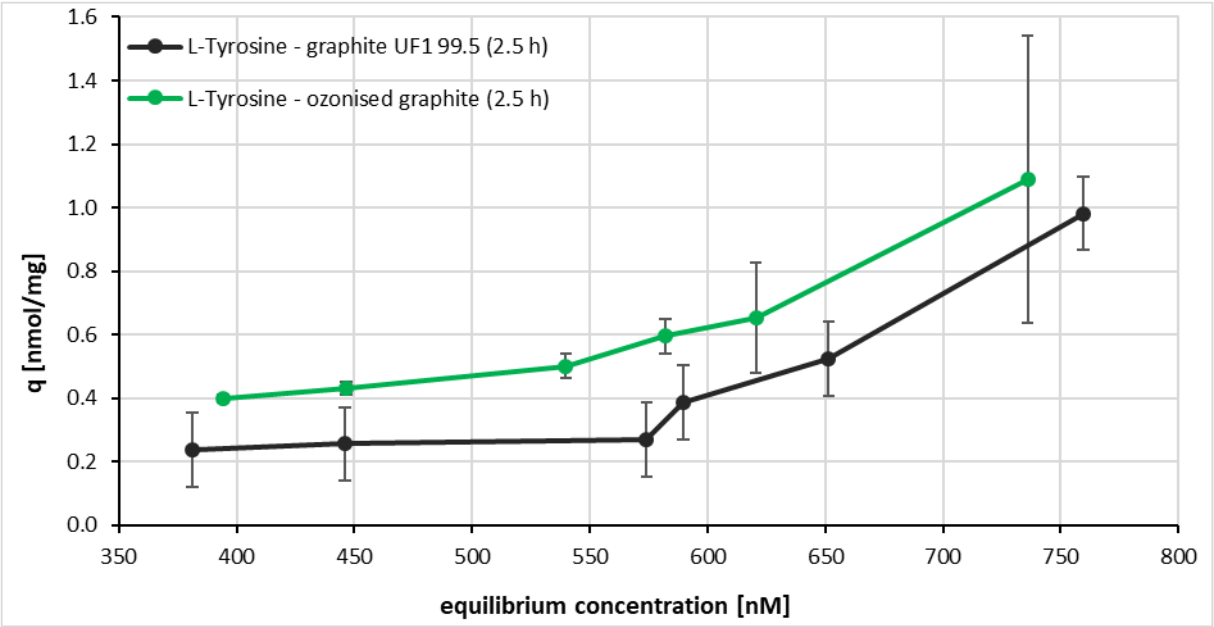

Figure 8.38: Averaged adsorption isotherms of L-tyrosine batch tests with the total error indication of *q*

8.7 Data sheet

UF1 99,5

Physikalische und chemische Daten

Spezifikation:

Kohlenstoffgehalt:		min. 99,5 %
Asche:		max. 0,5 %
Laserbeugung (Sympatec Helos):	d10	< 2 µm
	d50	2 - 4 µm
	d90	< 8 µm

Typische Werte:

Kohlenstoffgehalt:		99,7 %
Asche:		0,3 %
Laserbeugung (Sympatec Helos):	d10	1,5 µm
	d50	3,0 µm
	d90	5,5 µm

Graphit Kropfmühl GmbH
Langheinrichstraße 1
94051 Hauzenberg
GERMANY
Tel: +49 (0)8586 609-0
Fax: +49 (0)8586 609-114
info@gk-graphite.com
www.gk-graphite.com

Graphit als Modell-Adsorbens in wässrigen Lösungen

Vernillo, Marco

In: Selected theses from the Chair of Mechanical Process Engineering / Water technology

DOI: https://doi.org/10.17185/duepublico/49211

URN: urn:nbn:de:hbz:464-20190909-084000-7

Link: https://duepublico.uni-duisburg-essen.de:443/servlets/DocumentServlet?id=49211